cBAF generates subnucleosomes that expand OCT4 binding and function beyond DNA motifs at enhancers

Marina Nocente, Anida Mesihovic Karamitsos, Emilie Drouineau, Manon Soleil, Waad Albawardi, Cécile Dulary, Florence Ribierre, Hélène Picaud, Olivier Alibert, Joël Acker, et al.

nature structural & molecular biology

Article

https://doi.org/10.1038/s41594-024-01344-0

cBAF generates subnucleosomes that expand OCT4 binding and function beyond DNA motifs at enhancers

Received: 2 May 2023

Accepted: 3 June 2024

Published online: 2 July 2024

Check for updates

Marina C. Nocente[1,4], Anida Mesihovic Karamitsos[1,4], Emilie Drouineau[1,4], Manon Soleil[1], Waad Albawardi[2], Cécile Dulary[3], Florence Ribierre[3], Hélène Picaud[1], Olivier Alibert[3], Joël Acker[1], Marie Kervella[1], Jean-Christophe Aude[1], Nick Gilbert[2], Françoise Ochsenbein[1], Sophie Chantalat[3] & Matthieu Gérard[1]

The canonical BRG/BRM-associated factor (cBAF) complex is essential for chromatin opening at enhancers in mammalian cells. However, the nature of the open chromatin remains unclear. Here, we show that, in addition to producing histone-free DNA, cBAF generates stable hemisome-like subnucleosomal particles containing the four core histones associated with 50–80 bp of DNA. Our genome-wide analysis indicates that cBAF makes these particles by targeting and splitting fragile nucleosomes. In mouse embryonic stem cells, these subnucleosomes become an in vivo binding substrate for the master transcription factor OCT4 independently of the presence of OCT4 DNA motifs. At enhancers, the OCT4–subnucleosome interaction increases OCT4 occupancy and amplifies the genomic interval bound by OCT4 by up to one order of magnitude compared to the region occupied on histone-free DNA. We propose that cBAF-dependent subnucleosomes orchestrate a molecular mechanism that projects OCT4 function in chromatin opening beyond its DNA motifs.

Understanding how transcription factors (TFs) recognize their target *cis*-regulatory elements (CREs) on the mammalian genome and regulate transcription remains a major challenge[1,2]. Most mammalian TFs bind transiently to short (5–15 bp) and often degenerated DNA motifs[3,4]. Because of its large size, the genome provides nonfunctional binding opportunities that largely exceed the number of interaction events experimentally detected at CREs[5,6]. The nucleosomal organization and its dynamic regulation are the main mechanisms that orientate the binding of TFs to their proper targets on the genome.

The packaging of the genome into nucleosomes is a physical barrier to the binding of TFs and enzymes[2,7]. Nucleosome core particles contain two copies of each of the histones H2A, H2B, H3 and H4, around which 147 bp of DNA forms two gyres interacting with the surface of the histone core[8]. The rotational positioning of the motifs on the DNA helix impairs TF binding when the motif faces the core[9].

The nucleosomal barrier is dynamically regulated by a large family of enzymes called chromatin-remodeling factors (remodelers), which modulate nucleosome positioning and occupancy at CREs[10–13]. In particular, the BAF (BRG/BRM-associated factor) complexes (also known as mammalian SWI/SNF complexes), which bear tumor-suppressor properties[14], are essential for generating accessible DNA regions at enhancers[15–17]. It is generally assumed that the main product of BAF-mediated chromatin remodeling corresponds to DNA stripped of histones and that this histone-free DNA is the main genomic template bound by TFs

[1]Université Paris-Saclay, CEA, CNRS, Institute for Integrative Biology of the Cell (I2BC), Gif-sur-Yvette, France. [2]MRC Human Genetics Unit, Institute of Genetics and Cancer, University of Edinburgh, Western General Hospital, Edinburgh, UK. [3]Université Paris-Saclay, CEA, Centre National de Recherche en Génomique Humaine (CNRGH), Evry, France. [4]These authors contributed equally: Marina C. Nocente, Anida Mesihovic Karamitsos, Emilie Drouineau. e-mail: matthieu.gerard@i2bc.paris-saclay.fr

at CREs in vivo. However, some TFs can also interact with unstable, micrococcal nuclease (MNase)-sensitive nucleosomes (also called fragile nucleosomes) at CREs[18,19]. In yeast, these fragile nucleosomes correspond to partially unwrapped nucleosomes generated by the RSC (remodeling the structure of chromatin) complex[19], which is an ortholog of the mammalian BAF complexes.

In this study, we investigated the function of BRG1 (SMARCA4), the adenosine triphosphatase (ATPase) of SWI/SNF complexes in mouse embryonic stem cells (ES cells), using a method that distinguishes histone-free DNA from histone-containing genomic particles among the products of chromatin remodeling. In addition to generating histone-free DNA, we show that BRG1 produces hemisome-like subnucleosomal particles encompassing 50–80 bp of DNA at enhancer elements. We further demonstrate that this enhancer-specific activity of BRG1 occurs in the context of the canonical BAF (cBAF) complex. Moreover, we establish that these subnucleosomal particles are an in vivo binding substrate for OCT4 in mouse ES cells, independently of the presence of OCT4 motifs in the DNA. This interaction with the 50–80-bp subnucleosomes increases OCT4 occupancy and allows a striking expansion of the genomic interval occupied by OCT4 relative to the short interval it occupies on histone-free DNA. We also show that OCT4's potent function in chromatin opening at enhancers[15] is active precisely within the genomic interval delimited by the interaction between OCT4 and the 50–80-bp subnucleosomes. Together, these results reveal a molecular mechanism based on cBAF-generated subnucleosomal particles that expand OCT4's binding interval and project OCT4's function beyond the boundaries of its DNA motifs.

Results

Enhancers have a discrete nucleosomal and subnucleosomal organization

In mouse ES cells, enhancers are bound by a series of TFs that are required to maintain pluripotency and self-renewal, including OCT4, SOX2, NANOG, estrogen-related receptor-β (ESRRB) and Krüppel-like factor 4 (KLF4)[20]. The DNA-binding sites (BSs) for these TFs are located in relative proximity to each other yet without a constrained arrangement pattern[3,20–23]. Enhancers are also characterized by their hypersensitivity to DNase I, the presence of the Mediator complex and, for active enhancers, RNA polymerase II (Pol II) and TATA box-binding protein (TBP), as well as H3K27ac (refs. 24–27). We investigated nucleosomal organization at enhancers by MNase digestion of chromatin, followed by immunoprecipitation using antibodies against histone H3 and deep sequencing (MNase chromatin immunoprecipitation with DNA sequencing (ChIP-seq)) (Fig. 1a). We used an enhancer list corresponding to the genomic coordinates of DNase I hypersensitivity peaks coenriched for OCT4, SOX2, NANOG and Mediator[20,27,28](Methods). We show that *k*-means clustering based on the distribution patterns of canonical nucleosomes and subnucleosomal-size particles leads to identifying clusters of enhancers with different but highly related chromatin organizations (Extended Data Fig. 1a).

Using two-dimensional histograms (V-plots)[29], we detected in the central region of each cluster of enhancers the presence of short (50–120 bp) DNA fragments associated with histone H3, corresponding to subnucleosomal particles precisely positioned across the enhancers (Extended Data Fig. 1b). These subnucleosomal particles alternate in position with one or more full-size nucleosomes (that is, histone-associated 150–180-bp-long DNA fragments), depending on the distance that separates the two well-positioned nucleosomes, defined hereafter as nucleosomes −1 and +1, that flank the center of the enhancer (Fig. 1b and Extended Data Figs. 1b and 2). Enhancer clusters 1–3 that are representative of all subgroups differ from each other according to the distance between nucleosomes −1 and +1, with cluster 1 having the narrowest (340 bp) and cluster 3 having the widest (>480 bp) distance (Extended Data Fig. 1b).

In enhancer cluster 1 and related clusters 5, 8 and 12, a single centrally located nucleosome is present between nucleosomes −1 and +1 (Fig. 1b and Extended Data Fig. 1b). This central nucleosome is highly sensitive to MNase dosage, as it completely disappeared when mouse ES cells were incubated with a fourfold excess of MNase (Fig. 1c); we hereafter refer to this particle as a fragile nucleosome[18]. In contrast, the flanking nucleosomes −1 and +1 were only slightly affected by the high-dose MNase treatment, revealing their canonical nature. Enhancer cluster 2 and related clusters 4, 9 and 10 are characterized by the presence of fragile nucleosomes at two main positions instead of one in the central interval between nucleosomes −1 and +1 (Extended Data Fig. 2b,c). We observed that, in cluster 1, the single central fragile nucleosome is symmetrically flanked on each side of its dyad axis by a subnucleosomal particle protecting from MNase digestion of a minimum DNA length of 54 bp, as assessed by the length of the DNA fragments present at the vertex of the V-shaped signal (Fig. 1b). In cluster 2, each of the two fragile nucleosomes of the central interval is flanked by subnucleosomal particles in a pattern similar to cluster 1 (Extended Data Fig. 2b). Enhancer cluster 3 shows a variation of these patterns, with a wider central interval accommodating a larger number of subnucleosomal particles (Extended Data Fig. 1b). Thus, our analysis revealed that enhancers have a modular chromatin organization in which two positioned canonical nucleosomes delimit a central region containing a variable number of basic modules. Each basic module comprises one fragile nucleosome flanked on both sides of its dyad axis by two subnucleosomal particles occupying the same genomic interval, suggesting alternating chromatin configurations.

Enhancer subnucleosomal particles are enriched in TF-binding motifs

To investigate the relationship between this discrete chromatin architecture and TF motif distribution, we mapped the DNA-interacting motifs of the pluripotency-associated TFs OCT4, SOX2, NANOG and KLF4 (ref. 20). The genomic interval encompassing the central fragile nucleosome(s) and associated subnucleosomal particles corresponds precisely to the area in which TF motifs are enriched (Extended Data Fig. 2m–p). We then examined the distribution of TFs and epigenetic features that contribute to enhancer functions (Fig. 1g–l and Extended Data Fig. 2g–l). ChIP-seq analysis revealed that all tested TFs bind within the central interval of the enhancer in which subnucleosomal particles are interspersed with fragile nucleosome(s). Even TFs known to have pioneer functions, such as OCT4 and SOX2, were preferentially enriched on DNA fragments spanning 50 to 120 bp in length rather than the 150–180 bp typical of canonical nucleosomes (Fig. 1g,h and Extended Data Fig. 2g,h). The general TF TBP and Pol II were associated with 40–120-bp DNA fragments within the same central interval of the enhancer occupied by OCT4 and SOX2 (Fig. 1k,l and Extended Data Fig. 2j,l). In contrast to nucleosomes −1 and +1, the subnucleosomal particles were unexpectedly devoid of an H3K27ac signal (Fig. 1j and Extended Data Fig. 2k). The enhancers selected for this study lacked a CTCF ChIP-seq signal (Methods), excluding the possibility that this TF might organize nucleosome positioning.

BRG1 controls enhancer nucleosomal and subnucleosomal organization

We then investigated which factors control this enhancer-specific nucleosomal organization. ATP-dependent chromatin remodelers[10–13] are prime candidates, with BRG1 in particular forming accessible chromatin at enhancers[15–17]. Depletion of BRG1 using a short hairpin RNA (shRNA) resulted in striking alterations of both nucleosomal and subnucleosomal organization at enhancers. Subnucleosomal particles were almost completely absent at enhancers in cells depleted of BRG1 compared to control cells (Fig. 1e and Extended Data Fig. 2e). In addition, the positioning of canonical nucleosomes was severely

https://doi.org/10.1038/s41594-024-01344-0

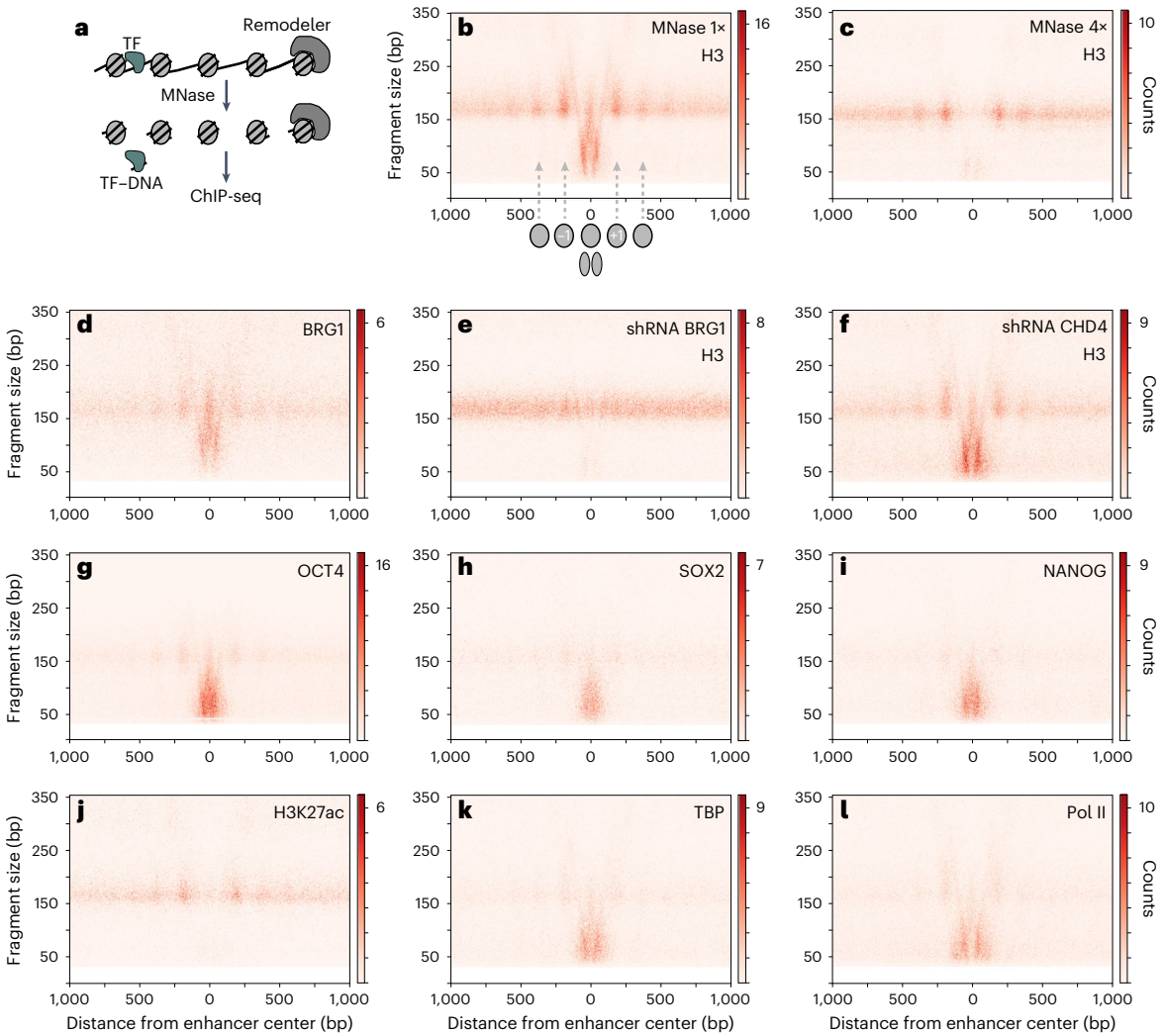

Fig. 1 | BRG1 controls nucleosomal and subnucleosomal organization at enhancers. a, MNase-digested chromatin was prepared from mouse ES cells for ChIP-seq experiments. **b**,**c**, V-plots of histone H3 ChIP-seq fragments spanning ±1,000 bp from the cluster 1 enhancer center, using either the standard MNase dose (**b**) or a fourfold excess (**c**). Red dots indicate the genomic position of the midpoint of each immunoprecipitated DNA fragment on the *x* axis and its length in bp on the *y* axis. The color scale corresponds to the number of DNA fragments. The schematic illustration in **b** indicates the positions of nucleosomes −1 and +1, which flank either the fragile nucleosome or the subnucleosomal particles that occupy the central region. **d**, V-plot of BRG1 ChIP-seq. **e**,**f**, V-plots of histone H3 ChIP-seq in mouse ES cells depleted of BRG1 (**e**) or CHD4 (**f**), using shRNAs. **g**–**l**, V-plots of OCT4 (**g**), SOX2 (**h**), NANOG (**i**), H3K27ac (**j**), TBP (**k**) and Pol II (**l**) ChIP-seq. The standard MNase dose was used in all panels except in **c**. Two biological replicates were performed for each ChIP-seq experiment.

altered, resulting in their apparently random redistribution across the enhancer. We detected identical alterations with antibodies against histone H3 and H2B and this was also the case when we used a second shRNA targeting a different region of BRG1 mRNA (Extended Data Fig. 3a). These perturbations of chromatin organization at enhancers were specific to BRG1 loss of function, as shRNA-mediated depletion of chromatin remodeler chromodomain-helicase-DNA-binding protein 4 (CHD4) did not prevent the generation of subnucleosomal particles or the positioning of canonical nucleosomes (Fig. 1f and Extended Data Fig. 2f). Depletion of BRG1 using the auxin-induced degron (AID) system[30] resulted in similar defects in chromatin organization even after a short period of auxin treatment, showing that impairment of subnucleosomal organization is not a secondary effect of BRG1 loss of function (Extended Data Fig. 3a,b).

The alterations in chromatin organization caused by BRG1 depletion are compatible with a scenario in which BRG1 binds the central fragile nucleosome to convert it into smaller particles, such as hexasomes ($(H3–H4)_2$ and H2A–H2B) or hemisomes (half-nucleosomes) containing one copy of each of the histones H3, H4, H2A and H2B (refs. 31–34). In support of this hypothesis, we detected BRG1 enriched both at the centrally located fragile nucleosome(s) and at subnucleosomal particles (Fig. 1d and Extended Data Fig. 2d). To analyze the nature of the subnucleosomal particles, we used centrifugation through a sucrose gradient in which the particles sediment as a function of their molecular mass and shape[35] (Fig. 2a). We loaded the MNase-digested mouse ES cell chromatin onto a 10–30% sucrose gradient. After centrifugation, individual fractions were collected and analyzed by agarose gel electrophoresis, revealing genomic DNA fragments ranging from 30 to 120 bp, which migrated slower than canonical nucleosomes through the gradient (Fig. 2b). To identify which fractions contained subnucleosomal particles, we performed ChIP-seq experiments with an antibody against histone H3 (Fig. 2c). At the top of the gradient, the DNA fragments in fractions 3–4 were not efficiently immunoprecipitated, suggesting that they mostly corresponded to histone-free DNA fragments. In contrast, the 50–80-bp-long particles collected in gradient fractions 5 and 6, which had a low sedimentation rate, were associated with histone H3 at enhancers and were, thus, genuine subnucleosomal particles (Fig. 2c).

https://doi.org/10.1038/s41594-024-01344-0

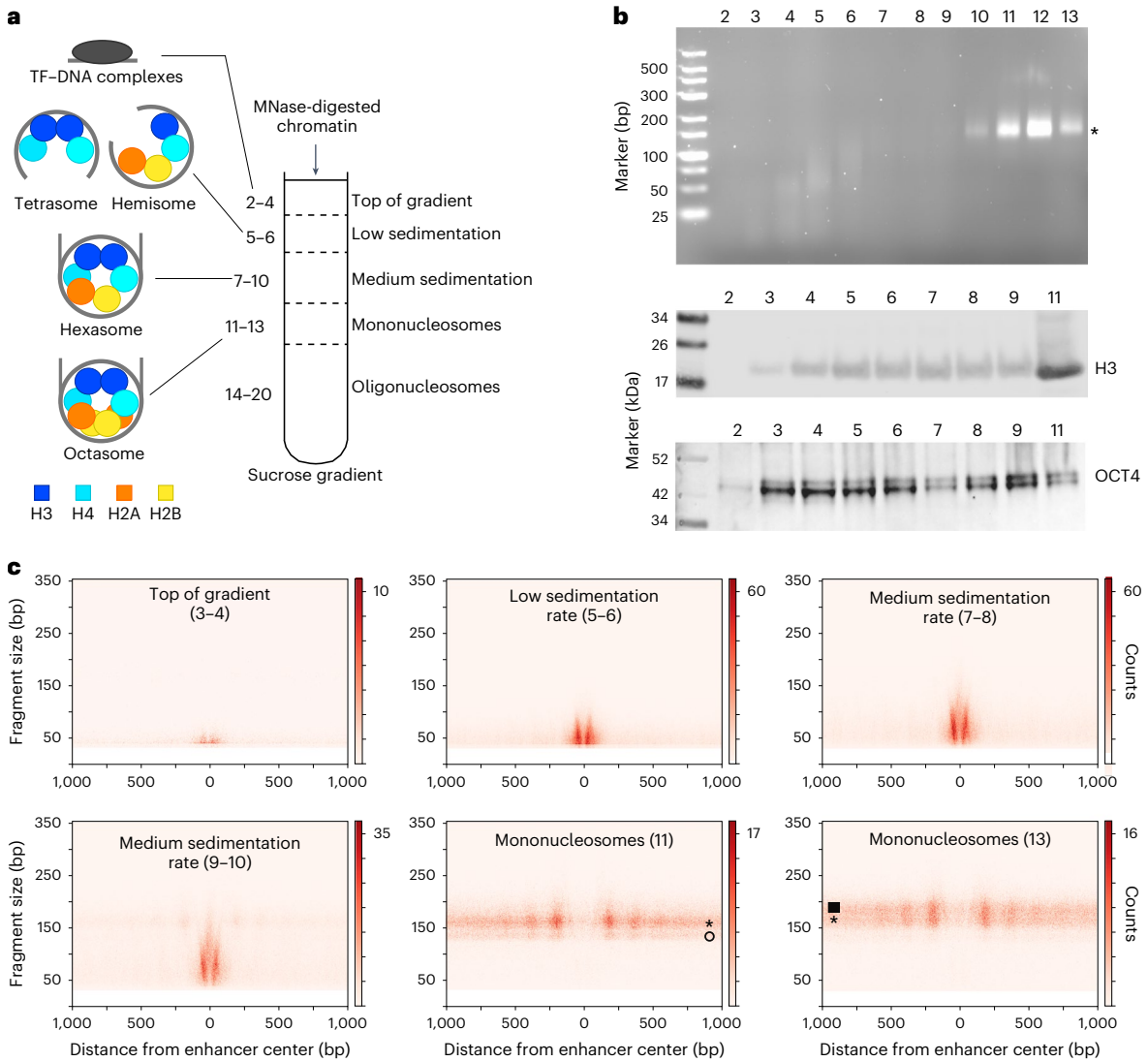

Fig. 2 | Identification of low-sedimentation-rate subnucleosomal particles associated with 50–80 bp of DNA at enhancers. a, MNase-digested chromatin was centrifugated through a 10–30% sucrose gradient to separate canonical nucleosomes from putative subnucleosomal particles and TF–DNA complexes. **b**, Top, the DNA fragments of each fraction were analyzed by electrophoresis in a 4% agarose gel. Middle and bottom, the distribution of histone H3 and OCT4 was revealed by western blot. The figure shows one representative example of two replicate experiments. The asterisk indicates the DNA fragments corresponding to mononucleosomes. **c**, V-plots of histone H3 ChIP-seq experiments performed with sucrose gradient fractions as the input, spanning ±1,000 bp from the cluster 1 enhancer center. The fractions or pools used for ChIP are indicated on each panel. The open circle and black square point to potential partially unwrapped nucleosomes and chromatosomes, respectively.

A particle containing 50–80 bp of DNA associated with the core histones

To define the histone content of the low-sedimentation-rate 50–80-bp subnucleosomal particles (hereafter called 50–80-bp subnucleosomes), we performed ChIP-seq experiments with antibodies against the remaining three histones (H4, H2A and H2B). These antibodies efficiently immunoprecipitated the 50–80-bp subnucleosomes but not the DNA fragments from the top of the gradient (Fig. 3). This result excludes the possibility that the 50–80-bp subnucleosomes might correspond to tetrasomes composed of two dimers of histones H3 and H4, which are nucleosome assembly intermediates detected during DNA replication[36]. The presence of the four core histones suggests that these particles correspond to either hexasomes or hemisomes[31,33,34,37]. However, the DNA length (50–80 bp) protected from MNase digestion is incompatible with the ~90-bp DNA associated with hexasomes[38]. The protection from MNase cleavage conferred by hexasomes yielded DNA fragments ranging from 90 to 130 bp (ref. 31). In our experimental setting, subnucleosomal particles associated with 90–130-bp DNA fragments had a medium sedimentation rate (fractions 7–8 and 9–10), suggesting a histone composition different from the 50–80-bp subnucleosomes that sedimented in fractions 5 and 6 (Fig. 2). A comprehensive examination of individual single-module enhancers from clusters 1 and 8 revealed that 50–80-bp subnucleosomes are systematically associated in pairs and separated by a DNA linker having a median length of 29 bp (Fig. 4g, Extended Data Fig. 4 and Methods). This unique genomic positioning of the 50–80-bp subnucleosomes, their histone content and their size properties suggest that they correspond to split nucleosomes that are composed of two hemisomes connected by a linker DNA fragment of variable length.

To test the distribution of these subnucleosomal particles on individual chromatin molecules, we used a single-molecule footprinting (SMF) dataset[3]. Examination of the footprints at two representative enhancers revealed that the genomic positions occupied by 50–80-bp subnucleosomes are frequently protected against DNA methylation

https://doi.org/10.1038/s41594-024-01344-0

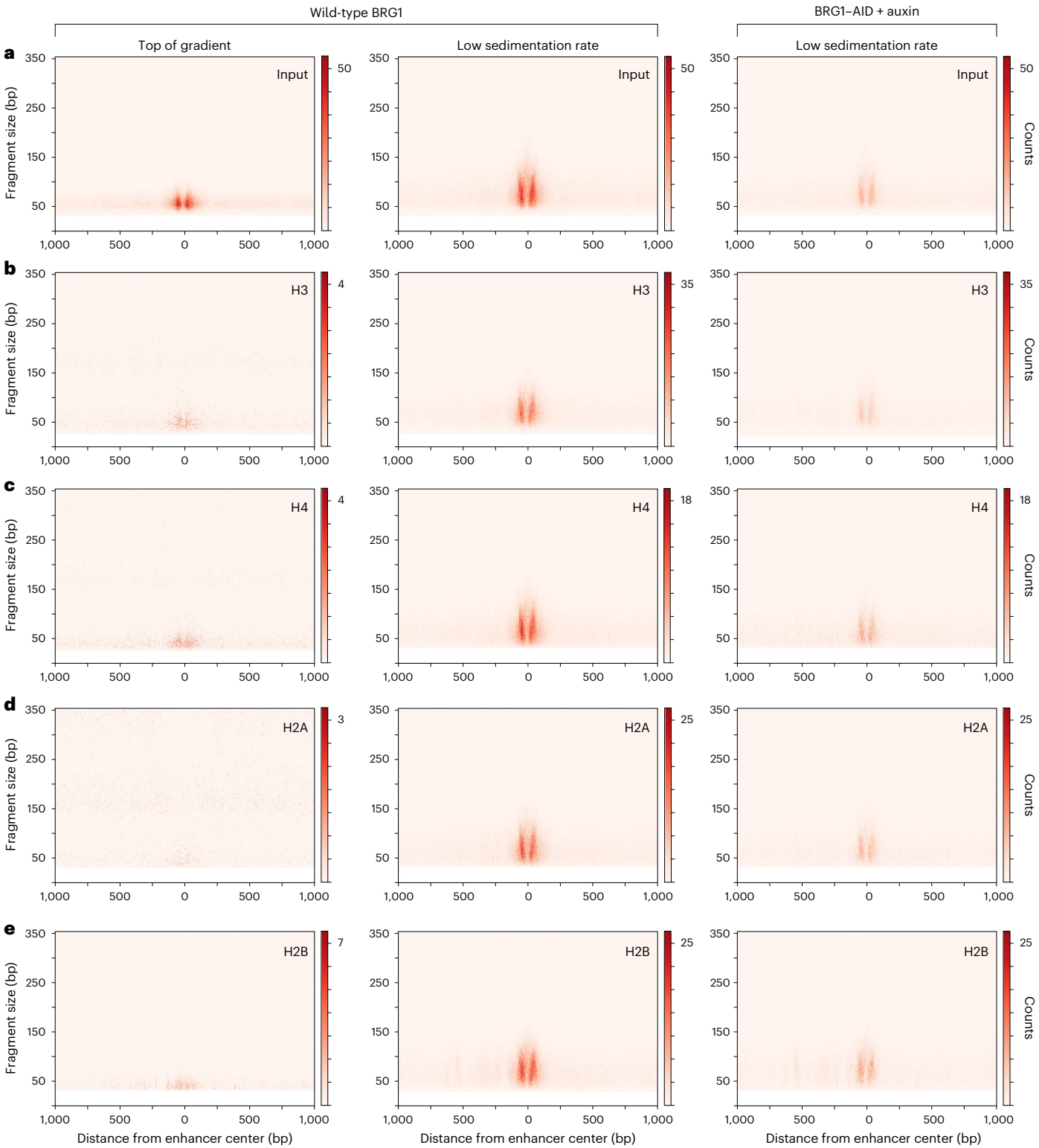

Fig. 3 | Histone composition of 50–80-bp subnucleosomes. Chromatin, prepared from mouse ES cells expressing WT BRG1 or from cells depleted of BRG1 using the AID system, was centrifugated through a sucrose gradient as in Fig. 2. **a**, V-plots of the DNA fragments that sedimented at the top of the gradient (pool of fractions 2–4) or of the DNA fragments present in low-sedimentation-rate fractions (pool of fractions 5 and 6), spanning ±1,000 bp from the cluster 1 enhancer center. Signals shown in the two right panels were adjusted according to the total number of fragments sequenced in each dataset. **b**–**e**, V-plots of histone H3 (**b**), H4 (**c**), H2A (**d**) and H2B (**e**) ChIP-seq experiments performed with the pools of sucrose gradient fractions indicated in **a** as the input. For each histone, the signals of the ChIP-seq experiments performed with subnucleosomal particles from mouse ES cells expressing WT BRG1 and from BRG1-depleted cells were adjusted according to the total number of DNA fragments in each dataset. Two biological replicates were performed for each ChIP-seq experiment.

https://doi.org/10.1038/s41594-024-01344-0

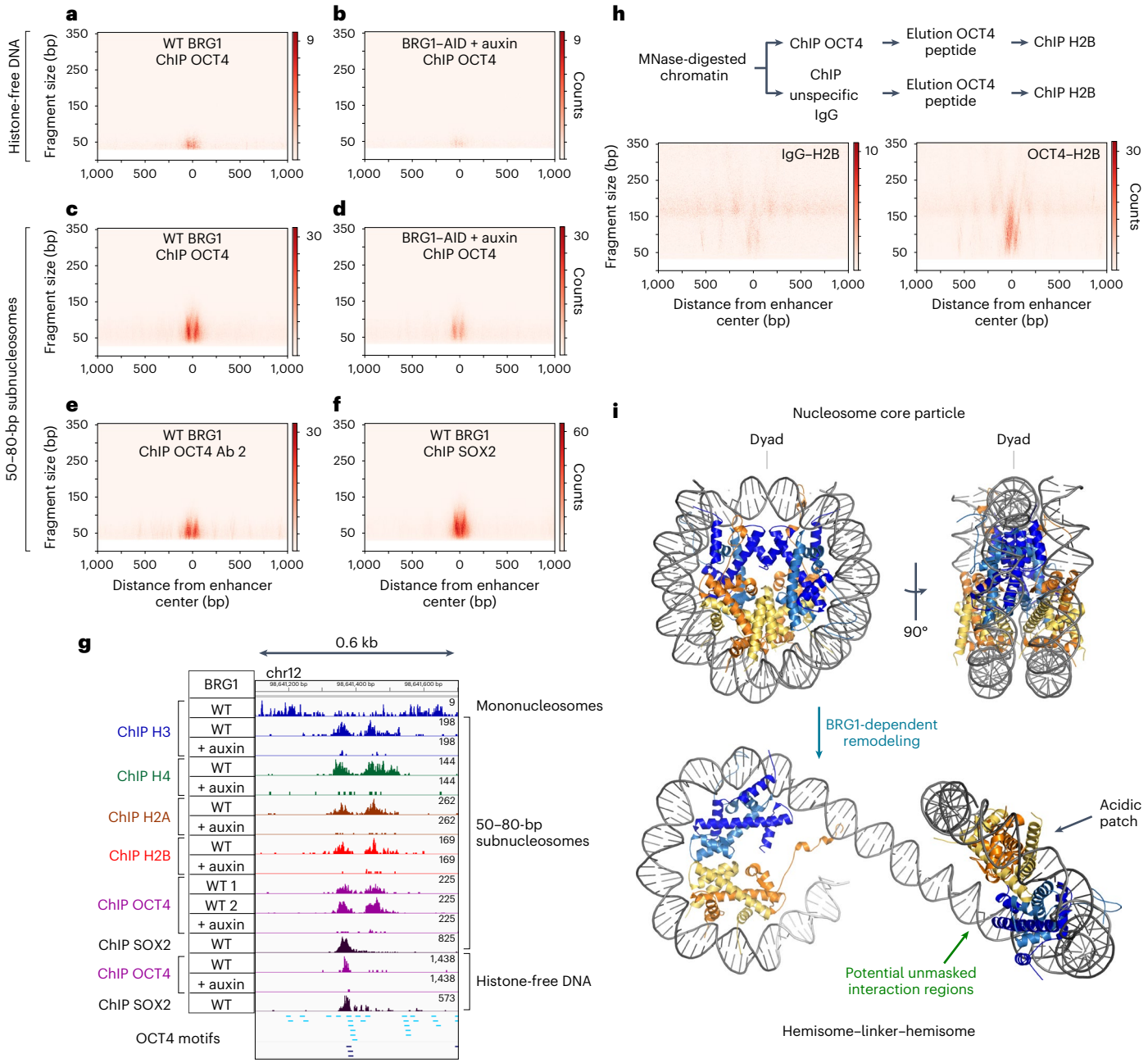

Fig. 4 | OCT4 binds to 50–80-bp subnucleosomes at enhancers. a–**f**, V-plots of ChIP-seq fragments spanning ±1,000 bp from the cluster 1 enhancer center. Chromatin, prepared from WT BRG1 or BRG1-depleted mouse ES cells (BRG1-AID + auxin), was centrifugated through a sucrose gradient as in Fig. 2. OCT4 (**a**–**e**) and SOX2 (**f**) ChIP experiments were performed using the chromatin from the top of the gradient (**a**,**b**, pool of fractions 2–4) or low-sedimentation-rate fractions (**c**–**f**, pool of fractions 5 and 6). Two distinct OCT4 antibodies were used in **a**–**d** and **e**. **g**, Density graphs showing the distribution of ChIP DNA fragment centers at a representative example of a cluster 1 enhancer. The top lane shows the positions of canonical nucleosomes detected by histone H3 ChIP-seq of sucrose gradient fractions 11 and 13. The next eight lanes show the distribution of 50–80-bp subnucleosomes, revealed by histone H3, H4, H2A and H2B ChIP-seq of sucrose gradient fractions 5 and 6. The subsequent lanes show the OCT4 or SOX2 ChIP-seq signal on 50–80-bp subnucleosomes or histone-free DNA from the top gradient fractions. Experiments were performed with chromatin from WT or BRG1-depleted mouse ES cells + auxin. Two antibodies against OCT4 were used in lanes WT 1 and WT 2. OCT4 consensus motifs with high ($P = 0.001$) and low ($P = 0.01$) confidence are indicated in black and blue, respectively. **h**, Sequential ChIP-seq experiments. Chromatin from WT mouse ES cells was first immunoprecipitated with an OCT4 antibody or an unspecific IgG. Elution was performed by peptide competition and each eluted fraction was subjected to a second round of immunoprecipitation with an antibody against H2B. The sequential OCT4-H2B ChIP-seq (right) and the unspecific IgG control (left) experiments. Two biological replicates were performed for each ChIP-seq experiment. **i**, Model proposing that BRG1 splits nucleosomes at enhancers to generate hemisome–linker–hemisome entities, which might display new interaction regions for TFs. The two hemisomes are separated by a DNA linker with a median length of 29 bp. Histones H3 and H4 are shown in two shades of blue, while histones H2A and H2B are in yellow and orange, respectively.

(Extended Data Fig. 5 and Methods). Importantly, 3–15% of the molecules displayed footprints compatible with the presence of two hemisomes, revealing that the split nucleosome can be detected onto single molecules (Extended Data Fig. 5). However, in a high percentage (~50%) of the molecules, the footprint analysis revealed a single hemisome co-occurring with a region of accessible DNA at the genomic position

of the expected second hemisome (Extended Data Fig. 5). This indicates that the single-hemisome configuration is more frequent than the paired hemisomes at the enhancers analyzed. Furthermore, 7–10% of the molecules had footprints indicative of a full-length nucleosome covering the genomic interval where both hemisomes are located. We speculate that they correspond to the fragile nucleosome detected by MNase ChIP-seq, although it is not possible to distinguish fragile and canonical nucleosomes by SMF. Lastly, 27–38% of the molecules did not display any footprint covering the genomic positions of the hemisomes, indicating accessible, histone-free DNA. These observations show that the chromatin-remodeling events controlled by BRG1 at enhancers can have at least three distinct outputs: the split nucleosome, one single hemisome adjacent to a segment of histone-free DNA (the most frequent output) and a region of fully accessible histone-free DNA (Extended Data Fig. 5c).

A subset of enhancers is organized in clusters called superenhancers, which contribute to the control of cell phenotype[28,39]. The nucleosomal and subnucleosomal organization of superenhancers, as well as their dependency on BRG1 activity, was identical to that of regular enhancers (Extended Data Fig. 4h).

We next used transmission electron microscopy (EM) to analyze the size of 50–80-bp subnucleosomes compared to mononucleosomes purified from sucrose gradients and nucleosomes assembled in vitro onto an array of 601 DNA fragments[40] (Extended Data Fig. 6d,e). Canonical nucleosomes have a front view diameter of 10–13 nm and a width of about 6 nm, the latter of which is defined by the sum of the two DNA gyres wrapped around the histone octamer[41]. If the particles generated at enhancers are hemisomes, they should retain a 10–13-nm diameter but have a width reduced to 3 nm, which corresponds to the size of a single DNA gyre. EM analysis should then reveal particles having an apparent size either smaller than or equal to that of canonical nucleosomes, depending on their orientation on the grid. Random selection and size measurement of both particles from gradient fractions 5 and 6 revealed a large proportion of small-sized particles (<10 nm), which were absent in control nucleosome-containing fractions (Extended Data Fig. 6d,e). We confirmed that the 50–80-bp subnucleosomes had a molecular size markedly inferior to that of mononucleosomes using size-exclusion chromatography (Extended Data Fig. 6a–c). These size analysis experiments, thus, further support the hypothesis that enhancer 50–80-bp subnucleosomes correspond to hemisomes.

We then considered whether the 50–80-bp subnucleosomes are specific to mouse ES cells or whether they are also produced in other mammalian cells. We used the histone MNase ChIP-seq approach combined with sucrose gradient sedimentation experiments to probe chromatin organization in a human melanoma cell line. We isolated clusters of putative enhancers enriched for 50–80-bp subnucleosomes, which have a chromatin organization very similar to that of mouse ES cell enhancer clusters (Extended Data Fig. 7). This analysis shows that the modular organization of nucleosomes and subnucleosomes we described at mouse ES cell enhancers is conserved in human cells.

The 50–80-bp subnucleosomes are produced at all categories of CREs

We used our high-coverage histone MNase ChIP-seq datasets to explore subnucleosomal organization at CTCF sites and promoters. This analysis revealed the presence of 50–80-bp subnucleosomes having distribution patterns distinct from that of enhancers (Extended Data Fig. 8). At CTCF sites, a single 50–80-bp subnucleosome was detected in the central region coinciding with the location of the CTCF motif (Extended Data Fig. 8a,b). Promoters contain a single 50–80-bp subnucleosome coinciding in genomic position with nucleosome −1, located upstream of the transcription start site (TSS) (Extended Data Fig. 8c,d). This nucleosome −1 was hypersensitive to an excess of MNase (Extended Data Fig. 8c), a hallmark of fragile nucleosomes. These observations suggest that, at promoters, chromatin-remodeling events target nucleosome −1 to convert it into a 50–80-bp subnucleosome occupying the same genomic position. In support of this hypothesis, we previously showed that a large variety of chromatin remodelers bind nucleosome −1 in mouse ES cells[13]. We detected a 30-bp protection against MNase digestion (footprint) within the 50–80-bp subnucleosome of promoters, which matches precisely the 30 bp of DNA upstream of the TSS. This footprint reveals that the binding on the subnucleosome of proteins is potentially involved in preinitiation complex formation (Extended Data Fig. 8e).

cBAF generates the 50–80-bp subnucleosomal particles at enhancers

The chromatin perturbation pattern caused by BRG1 depletion (Fig. 1) suggests that this remodeler might generate the 50–80-bp subnucleosomes at enhancers. We tested this possibility by repeating the sucrose gradient sedimentation experiments, using chromatin prepared from BRG1-depleted or control cells. ChIP-seq experiments with antibodies against histones H3, H4, H2A and H2B revealed that BRG1 depletion results in a strong reduction in the number of 50–80-bp subnucleosomes, thus indicating that their production at enhancers is indeed dependent on BRG1 (Fig. 3). BRG1 depletion also reduced the number of medium-sedimentation-rate 90–130-bp subnucleosomal particles, showing that BRG1 activity was required for the generation of all classes of subnucleosomal particles detected at enhancers in this study (Extended Data Fig. 9c–f). In contrast, BRG1 depletion did not alter the distribution or number of subnucleosomes at CTCF sites, showing that they were generated independently of BAF complexes at these loci (Extended Data Fig. 8a,b). This result agrees with a previous study demonstrating that the chromatin remodeler SNF2H, but not BRG1, assists CTCF binding to its DNA motifs[42]. At promoters, BRG1 loss of function did not affect nucleosome positioning but the number of 50–80-bp subnucleosomes was slightly decreased, suggesting a minor function of BRG1 at this category of CRE (Extended Data Fig. 8c,d).

We also tested whether BRG1 is involved in producing histone-free DNA fragments at enhancers. Deep sequencing of the DNA prepared from the top sucrose gradient fractions revealed that BRG1 depletion resulted in a pronounced reduction in these DNA fragments at enhancers but not at CTCF sites (Extended Data Fig. 9a,b). DNA fragments containing motifs for OCT4, SOX2, ESRRB, KLF4 and NANOG were markedly depleted in the top gradient fractions prepared from BRG1-depleted cells (Extended Data Fig. 9g), demonstrating that BRG1 is required for the efficient production of histone-free, accessible DNA for these TFs at enhancers. BRG1 is, thus, essential at enhancers for producing two main chromatin-remodeling products: histone-free DNA and 50–80-bp subnucleosomal particles.

BRG1 belongs to three distinct BAF complexes in mouse ES cells: cBAF, pBAF (polybromo-associated) and ncBAF (noncanonical)[43,44]. We wondered which of these three complexes generates the 50–80-bp subnucleosomes at enhancers. We produced a series of mouse ES cell lines in which the genes encoding distinct BAF complex subunits were fused with a sequence encoding the auxin degron. We obtained homozygous cell lines for the genes encoding SMARCB1, which is a component of both cBAF and pBAF (but not ncBAF), and the genes encoding ARID1A (cBAF-specific), BRD7 (pBAF-specific), PBRM1 (pBAF-specific) and BRD9 (ncBAF-specific) (Methods and Extended Data Fig. 3c). Depletion of SMARCB1 and ARID1A severely affected the production of 50–80-bp subnucleosomes at enhancers (Fig. 5). In contrast, depletion of BRD7, PBRM1 or BRD9 had no detectable effect (Fig. 5). We concluded that the cBAF complex is specifically responsible for the generation of enhancer subnucleosomal particles.

The 50–80-bp subnucleosomes interact with OCT4 independently of its DNA motif

We observed that, in the OCT4, SOX2 and NANOG ChIP-seq experiments (Fig. 1g–i), the sizes and position on the genome of the

https://doi.org/10.1038/s41594-024-01344-0

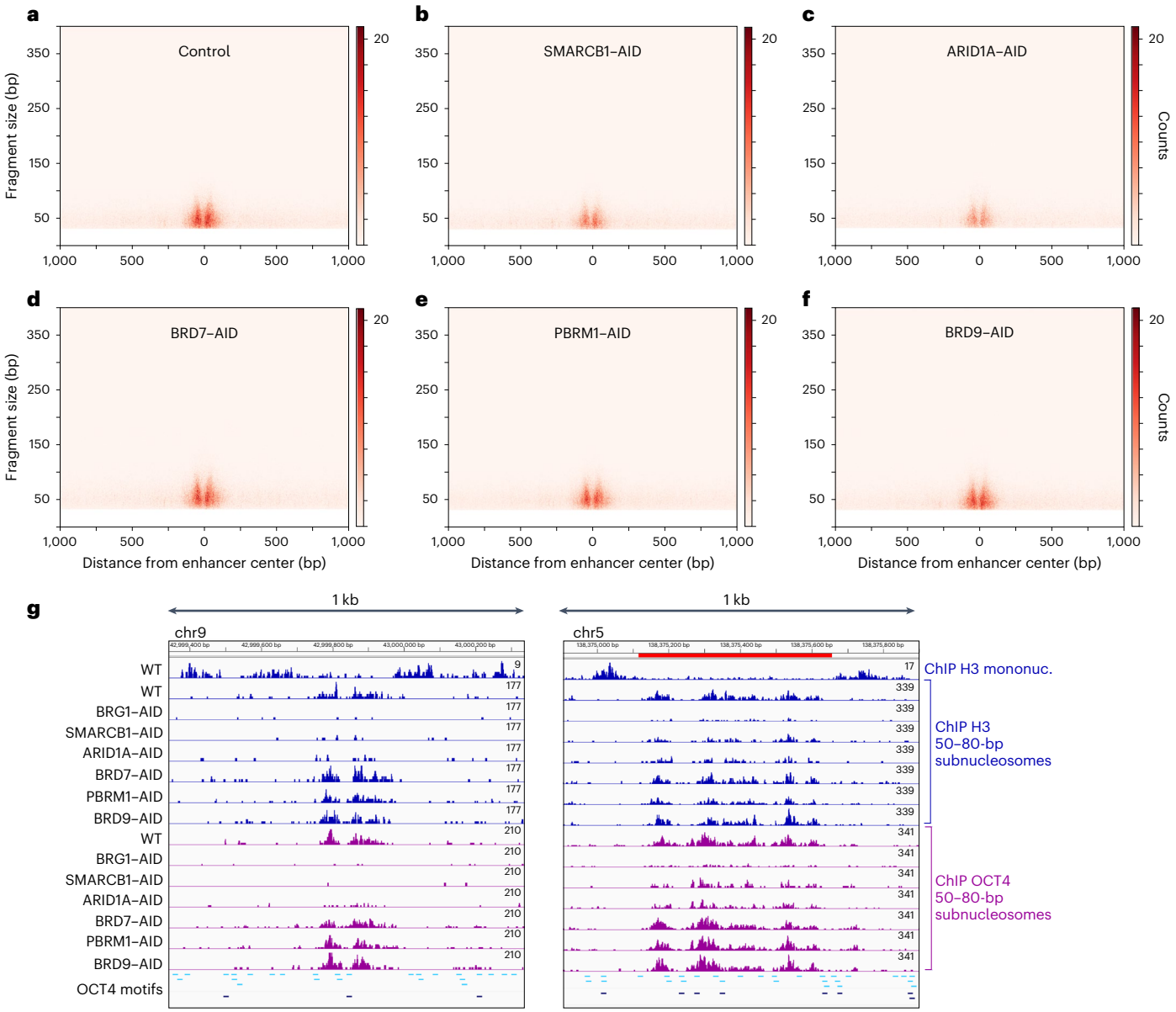

Fig. 5 | The cBAF complex controls the formation of 50–80-bp subnucleosomes at enhancers. a–**f**, V-plots of ChIP-seq fragments spanning ±1,000 bp from the cluster 1 enhancer center. Chromatin, prepared from mouse ES cells expressing WT BAF complexes (control, **a**) or from cells depleted of SMARCB1 (**b**), ARID1A (**c**), BRD7 (**d**), PBRM1 (**e**) and BRD9 (**f**), was centrifugated through a sucrose gradient as in Fig. 2. Histone H3 ChIP experiments were performed using chromatin fragments present in low-sedimentation-rate fractions. **g**, Density graphs showing the distribution of ChIP DNA fragment centers at representative examples of enhancers. The top lane shows the positions of canonical nucleosomes detected by histone H3 ChIP-seq of sucrose gradient fractions 11 and 13. The next seven lanes show the distribution of 50–80-bp subnucleosomes, revealed by histone H3 ChIP-seq of sucrose gradient fractions 5 and 6, in cells depleted of distinct BAF subunits, as indicated. The subsequent lanes show the OCT4 ChIP-seq signal on 50–80-bp subnucleosomes in the same contexts as above. Two biological replicates were performed for each ChIP-seq experiment. OCT4 consensus binding motifs with high ($P = 0.001$) and low ($P = 0.01$) confidence are indicated in black and blue, respectively. mononuc., mononucleosomes.

immunoprecipitated DNA fragments were similar to those of the 50–80-bp subnucleosomes (Fig. 3). This specific pattern, reproduced with three distinct antibodies against OCT4 (Figs. 1 and 4 and Methods), suggests that 50–80-bp subnucleosomes might represent a previously undetected binding substrate for TFs in vivo. To test whether OCT4 is genuinely bound to histone-associated subnucleosomal particles, we carried out sequential ChIP experiments using antibodies against OCT4 in the first step. Elution of OCT4-bound chromatin was performed using a competitor peptide and the eluted chromatin was used in a second step of ChIP with antibodies against histone H2B. Deep sequencing of the DNA associated with both OCT4 and histone H2B revealed DNA fragments of subnucleosomal size, thus demonstrating that OCT4 is bound to subnucleosomal particles in vivo (Fig. 4h). Analysis of OCT4-immunopurified 50–80-bp subnucleosomes by EM revealed particle sizes compatible with the hypothesis that OCT4 interacts in vivo with hemisomes (Extended Data Fig. 6d,e).

We next compared how OCT4 binds to 50–80-bp subnucleosomes and histone-free DNA present in the top gradient fractions. OCT4 antibodies successfully immunoprecipitated both histone-free DNA fragments and 50–80-bp subnucleosomes (Fig. 4a,c). However, OCT4 enrichment profiles were different at these two distinct genomic templates. At histone-free DNA fragments, OCT4 peaks coincided with OCT4 consensus motifs, whereas, in 50–80-bp subnucleosomes, OCT4 enrichment coincided with histones (Fig. 4g and Extended Data Fig. 4).

We verified the specificity of this unexpected OCT4 ChIP-seq enrichment profile on 50–80-bp subnucleosomes with a second antibody against OCT4 and by performing the elution step of the ChIP experiment using a competitor peptide (Fig. 4e and Extended Data Fig. 4). Because OCT4 often binds to its sites in association with SOX2 (refs. 45,46), we also investigated SOX2 ChIP-seq enrichment profiles. Similar to OCT4, SOX2 was enriched at enhancers onto both histone-free DNA and 50–80-bp subnucleosomes (Fig. 4f,g and Extended Data Fig. 4). However, the binding profile of SOX2 was different from that of OCT4. We observed the coincidence between OCT4 and histone enrichment even when OCT4-binding motifs were absent from the DNA wrapped around the subnucleosome (Extended Data Fig. 10 and Methods). In contrast, the SOX2 enrichment profile on 50–80-bp subnucleosomes systematically matched its profile on histone-free DNA and was less correlated to histone enrichment (Fig. 4g and Extended Data Fig. 4). This result suggests that, for efficiently interacting with the subnucleosomes in vivo, SOX2 is more dependent than OCT4 on the presence of its consensus motif on the DNA.

It remained possible that partial OCT4 motifs could be enriched on subnucleosomes and compensate for the absence of full motifs, in a manner reminiscent of the interaction between OCT4 and the nucleosomes[47,48]. However, examination of the distribution of partial motifs did not reveal their enrichment on subnucleosomes, invalidating this hypothesis (Extended Data Fig. 10g and Methods). These observations suggest that OCT4 interactions with 50–80-bp subnucleosomes involve contacts with the histone component in addition to those with its DNA-binding motif. An intriguing possibility is that the internal histone surface of the split nucleosome, which is inaccessible in canonical nucleosomes, provides an interaction domain for OCT4 and potentially for other TFs and chromatin-binding proteins in a manner reminiscent of the acidic patch of the nucleosome, which is present on the other side (Fig. 4i).

We designed a pull-down assay to investigate whether we could recapitulate the interaction between OCT4 and the 50–80-bp subnucleosome in vitro. Using mouse ES cells expressing a tagged version of histone H3.3, we purified native subnucleosomes from unfixed chromatin by immunoaffinity followed by centrifugation through a sucrose gradient (Methods). Deep sequencing of the purified native subnucleosomes revealed that their distribution across the genome is identical to that of formaldehyde-fixed particles (Fig. 6 and Supplementary Fig. 1). Importantly, the unfixed 50–80-bp subnucleosomes from enhancers could still be detected after 72 h in solution, revealing that they are stable particles. We incubated these purified native subnucleosomes with a tagged OCT4 protein immobilized onto agarose beads (Fig. 6a). After a series of washes, OCT4 was released by tobacco etch virus (TEV) protease digestion and we extracted the DNA associated with the eluted OCT4–subnucleosome complexes. Deep sequencing of this DNA revealed the genomic coordinates of the 50–80-bp subnucleosomes that established a stable interaction with OCT4 in vitro (Fig. 6b–g, Supplementary Fig. 1 and Methods). These coordinates globally match the distribution of the subnucleosomes bound by OCT4 in vivo established by MNase ChIP-seq (Fig. 6f,g and Supplementary Fig. 1). However, not all subnucleosome positions were equally represented at enhancers in the pull-down datasets (Fig. 6f,g and Supplementary Fig. 1), suggesting that, at some genomic positions, the OCT4–subnucleosome complexes were not stable enough to survive the washes of the protocol. Another possibility is that, in the context of a subset of loci, the interaction between OCT4 and subnucleosomes may involve additional nuclear proteins not present in the pull-down assay.

The 50–80-bp subnucleosomes expand the genomic interval bound by OCT4

To address the function of the interaction between OCT4 and 50–80-bp subnucleosomes, we first compared the size of the genomic intervals bound by OCT4 at either 50–80-bp subnucleosomes or histone-free DNA. This comparison revealed an up to sevenfold size increase for 50–80-bp subnucleosomes relative to histone-free DNA (Fig. 7a–d). Thus, the function of the interaction between OCT4 and 50–80-bp subnucleosomes is to dramatically increase the size of the genomic interval bound by OCT4 at enhancers. A second potential function of the 50–80-bp subnucleosomes could be to augment the OCT4 occupancy of enhancers. A previous SMF analysis revealed a low OCT4 occupancy on nucleosome-free DNA molecules bearing its consensus motif in mouse ES cells[3]. In agreement with this result, we observed that about 10% of the enhancers displayed a robust OCT4 ChIP-seq signal on histone-free DNA, whereas 90% had a low or undetectable signal (Fig. 4g, Extended Data Fig. 4, Supplementary Figs. 1 and 2 and Methods). In contrast, the OCT4 ChIP-seq signal on 50–80-bp subnucleosomes was high at most enhancers. These data show that the 50–80-bp subnucleosomes form a genomic template that augments the OCT4 occupancy of enhancers.

We next hypothesized that the remarkable increase in size of OCT4's binding interval on 50–80-bp subnucleosomes might project this TF's activity beyond the short interval that it binds onto histone-free DNA. Several studies reported that OCT4 carries a potent function in chromatin opening at enhancers[15,49]. We used the transposase-accessible chromatin with sequencing (ATAC-seq) datasets generated in these studies to test whether OCT4 performs its function in chromatin opening within the genomic interval that it occupies on either histone-free DNA or 50–80-bp subnucleosomes (Fig. 7e–h). We observed a striking coincidence of the interval spanned by the OCT4-dependent ATAC-seq signal and the interval occupied by OCT4 on 50–80-bp subnucleosomes (Fig. 7). In contrast, the interval occupied by OCT4 on histone-free DNA was much smaller than the extent of the OCT4-dependent ATAC-seq signal (Fig. 7). Thus, an essential role of the OCT4–subnucleosome interaction is to expand OCT4's binding interval to project its function in chromatin opening beyond the short region it occupies on histone-free DNA.

The critical requirement for OCT4 in chromatin opening suggests that this TF might be involved in the mechanism controlling the formation of subnucleosomes at enhancers. We tested this possibility by performing histone H3 MNase ChIP-seq experiments in OCT4-depleted cells. We found that OCT4 depletion severely altered the formation of the 50–80-bp subnucleosomes at enhancers (Fig. 7i and Supplementary Fig. 2). This result shows that OCT4 and cBAF are both critical actors in the mechanism generating the subnucleosomes.

Discussion

We identified a well-defined organization of open chromatin at enhancers in mouse ES cells, containing five essential components: (1) two canonical nucleosomes that flank and delimit the open chromatin region; (2) one or several fragile nucleosome(s); (3) hemisome-like subnucleosomal particles associated to 50–80-bp of DNA, containing the four core histones H2A, H2B, H3 and H4; (4) subnucleosomal particles associated to 81–110 bp of DNA, which could correspond to hexasomes; and (5) histone-free DNA fragments bound by TFs.

Our comprehensive MNase ChIP-seq analysis revealed that the 50–80-bp subnucleosomes are always detected as pairs where a median distance of 29 bp separates the two particles. The two particles of the pair are symmetrically distributed on each side of the dyad axis of a fragile nucleosome. SMF analysis confirmed the copresence of the two hemisomes at a subset of the chromatin molecules. Most molecules contained only one of the two hemisomes detected by MNase ChIP-seq, suggesting a dynamic equilibrium between the subnucleosome and histone-free DNA. We hypothesize that the remodeling event leading to the split nucleosome frequently results in asymmetric products in which only one subnucleosome remains while the second is further remodeled into histone-free DNA (Fig. 8). In this context, TFs can bind to both the subnucleosome and the histone-free DNA

https://doi.org/10.1038/s41594-024-01344-0

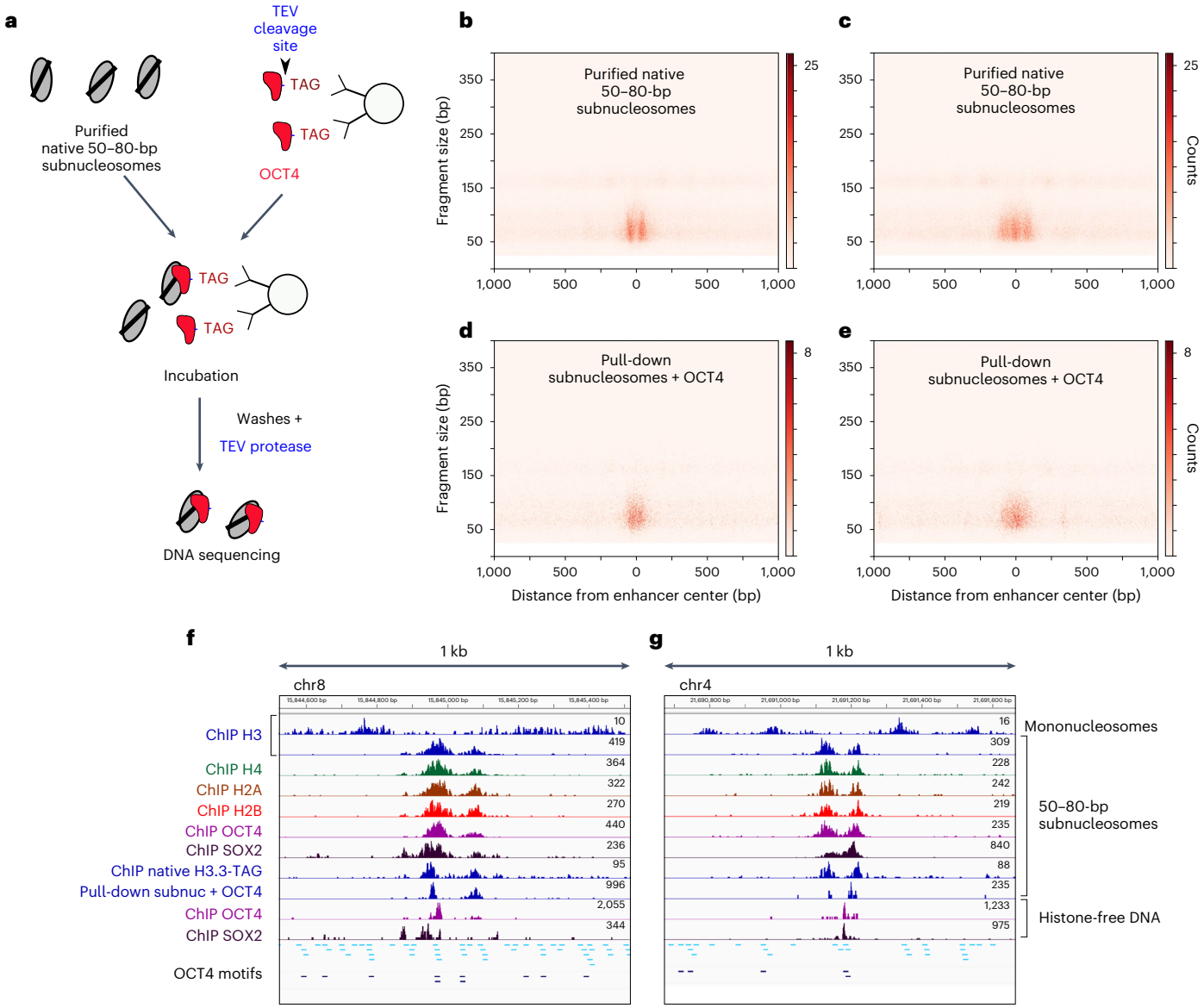

Fig. 6 | Native 50–80-bp subnucleosomes are stable and interact with OCT4 in vitro. a, Overview of the pull-down protocol used to test the interaction between OCT4 and 50–80-bp subnucleosomes in vitro. Unfixed chromatin prepared from mouse ES cells expressing a tagged histone H3.3 was immunopurified with anti-HA agarose beads and centrifugated through a sucrose gradient as in Fig. 2. The low-sedimentation fractions, containing the purified native 50–80-bp subnucleosomes (top left), were incubated with tagged OCT4 immobilized onto agarose beads (top right). After several washes, the potential OCT4–subnucleosome complexes were eluted by TEV protease cleavage. DNA was extracted from the eluted fraction and deep-sequenced. **b**–**e**, V-plots of DNA fragments from the purified subnucleosomes (**b**,**c**) and the TEV protease-eluted fractions (**d**,**e**), spanning ±1,000 bp from enhancer cluster 1 (**b**,**d**) and enhancer cluster 2 (**c**,**e**). DNA fragments from two biological replicates were merged. **f**,**g** Density graphs showing the distribution of ChIP DNA fragment centers at representative examples of enhancers. The top five lanes show the positions of canonical nucleosomes and subnucleosomes, as in Fig. 5. Lanes 6 and 7 show the OCT4 and SOX2 ChIP-seq signal on fixed 50–80-bp subnucleosomes. The next lane shows the distribution of native 50–80-bp subnucleosomes, revealed by ChIP of tagged histone H3.3. The subsequent lane indicates the native subnucleosomes that efficiently interacted with OCT4 in the pull-down assay. The last two lanes show the OCT4 and SOX2 ChIP-seq signal on histone-free DNA from the top gradient fractions. In **f**, the two OCT4 peaks detected in vivo on the subnucleosomes are recapitulated in the pull-down experiment. In **g**, only one of the two OCT4 peaks is robustly detected. subnuc, subnucleosomes.

moiety of the same molecule. Interactions between TFs and potential subnucleosomal particles were previously detected by MNase-SSP (single-stranded protocol)[50].

We demonstrated that BRG1 is required within the cBAF complex to generate the 50–80-bp subnucleosomes at enhancers, thus identifying a previously unknown in vivo function of this remodeler. Because BRG1 binds the centrally located fragile nucleosomes, these particles likely correspond to the substrate converted by BRG1 into subnucleosomes. By investigating how TFs interact with enhancers, we observed that their highest ChIP-seq enrichment signal coincided with the 50–80-bp subnucleosomes. This binding pattern suggested that the subnucleosomes might form a genuine genomic binding target for TFs at CREs. To test this hypothesis, we compared how the master TF OCT4 interacts with 50–80-bp subnucleosomes and histone-free DNA. As expected, we detected the binding of OCT4 to histone-free DNA at the level of its consensus DNA-binding motifs; however, we also found that OCT4, unlike SOX2, interacts with 50–80-bp subnucleosomes independently of an OCT4 motif within the particle. We showed that this absence of OCT4 motifs was not compensated for by the presence of degenerated motifs or by half-sites that OCT4 can target onto canonical nucleosomes[47,48].

https://doi.org/10.1038/s41594-024-01344-0

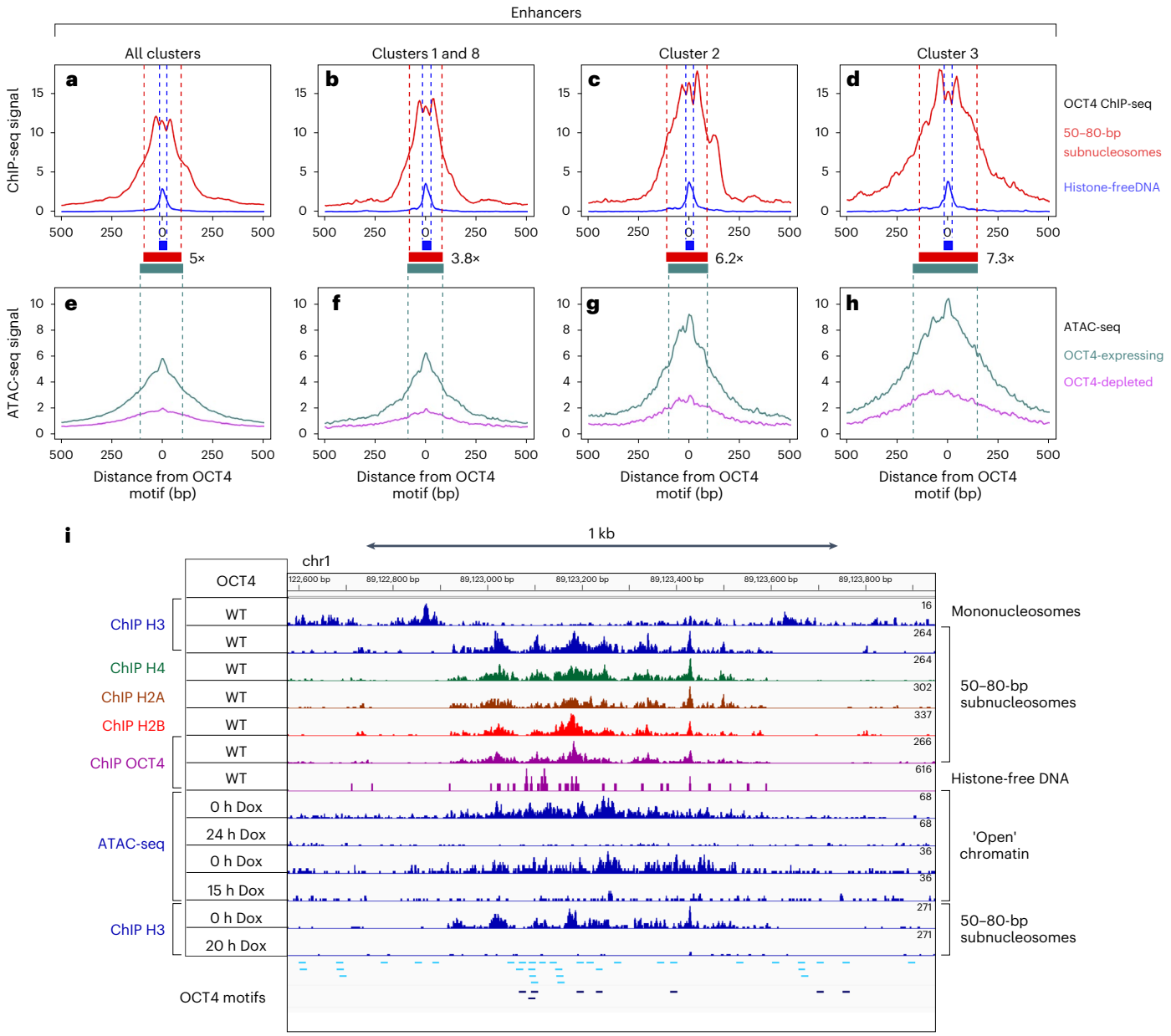

Fig. 7 | The 50–80-bp subnucleosomes expand OCT4's binding interval and function in chromatin opening at enhancers. a–**d**, Average OCT4 ChIP-seq profiles of 50–80-bp subnucleosomes (red) and histone-free DNA (blue) at enhancers centered on their OCT4 motif. The dashed lines and associated bars delimit the OCT4 enrichment domain by pointing to the positions at which the OCT4 ChIP-seq signal reached 50% of its maximum. **a**, All enhancers (clusters 1–12 from Extended Data Fig. 1); **b**, single-module enhancers (clusters 1 and 8); **c**,**d**, multimodule enhancers of clusters 2 (**c**) and 3 (**d**). We selected enhancers containing a single OCT4 high-confidence consensus motif for this analysis (n = 3,266 (**a**), 527 (**b**), 234 (**c**) and 230 (**d**)). Numbers associated with the red bars quantify the expansion of OCT4's binding interval on 50–80-bp subnucleosomes relative to histone-free DNA. **e**–**h**, Average ATAC-seq profiles of the enhancers selected in the top panels in OCT4-expressing (0 h Dox) and OCT4-depleted (24 h Dox) mouse ES cells. **e**, All enhancers (clusters 1–12); **f**, single-module enhancers (clusters 1 and 8); **g**,**h**, multimodule enhancers of clusters 2 (**g**) and 3 (**h**). The green dashed lines and bar indicate the positions at which the ATAC-seq signal detected in OCT4-expressing cells was at 50% of its maximum. **i**, Density graphs comparing OCT4 ChIP-seq and OCT4-dependent ATAC-seq signals at a representative enhancer of cluster 3. The top lane shows the positions of canonical nucleosomes detected by histone H3 ChIP-seq of sucrose gradient fractions 11 and 13 in WT mouse ES cells. The next four lanes show the distribution of 50–80-bp subnucleosomes, revealed by histone H3, H4, H2A and H2B ChIP-seq of sucrose gradient fractions 5 and 6. The subsequent two lanes show OCT4 enrichment detected by ChIP-seq of 50–80-bp subnucleosomes (fractions 5 and 6) or histone-free DNA from the top gradient fractions (fractions 2–4). The next four lanes show the distribution of ATAC-seq signal in OCT4-expressing (0 h Dox; two independent datasets) or OCT4-depleted (15 h or 24 h Dox) mouse ES cells. The last two lanes display the distribution of 50–80-bp subnucleosomes in OCT4-depleted (20 h Dox) and control mouse ES cells. Two biological replicates were performed for each ChIP-seq experiment. OCT4 consensus binding motifs with high (P = 0.001) and low (P = 0.01) stringency are indicated in black and blue, respectively.

This result suggests that OCT4 binds a histone domain accessible on the 50–80-bp subnucleosomes but not on the canonical nucleosomes. Our data support a model in which BRG1 converts its target fragile nucleosome into half-nucleosomes (or hemisomes). Each hemisome exposes to the solvent a new histone domain that was hidden before the nucleosome splitting event (Fig. 4i). We hypothesize that TFs such as OCT4 recognize and interact with this histone domain to increase their interaction with the open chromatin region of each enhancer.

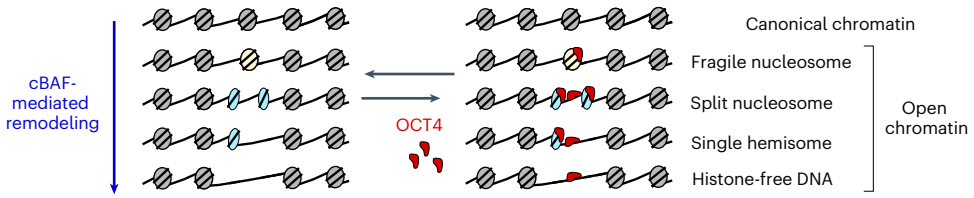

Fig. 8 | Model of how cBAF generates mixed states of open chromatin that strengthen TF binding at enhancers. Five chromatin states are indicated, from 'closed' canonical chromatin to histone-free DNA. cBAF is required at all steps of chromatin opening: generation of fragile nucleosomes, split nucleosomes, single hemisomes and histone-free DNA.

Our study revealed that promoters and CTCF sites also exhibit 50–80-bp subnucleosomes positioned within their open chromatin region. In contrast to the situation observed at enhancers, BAF complexes are not involved at CTCF sites to generate the subnucleosomes but they might have a minor function at promoters.

At the level of enhancers, the interaction of OCT4 with 50–80-bp subnucleosomes expands the genomic interval occupied by this TF by up to one order of magnitude, compared to the smaller interval it occupies on histone-free DNA (Fig. 7). This interaction allows OCT4 to cover the entire length of each enhancer independently of the number and distribution of OCT4 motifs on the DNA. A second function of the OCT4–subnucleosome interaction is to increase OCT4 occupancy.

Our data revealed that OCT4's potent function in chromatin opening is active precisely within the genomic interval delimited by the interaction between OCT4 and the 50–80-bp subnucleosomes. We also demonstrated that OCT4 is critically required within the same interval to form the subnucleosomes properly. This domain of OCT4 activity largely exceeds the size of the interval it occupies on histone-free DNA. Our work, thus, revealed a molecular mechanism in which OCT4 and cBAF cooperate to generate subnucleosomes that interact with OCT4 to expand its own binding interval and project its function beyond the boundaries of its DNA motifs.

Online content

Any methods, additional references, Nature Portfolio reporting summaries, source data, extended data, supplementary information, acknowledgements, peer review information; details of author contributions and competing interests; and statements of data and code availability are available at https://doi.org/10.1038/s41594-024-01344-0.

References

1. Ferrie, J. J., Karr, J. P., Tjian, R. & Darzacq, X. "Structure"–function relationships in eukaryotic transcription factors: the role of intrinsically disordered regions in gene regulation. *Mol. Cell* **82**, 3970–3984 (2022).
2. Isbel, L., Grand, R. S. & Schübeler, D. Generating specificity in genome regulation through transcription factor sensitivity to chromatin. *Nat. Rev. Genet.* **23**, 728–740 (2022).
3. Sönmezer, C. et al. Molecular co-occupancy identifies transcription factor binding cooperativity in vivo. *Mol. Cell* **81**, 255–267 (2021).
4. Inukai, S., Kock, K. H. & Bulyk, M. L. Transcription factor–DNA binding: beyond binding site motifs. *Curr. Opin. Genet. Dev.* **43**, 110–119 (2017).
5. Slattery, M. et al. Absence of a simple code: how transcription factors read the genome. *Trends Biochem. Sci.* **39**, 381–399 (2014).
6. Neph, S. et al. An expansive human regulatory lexicon encoded in transcription factor footprints. *Nature* **489**, 83–90 (2012).
7. Kornberg, R. D. & Lorch, Y. Primary role of the nucleosome. *Mol. Cell* **79**, 371–375 (2020).
8. Luger, K., Mäder, A. W., Richmond, R. K., Sargent, D. F. & Richmond, T. J. Crystal structure of the nucleosome core particle at 2.8 Å resolution. *Nature* **389**, 251–260 (1997).
9. Luzete-Monteiro, E. & Zaret, K. S. Structures and consequences of pioneer factor binding to nucleosomes. *Curr. Opin. Struct. Biol.* **75**, 102425 (2022).
10. Clapier, C. R., Iwasa, J., Cairns, B. R. & Peterson, C. L. Mechanisms of action and regulation of ATP-dependent chromatin-remodelling complexes. *Nat. Rev. Mol. Cell Biol.* **18**, 407–422 (2017).
11. Narlikar, G. J., Sundaramoorthy, R. & Owen-Hughes, T. Mechanisms and functions of ATP-dependent chromatin-remodeling enzymes. *Cell* **154**, 490–503 (2013).
12. Markert, J. & Luger, K. Nucleosomes meet their remodeler match. *Trends Biochem. Sci.* **46**, 41–50 (2021).
13. de Dieuleveult, M. et al. Genome-wide nucleosome specificity and function of chromatin remodellers in ES cells. *Nature* **530**, 113–116 (2016).
14. Kadoch, C. et al. Proteomic and bioinformatic analysis of mammalian SWI/SNF complexes identifies extensive roles in human malignancy. *Nat. Genet.* **45**, 592–601 (2013).
15. King, H. W. & Klose, R. J. The pioneer factor OCT4 requires the chromatin remodeller BRG1 to support gene regulatory element function in mouse embryonic stem cells. *eLife* **6**, e22631 (2017).
16. Schick, S. et al. Acute BAF perturbation causes immediate changes in chromatin accessibility. *Nat. Genet.* **53**, 269–278 (2021).
17. Iurlaro, M. et al. Mammalian SWI/SNF continuously restores local accessibility to chromatin. *Nat. Genet.* **53**, 279–287 (2021).
18. Iwafuchi-Doi, M. et al. The pioneer transcription factor FoxA maintains an accessible nucleosome configuration at enhancers for tissue-specific gene activation. *Mol. Cell* **62**, 79–91 (2016).
19. Brahma, S. & Henikoff, S. RSC-associated subnucleosomes define MNase-sensitive promoters in yeast. *Mol. Cell* **73**, 238–249 (2019).
20. Chen, X. et al. Integration of external signaling pathways with the core transcriptional network in embryonic stem cells. *Cell* **133**, 1106–1117 (2008).
21. Singh, G. et al. A flexible repertoire of transcription factor binding sites and a diversity threshold determines enhancer activity in embryonic stem cells. *Genome Res.* **31**, 564–575 (2021).
22. King, D. M. et al. Synthetic and genomic regulatory elements reveal aspects of *cis*-regulatory grammar in mouse embryonic stem cells. *eLife* **9**, e41279 (2020).
23. Spitz, F. & Furlong, E. E. M. Transcription factors: from enhancer binding to developmental control. *Nat. Rev. Genet.* **13**, 613–626 (2012).
24. Kagey, M. H. et al. Mediator and cohesin connect gene expression and chromatin architecture. *Nature* **467**, 430–435 (2010).
25. Koch, F. et al. Transcription initiation platforms and GTF recruitment at tissue-specific enhancers and promoters. *Nat. Struct. Mol. Biol.* **18**, 956–963 (2011).
26. Creyghton, M. P. et al. Histone H3K27ac separates active from poised enhancers and predicts developmental state. *Proc. Natl Acad. Sci. USA* **107**, 21931–21936 (2010).
27. Yue, F. et al. A comparative encyclopedia of DNA elements in the mouse genome. *Nature* **515**, 355–364 (2014).

28. Whyte, W. A. et al. Master transcription factors and mediator establish super-enhancers at key cell identity genes. *Cell* **153**, 307–319 (2013).
29. Henikoff, J. G., Belsky, J. A., Krassovsky, K., MacAlpine, D. M. & Henikoff, S. Epigenome characterization at single base-pair resolution. *Proc. Natl Acad. Sci. USA* **108**, 18318–18323 (2011).
30. Natsume, T., Kiyomitsu, T., Saga, Y. & Kanemaki, M. T. Rapid protein depletion in human cells by auxin-inducible degron tagging with short homology donors. *Cell Rep.* **15**, 210–218 (2016).
31. Ramachandran, S., Ahmad, K. & Henikoff, S. Transcription and remodeling produce asymmetrically unwrapped nucleosomal intermediates. *Mol. Cell* **68**, 1038–1053 (2017).
32. Rhee, H. S., Bataille, A. R., Zhang, L. & Pugh, B. F. Subnucleosomal structures and nucleosome asymmetry across a genome. *Cell* **159**, 1377–1388 (2014).
33. Zlatanova, J., Bishop, T. C., Victor, J.-M., Jackson, V. & van Holde, K. The nucleosome family: dynamic and growing. *Structure* **17**, 160–171 (2009).
34. Fatmaoui, F. et al. Cryo-electron tomography and deep learning denoising reveal native chromatin landscapes of interphase nuclei. Preprint at *bioRxiv* https://doi.org/10.1101/2022.08.16.502515 (2022).
35. Noll, H. & Noll, M. Sucrose gradient techniques and applications to nucleosome structure. *Methods Enzymol.* **170**, 55–116 (1989).
36. Clément, C. & Almouzni, G. MCM2 binding to histones H3–H4 and ASF1 supports a tetramer-to-dimer model for histone inheritance at the replication fork. *Nat. Struct. Mol. Biol.* **22**, 587–589 (2015).
37. Ramachandran, S. & Henikoff, S. Nucleosome dynamics during chromatin remodeling in vivo. *Nucleus* **7**, 20–26 (2016).
38. Farnung, L., Ochmann, M., Garg, G., Vos, S. M. & Cramer, P. Structure of a backtracked hexasomal intermediate of nucleosome transcription. *Mol. Cell* **82**, 3126–3134 (2022).
39. Blobel, G. A., Higgs, D. R., Mitchell, J. A., Notani, D. & Young, R. A. Testing the super-enhancer concept. *Nat. Rev. Genet.* **22**, 749–755 (2021).
40. Lowary, P. T. & Widom, J. New DNA sequence rules for high affinity binding to histone octamer and sequence-directed nucleosome positioning. *J. Mol. Biol.* **276**, 19–42 (1998).
41. Zhou, K., Gaullier, G. & Luger, K. Nucleosome structure and dynamics are coming of age. *Nat. Struct. Mol. Biol.* **26**, 3–13 (2019).
42. Barisic, D., Stadler, M. B., Iurlaro, M. & Schübeler, D. Mammalian ISWI and SWI/SNF selectively mediate binding of distinct transcription factors. *Nature* **569**, 136–140 (2019).
43. Mashtalir, N. et al. Modular organization and assembly of SWI/SNF family chromatin remodeling complexes. *Cell* **175**, 1272–1288 (2018).
44. Gatchalian, J. et al. A non-canonical BRD9-containing BAF chromatin remodeling complex regulates naive pluripotency in mouse embryonic stem cells. *Nat. Commun.* **9**, 5139 (2018).
45. Ambrosetti, D.-C., Basilico, C. & Dailey, L. Synergistic activation of the fibroblast growth factor 4 enhancer by Sox2 and OCT-3 depends on protein–protein interactions facilitated by a specific spatial arrangement of factor binding sites. *Mol. Cell. Biol.* **17**, 6321–6329 (1997).
46. Mistri, T. K. et al. Selective influence of Sox2 on POU transcription factor binding in embryonic and neural stem cells. *EMBO Rep.* **16**, 1177–1191 (2015).
47. Soufi, A. et al. Pioneer transcription factors target partial DNA motifs on nucleosomes to initiate reprogramming. *Cell* **161**, 555–568 (2015).
48. Roberts, G. A. et al. Dissecting OCT4 defines the role of nucleosome binding in pluripotency. *Nat. Cell Biol.* **23**, 834–845 (2021).
49. Xiong, L. et al. OCT4 differentially regulates chromatin opening and enhancer transcription in pluripotent stem cells. *eLife* **11**, e71533 (2022).
50. Ramani, V., Qiu, R. & Shendure, J. High sensitivity profiling of chromatin structure by MNase-SSP. *Cell Rep.* **26**, 2465–2476 (2019).

Methods

Cell lines and culture

The Brg1-3FTH mouse ES cell line (parental cell line 46C) was generated as previously described[13]. The E14Tg2a-Tir1 cell line was obtained from E. Nora and B. Bruneau[51]. The 501Mel cell line was obtained from I. Davidson[52]. All mouse ES cell lines were grown on mitomycin C-inactivated mouse embryonic fibroblasts at 37 °C, 5 % CO_2, in DMEM (Sigma) supplemented with leukemia inhibitory factor, 1× nonessential amino acids (Invitrogen), 15% fetal calf serum (Invitrogen), 0.2% β-mercaptoethanol (Sigma) and 1× penicillin–streptomycin (Invitrogen)[53]. The human melanoma 501Mel cell line was grown in RPMI-1640 medium (Sigma) supplemented with 10% fetal calf serum and 1× penicillin–streptomycin.

Plasmid construction

We designed the shRNA-expressing plasmids as previously described[54]. Sequences of the sense strand of shRNAs targeting BRG1 were as follows: shRNA O5, 5′-GCTCCAGTAAAGATGTCTACT-3′; shRNA O7, 5′-GAGCGAATGCGGAGGCTTATG-3′. Sequences targeting *Chd4* were already described[13].

The AID system is based on the fusion, at the C terminus of the target protein, of a mini AID (mAID) tag (68 amino acids, 7.4 kDa)[30]. We adopted the two-selection marker strategy to target the *Smarca4* and *Smarcb1* alleles with the sequence encoding mAID[30]. We assembled the *Smarca4*–mAID and *Smarcb1*–mAID targeting vectors by a serial modification of the base vectors pMK287 (mAID-Hygro, Addgene 72825) and pL452 (ref. 13). We amplified the left and right homology arms (400–500 bp each) corresponding to the last exon and 3′ untranslated region of *Smarca4* and *Smarcb1* by PCR from E14Tg2A genomic DNA. We designed the oligonucleotides that amplify homology arms to introduce silent mutations after integrating the mAID cassette downstream of the *Smarca4* and *Smarcb1* genes to prevent recutting by the Cas9 enzyme. In the next cloning steps, we introduced the PCR products of left and right homology arms using restriction enzyme digestions into both vectors (pMK287-mAID-Hygro and pL452-mAID-Neo).

We assembled the CRISPR–Cas9 vectors by annealing pairs of oligos carrying the single guide RNA (sgRNA) sequences and cloning them into pSpCas9(BB)-2A-Puro (PX459) (Addgene 62988) as described[55]. Two distinct *Smarca4*-targeting sgRNAs were cloned separately by annealing oligos caccgTTGGCTGGGACGAGCGCCTC and aaacGAGGCGCTCGTCCCAGCCAAc for the first sgRNA and caccgGCGCCTCGGGGTCAGGACTC and aaacGAGTCCTGACCCCGAGGCGCc for the second sgRNA. We designed the sgRNAs to target the area close to the last exon of *Smarca4* using the Zhang lab guide design tool (https://zlab.bio/guide-design-resources). Similarly, two *Smarcb1*-targeting sgRNAs were cloned into pSpCas9(BB)-2A-Puro by annealing the oligonucleotides described in Supplementary Table 5. We followed a similar strategy to design the plasmids required for tagging the *Arid1a*, *Pbrm1*, *Brd7, Brd9, Pou5f1* (encoding OCT4) and *H3f3b* (encoding histone H3.3) genes. For these genes, the sequence encoding the mAID tag was fused in frame with a sequence encoding the 3FTH tag. The 3FTH tag was composed, from the N to C terminus, of three FLAG epitopes followed by a TEV protease cleavage site and a single hemagglutinin (HA) epitope as previously described[13]. In the fused tag (3FTH-mAID), mAID was located at the C-terminal end. The sequences of the oligonucleotides encoding the sgRNAs targeting *Arid1a*, *Pbrm1*, *Brd7*, *Brd9*, *Pou5f1* and *H3f3b* are in Supplementary Table 5.

Generation of the mAID-tagged cell lines

We used the E14Tg2a-Tir1 cell line, which was obtained by targeting the *Tigre* locus of E14Tg2a cells with a transgene expressing *Oryza sativa* Tir1 (ref. 51). Using the Neon electroporation kit (ThermoFisher), we transfected this cell line with the two vectors encoding the Cas9 enzyme and sgRNAs (2.5 µg each) and with the two linearized plasmids carrying the targeted gene homology arms and the mAID tag (pMK287 and pL452; 10 µg each). Neomycin (250 µg ml^{-1}; G-418, Sigma) and hygromycin B (300 µg ml^{-1}; Thermo Fisher Scientific) selection was started after 24 h. After 6 days of selection, single clones were manually picked, expanded in 24-well plates and subjected to genotyping by PCR and sequencing of the knock-in region. Western blotting of protein extracts from auxin-treated cells confirmed selected clones with a homozygous insertion of the mAID or 3FTH-mAID tag at the *Smarca4*, *Smarcb1*, *Arid1a*, *Pbrm1*, *Brd7* and *Brd9* loci. We obtained cell lines heterozygous for the *H3f3b-3FTH-mAID* and *Pou5f1-3FTH-mAID* alleles.

Chromatin remodeler subunit depletion

We performed shRNA-mediated depletion as described[13]. For auxin-mediated protein depletion, we supplemented the cell culture medium of cells expressing BRG1-mAID with 1 mM auxin (IAA, indole-3-acetic acid; Cayman Chemical) for 3 h or 20 h. Unless specified otherwise, we realized all auxin-mediated depletion of BAF complex subunit experiments described in the manuscript at the 20-h auxin time point.

Chromatin preparation from formaldehyde-fixed cells

Mouse ES cells were treated with trypsin to obtain a single-cell suspension and separated from mouse embryonic fibroblast feeders by a 30-min incubation at 37 °C in D15 medium on a gelatin-coated culture plate. Mouse ES cells and 501Mel cells were collected and fixed in culture medium containing 1% formaldehyde (Sigma) for 10 min at 20 °C. We stopped fixation by adding glycine to 125 mM and the cells were centrifugated and washed three times with PBS. Cells were then permeabilized in 15 mM Tris-HCl pH 7.5, 15 mM NaCl, 5 mM $MgCl_2$, 0.1 mM EGTA, 60 mM KCl, 0.3 M sucrose and 0.4% IGEPAL CA-630 (I3021, Sigma) during 15 min on ice. We next diluted the cells with two volumes of MNase buffer (20 mM Tris-HCl pH 7.5, 20 mM NaCl, 2 mM $CaCl_2$, 4 mM $MgCl_2$ and 15 mM KCl) and chromatin was digested for 10 min at 37 °C with 6 Kunitz units of MNase (New England Biolabs, 200 Kunitz units per µl) per 1 million cells. We stopped MNase digestion by adding a final concentration of 10 mM EDTA. We released chromatin from MNase-treated mouse ES cells by passing the cell suspension 13 times through a 26-gauge syringe. Next, we centrifugated the samples and the supernatants containing the solubilized chromatin were used directly for ChIP-seq experiments or sucrose gradient centrifugation. The quality and reproducibility of the MNase digestion pattern of all samples were validated after crosslink reversal by electrophoresis on a 1.7% agarose gel.

Fractionation of MNase-digested chromatin by sucrose gradient centrifugation

Chromatin samples prepared from 40 million formaldehyde-fixed mouse ES cells or 501Mel cells were supplemented with protease inhibitors (Complete Protease Inhibitor Cocktail, Roche) and loaded on a 9.9-ml manually poured 10–30% sucrose gradient containing 10 mM Tris-HCl pH 7.5, 1 mM EDTA, 1 mM EGTA, 80 mM NaCl and protease inhibitors. For unfixed chromatin samples, we used sucrose gradients containing 10 mM EDTA and 20 mM EGTA in addition to the other ingredients. We centrifugated the chromatin samples for 16 h at 197,000*g* using a Beckman Coulter SW 41 swinging-bucket rotor, at 4 °C. After centrifugation, 20 chromatin fractions of 500 µl were collected from top to bottom of the tube and stored at −80 °C. Aliquots of each chromatin fraction were treated with RNAse A and proteinase K and subjected to reverse crosslinking for 16 h at 65 °C, followed by phenol–chloroform DNA extraction and ethanol precipitation. DNA was quantified using the Qubit system (Thermo) and analyzed on a 4% agarose gel or used for library preparation and deep sequencing.

MNase ChIP-seq using formaldehyde-fixed chromatin

ChIP-seq experiments were performed with individual sucrose gradient fractions, pools of gradient fractions or whole-cell chromatin extracts.

For the whole-cell chromatin extracts, we used chromatin solubilized from 1.2 million mouse ES cells for ChIP-seq with antibodies against histones or from 10 million cells for ChIP-seq with antibodies against TFs and Pol II. Chromatin samples were incubated with antibodies (20 µg of antibodies against TFs or Pol II and 5 µg of antibodies against histones) overnight at 4 °C. Chromatin–antibody complexes were next incubated with 50 µl of protein G agarose beads (Roche 11243233001) for 4 h at 4 °C. Then, chromatin–antibody–bead complexes were washed three times with TEN buffer (20 mM Tris-HCl pH 7.5, 150 mM NaCl, 3 mM $MgCl_2$, 0.1 mM EDTA and 0.01% IGEPAL), four times with WBLiCl buffer (50 mM HEPES pH 7.5, 500 mM LiCl, 1 mM EDTA, 1% IGEPAL and 0.7% Na-deoxycholate) and once with TEN buffer. Between each wash, we centrifugated the beads for 3 min at 800*g* and 4 °C. Elution was realized by resuspending the beads in elution buffer (50 mM Tris-HCl pH 8, 10 mM EDTA and 1% SDS). For ChIP-seq experiments realized with the antibody targeting the 20 C-terminal amino acids of OCT4 (Fig. 4e, WT 1 lane of Fig. 4g and Extended Data Fig. 4), we performed the washes and elution by peptide competition as described below for sequential ChIP-seq of OCT4-bound and H2B-bound chromatin. Eluted chromatin was treated with proteinase K and subjected to reverse crosslinking and phenol–chloroform extraction, followed by ethanol precipitation. We prepared DNA libraries using a MicroPlex Library Preparation Kit v2 or v3 (Diagenode). Sequencing was performed on a NextSeq 500 Illumina platform using a NextSeq 500 High Output v2 (75 cycles) kit. At least two biological replicates were realized and sequenced for each histone or TF ChIP-seq experiment.

Sequential ChIP-seq of OCT4-bound and H2B-bound genomic DNA

We used chromatin prepared from 240 million E14Tg2a mouse ES cells for each experiment. We incubated the chromatin with either 45 µg of antibodies against OCT4 (MBS420786, MyBioSource) or 45 µg of nonspecific immunoglobulin G (IgG) as a control. After 16 h at 4 °C, we added protein G agarose beads to chromatin–antibody complexes and further incubated for 4 h at 4 °C. After seven washes with TEN buffer, we incubated the beads with TEN buffer containing OCT4 peptide (C-terminal part of OCT4 sequence: H-Cys-Lys-Lys-Lys-Lys-Pro-Ser-Val-Pro-Val-Thr-Ala-Leu-Gly-Ser-Pro-Met-His-Ser-Asn-OH) for elution by competition. We performed three consecutive elution steps: 2 h at room temperature with TEN buffer containing 2 mg ml^{-1} of OCT4 peptide, 2 h at room temperature with 1 mg ml^{-1} of peptide and 16 h at 4 °C with 1 mg ml^{-1} peptide. The three elution fractions were pooled and incubated with 5 µg of antibodies against histone H2B for 16 h at 4 °C. Protein G agarose beads were next added and incubated for 4 h at 4 °C. We performed the wash and elution steps of this second ChIP as described above for regular ChIP-seq experiments. Two biological replicates were obtained for each OCT4 and nonspecific IgG antibody.

Chromatin preparation from unfixed mouse ES cells expressing the tagged histone H3.3-3FTH-mAID

Mouse ES cells were treated with trypsin to obtain a single-cell suspension and separated from mouse embryonic fibroblast feeders by a 30-min incubation at 37 °C in D15 medium on a gelatin-coated culture plate. Mouse ES cells were then washed in PBS and permeabilized in 15 mM Tris-HCl pH 7.5, 15 mM NaCl, 5 mM $MgCl_2$, 0.1 mM EGTA, 60 mM KCl, 0.3 M sucrose, 0.2% IGEPAL CA-630 and protease inhibitors for 10 min on ice. The cells were then centrifugated at 10,000*g* for 30 min through an 8-ml sucrose cushion (15 mM Tris-HCl pH 7.5, 15 mM NaCl, 5 mM $MgCl_2$, 0.1 mM EGTA, 60 mM KCl and 1.2 M sucrose). The pellet of nuclei was gently resuspended in MNase buffer. The nuclei were digested for 10 min at 37 °C with 1.4 Kunitz units of MNase (New England Biolabs, 200 Kunitz units per µl) per 1 million cells. We stopped the digestion by adding a final concentration of 10 mM EDTA and 20 mM EGTA. The nuclei were incubated for 1 h onto a rotative agitator at 4 °C. We released the chromatin by passing the nuclei suspension 13 times through a 26-gauge syringe. After centrifugation, the supernatants containing the solubilized chromatin were used directly for ChIP onto agarose beads coupled to a mouse monoclonal anti-HA antibody (Sigma A2095).

Preparation of purified native 50–80-bp subnucleosomes from unfixed chromatin

The chromatin prepared from ~240 million H3.3-3FTH-mAID-expressing and TIR1 mouse ES cells was solubilized in MNase buffer and divided into two 500-µl batches. Each tube was incubated under agitation at 4 °C with 60 µl of agarose beads coupled to a mouse monoclonal anti-HA antibody. After overnight incubation at 4 °C, the beads were collected by centrifugation for 3 min at 800*g* and washed two times with 10 ml of TEN buffer. The beads were then washed five times for 15 min at 4 °C with 8 ml of buffer A (10 mM Tris-HCl pH 7.5, 1 mM EDTA, 1 mM EGTA and 80 mM NaCl). Each batch of beads was resuspended in 400 µl of buffer A with 1 mM DTT. Elution was performed by adding 6 µl of TEV protease (New England Biolabs, 10 units per µl), followed by overnight incubation at 4 °C under agitation. The next day, the beads were centrifugated for 3 min at 800*g* and the eluate (supernatant) was collected and stored on ice. The beads were then resuspended in 400 µl of buffer A with 1 mM DTT and 3 µl of TEV protease. After 1.5 h at 30 °C, the second eluate was collected, cooled on ice and mixed with the first eluate. The combined eluate was then divided into two 400-µl aliquots that were each centrifugated for 16 h at 197,000*g* through a sucrose gradient as described above. Then, 500-µl fractions were collected as described above. The DNA was extracted from a 150-µl aliquot of each low-sedimentation fraction. Only the DNA prepared from H3.3-3FTH-mAID-expressing cells allowed the preparation of libraries using the Diagenode microplex v3 kit. Four biological replicates were realized and sequenced. The DNA prepared from the control untagged TIR1 cells did not contain enough DNA to prepare a library using the same amplification conditions. The remaining 350 µl of the low-sedimentation fractions were used as the input 50–80-bp subnucleosome fraction for the pull-down assay (below).

OCT4 pull-down assay

The nuclei of ~240 million cells expressing the tagged OCT4-3FTH-mAID protein were resuspended in 4 ml of buffer C (20 mM HEPES pH 7.9, 25% (v/v) glycerol, 0.42 M NaCl, 1.5 mM $MgCl_2$, 0.2 mM EDTA, 0.5 mM DTT and protease inhibitors) as previously described[56]. The nuclei were lysed with ten strokes of a Dounce homogenizer (B-type pestle). After a 30-min agitation at 4 °C, the extract was centrifugated at 21,000*g* for 30 min at 4 °C. The supernatant was collected and diluted with an equal volume of buffer C without NaCl. The diluted extract was then distributed in six tubes each containing 50 µl of anti-HA agarose beads. The beads and extract were incubated under agitation at 4 °C overnight. The next day, the beads were washed twice with TEN buffer, three times with WBLiCl buffer, once with TEN buffer and twice with buffer A. Each batch of agarose beads carrying immobilized OCT4 was next incubated with 700 µl (pool of two low-sedimentation fractions) of the purified native 50–80-bp subnucleosomes or, as a control, with buffer A. After a 90-min incubation at 20 °C with agitation, the beads were washed twice for 5 min with 6 ml of buffer A with 1 mM DTT. Elution was performed by adding 150 µl of buffer A containing 2 µl of TEV protease and 200 µg ml^{-1} BSA. After 90 min at 30 °C under agitation, the beads were centrifugated and the supernatant was collected for DNA extraction and library preparation using the Diagenode MicroPlex Library Preparation Kit v3. Using an aliquot of the eluted fraction, we verified by western blotting that OCT4 was efficiently released from the beads. An additional series of control experiments was performed by conducting the same series of tests with 'control' agarose beads that were not incubated with tagged OCT4. The two controls, thus, consisted of incubating the purified subnucleosomes

with beads without immobilized OCT4 and incubating the beads carrying immobilized OCT4 without subnucleosomes. Neither of these controls allowed the synthesis of a library, showing that the background level of the experiment was appropriate. In contrast, incubating the purified 50–80-bp subnucleosomes with agarose beads bearing immobilized OCT4 allowed the amplification of libraries in both replicate experiments.

Depletion of OCT4 in ZHBTc4 mouse ES cells

ZHBTc4 mouse ES cells were treated with 1 µg ml^{-1} doxycycline (Dox; Takara) for 20 h in D15 medium as previously described[57]. We controlled the efficiency of OCT4 depletion by western blotting.

Transmission EM

Chromatin samples were prepared from 80 million E14Tg2a mouse ES cells and centrifugated through a sucrose gradient as described above for MNase ChIP-seq. We examined subnucleosomal particles collected from fractions 5, 6, 11 and 12 of the sucrose gradient and particles further purified from a pool of fractions 5 and 6 by immunoprecipitation with the antibody targeting the 20 C-terminal amino acids of OCT4, as described above. Aliquots of sucrose gradient fractions were dialyzed overnight into TEAP10 buffer (10 mM triethanolamine-HCl pH 7.5, 0.2 mM EDTA, 10 mM NaCl and 0.2 mM PMSF), then crosslinked with 0.1% glutaraldehyde at 4 °C for 2 h and quenched by the addition of Tris (pH 8) to a final concentration of 50 mM. Samples were coated with 2 × 10^{-4}% benzalkonium chloride for 1 h at room temperature and 5 µl of the sample (approximately 0.02 ng µl^{-1}) was adsorbed onto carbon–formvar-supported 200-mesh copper grids (TAAB technologies). Grids were washed twice with deionized water, dehydrated with 90% ethanol and blotted dry. Grids were rotary-shadowed with 3 nm of platinum at a 7° angle and examined on a JEOL JEM-1400Plus Transmission EM instrument.

We randomly selected the particles and measured them with ImageJ for statistical analysis of particle size. Most particles had a disk-like structure and we measured them along the diameter. We measured particles having an elliptical shape along the major axis, as this likely represented the front view of the nucleosomal particles. We built the box plot shown in Extended Data Fig. 6e with sizes of 92, 102, 97, 71 and 100 particles from one sample of sucrose gradient fraction 6, two independent samples of OCT4-immunopurified particles (OCT4 (fractions 5 and 6) R1 and R2), one sample of fraction 12 (mononucleosomes) and one preparation of in vitro assembled 601 nucleosomes, respectively. To choose the appropriate statistical test to compare the different groups of particles, we first verified the size distribution in each group and performed Shapiro–Wilk normality tests. This analysis revealed that the data collected for all groups of subnucleosomal particles did not display a normal distribution. We, thus, selected a Mann–Whitney test (R: Wilcox.test function, two-sided; parameters: paired = FALSE and conf.level = 0.95) to determine whether the sizes of subnucleosomal particles and canonical nucleosomes were significantly different. This statistical analysis revealed that subnucleosomal particles of each group were significantly different in size from canonical nucleosomes; particles from fraction 6 versus those from fraction 12, $P = 6.6 \times 10^{-5}$; particles from OCT4 (fractions 5 and 6) R1 versus those from fraction 12, P value = 1.5×10^{-7}; particles from OCT4 (fractions 5 and 6) R2 versus those from fraction 12, $P = 2.9 \times 10^{-11}$; particles from fraction 6 versus 601 nucleosomes, $P = 2.4 \times 10^{-14}$; particles from OCT4 (fractions 5 and 6) R1 versus 601 nucleosomes, $P < 2.2 \times 10^{-16}$; particles from OCT4 (fractions 5 and 6) R2 versus 601 nucleosomes, $P < 2.2 \times 10^{-16}$.

Size-exclusion chromatography

Chromatin samples were sucrose gradient fraction 6 for 50–80-bp subnucleosomes and fraction 11 for mononucleosomes. First, 400 µl of chromatin sample was loaded at 0.25 ml min^{-1} onto a Superdex 200 increase 10/300 GL column (Cytiva) equilibrated in 10 mM Tris-HCl pH 7.5, 80 mM NaCl and 1 mM EDTA. Then, 250-µl fractions were collected. The column was calibrated with gel filtration protein markers thyroglobulin (669 kDa), apoferritin (440 kDa), β-amylase (200 kDa) and BSA (67 kDa) from MWGF1000 (Sigma).

Construction of the hemisome–link–hemisome model

To generate the hemisome–linker–hemisome molecular model, we separated the best resolution nucleosome structure (1,000 × 5 bp) into two hemisomes by cutting the DNA at the dyad position. We positioned a B-DNA linker at the generated DNA extremity by overlapping four base pairs. We choose a representative length of 29 bp corresponding to the median distance between two hemisome-like particles at enhancers. The second hemisome was positioned similarly at the second extremity of the DNA linker. The exposed DNA was highly sensitive to MNase and, thus, digested before the ChIP experiment. The resulting isolated particles, corresponding to hemisomes, contained 50–70-bp DNA fragments linked to histones H3–H4–H2A and H2B.

Computational analyses

Lists of mouse ES cell enhancers. We first mapped the distribution of CREs onto the mouse ES cell genome using DNaseI-seq data (GSM1014187), identifying 139,454 DNase-hypersensitive (DHS) regions, as previously described[13]. Gene promoters were filtered out using RefSeq coordinates of TSSs and putative enhancers were identified on the basis of the co-occurring binding of pluripotency-associated TFs OCT4 (GSM1082340), SOX2 (GSM1082341) and NANOG (GSM1082342), as well as of Mediator (GSM560347)[20,28]. To avoid potential interferences with CTCF-bound regions in our nucleosomal organization analysis, we removed from these putative enhancers those bound by CTCF using mouse ES cell datasets GSM723015 and GSM1828650. A total of 19,365 loci displaying a high ChIP-seq signal for OCT4, SOX2, NANOG and Mediator but negative for CTCF were identified as putative enhancer elements. We then used the histone H3 MNase ChIP-seq datasets generated in this study to analyze nucleosomal and subnucleosomal organization at these putative enhancers. One of these H3 MNase ChIP-seq datasets was converted into a BED (browser extensible data) file and subdivided into five files containing DNA fragments of 30–80, 81–110, 111–140, 141–180 and >181 bp. The number of DNA fragments in each subgroup was as follows. 30–80 bp, 13,806,227 DNA fragments; 81–110 bp, 9,480,961 fragments; 111–140 bp, 13,589,276 fragments; 141–180 bp, 64,258,774 fragments; >180 bp, 51,518,836 fragments. Next, in each BED file, DNA fragments were reduced to 10 bp and centered at the level of the fragment midpoint. Using seqMINER[58], fragment densities from these modified BED files were collected in a ±1,500 bp window around the center of each enhancer (defined in this study as the center of the DHS peak) and subjected to several rounds of *k*-means clustering. This analysis allowed us to classify 10,304 (of the initial 19,365) putative enhancers into the 12 clusters shown in Extended Data Fig. 1.

We developed the exPATT.R tool (https://github.com/jcaude/exPATT) to detect OCT4 DNA-binding motifs and change the genomic coordinates of each enhancer to have the OCT4 motif at its center. The exPATT.R R script filters genomic regions, recorded in an input BED file, that match a given DNA pattern (OCT4 consensus motif in this study) depicted as a position weight matrix (PWM). These pattern matrices were matched in terms of genomic region using the PWM-related functions of the Bioconductor package Biostrings[59] with a minimum of 80% of the highest possible score. Then, genomic regions with at least one pattern hit were filtered. The output of this script was a new bedGraph file with filtered DNA regions of 2 kb centered around the pattern. All BED file input and output operations were performed using the rtracklayer package. Then, we used BEDTools to select enhancers bearing a single central OCT4 motif per enhancer (n = 1,302; Extended Data Fig. 10).

Lists of 501Mel cell enhancers. On the basis of the hypothesis that subnucleosomal particles are conserved in human cells, we mapped CREs in human 501Mel cells using the histone H3 ChIP-seq dataset from 50–80-bp subnucleosomes purified from these cells. We used MACS2 to call 91,205 peaks from this dataset. We next focused our analysis on putative enhancer elements located in intergenic regions. We filtered out all regions of the human genome located within 3 kb of gene TSSs or 10 kb of gene end coordinates. We also set up a strategy to remove CTCF-bound loci from this list of peaks. Because the CTCF ChIP-seq distribution has not been defined in 501Mel cells, we took advantage of the observation that CTCF binding to mammalian genomes is relatively independent of cell type[60,61]. We removed all loci bound by CTCF in two cancer cell lines from the putative enhancer list, using ENCODE CTCF ChIP-seq datasets GSM749683, GSM749715, GSM749679 and GSM749768. This combination of filtering steps led to a list of 14,502 putative 501Mel cell enhancers. The *k*-means clustering of these 14,502 elements using the H3 ChIP-seq datasets from sucrose gradient-purified 50–80-bp subnucleosomes and from the fraction containing canonical nucleosomes allowed us to isolate the five clusters of putative 501Mel cell enhancers shown in Extended Data Fig. 7.

List of CTCF sites. We identified mouse ES cell genomic CTCF sites on the basis of the ChIP-seq signal of several CTCF datasets (GSM723015, GSM1828650, GSM288351 and GSM560352) at DHS regions, as described above for enhancers. All loci proximal (<2 kb) to gene promoters and putative enhancers were removed. We used a subset (n = 9,850) of these CTCF-positive regions to generate the V-plots shown in Extended Data Fig. 8 and 9.

List of promoters. We rank-ordered gene promoters transcribed in mouse ES cells according to the distance between the two divergent TSSs located on the plus and minus strands, using 5′ ends of start RNA reads (GSE43390), as previously described[62]. Mouse ES cell start RNA read datasets were first aligned to mm9 using Bowtie 1.3.0. We conserved only the reads mapping to a single position with a maximum of two mismatches. We derived the reference promoter list from RefSeq annotation. We defined promoter windows as ±1,000 bases around the TSS position. We discarded windows with more than one TSS on the plus strand. We also removed the promoters associated with fewer than five overlapping start RNA reads. We calculated the coverage using a bin of one base. We selected the first six bases of the 5′ reads as the signal to adjust the position of the TSS on the plus strand. We used a Python (version 3) script to find the nearest local maximum upstream of the RefSeq annotation, which we defined as the TSS position in this study. Next, we determined the location of the antisense start RNA signal on the minus strand in the region located upstream of the plus-strand TSS. We selected the first six bases of the 5′ reads to define the position of the antisense TSS. We then designated the coordinate of the antisense TSS as the location having maximum start RNA expression on the minus strand, upstream of the sense TSS. We next sorted the promoters according to the distance between sense and antisense TSS coordinates. In this study, we focused our analysis on the 1,000 TSSs with the smallest distance between sense and antisense TSSs. The nucleosomal and subnucleosomal organization of the other groups of TSSs is similar and will be presented in a separate publication.

MNase ChIP-seq, MNase-seq and ATAC-seq analysis

Data collection, quality controls, mapping and postmapping process. Illumina RTA 2.4.11 or 2.11.3 (NextSeq550) and bcl2fastq Conversion Software version 2.20.0.422 were used for base calling and demultiplexing. Data analysis was performed using Snakemake 7.15.2 (ref. 63), Conda 4.11.0 and in-house Python scripts (https://github.com/Edmri/hist2D/releases/tag/v1.0.0). We controlled the quality of sequencing data with FastQC 0.11.9 using default parameters)[64] and FastQ Screen 0.14.0 using Bowtie 2 (version 2.4.2) as the default aligner[65]. Depending on their quality, sequencing files were trimmed with fastp 0.20.1 using the process described hereafter. Reads with a size below 25 bp were discarded to keep mapping specificity. Adaptor sequences were autodetected over ~1 million reads and removed. Reads with a base quality under 10 through a window size of six bases were discarded and poly(G) sequences were filtered out. Potential artifactual enrichments were assessed over 1/20 of the raw reads and removed[66]. Trimmed paired-end reads were mapped with Bowtie 2 (version 2.4.2)[67] over Gencode's 9th mouse genome version for mouse ES cells or the 38th human genome version for 501Mel cells. After mapping, reads were sorted by genomic coordinates using SAMtools 1.11. Artifactual fragment duplication (optical and local) was assessed with Picard 2.23.8 (Picard Toolkit; http://broadinstitute.github.io/picard/). SAMtools was used to remove marked duplicates, unmapped reads and reads involving a mapping quality below 30. The reads per kilobase per million mapped reads (RPKM) normalized genomic coverage was calculated with deepTools for MNase data with a bin size of one base and centered on the fragment center for a fragment size of 10–500 bp. For the OCT4 MNase ChIP-seq datasets of the BAF complex loss-of-function series, we fixed the fragment size from 10 to 100 bp. Chromosomes M, Y and X were not used for the normalization. The effective mouse genome size was set to 2,652,783,500 bp (deepTools 3.5.0)[68].

IGV visualizations and V-plots. Peaks and normalized coverage profiles were visualized as IGV (Integrative Genomics Viewer) screenshots, heat maps and V-plots. We converted BAM files containing paired-end mapped reads to BED files containing DNA fragments using BEDTools bamtobed (version 2.29.2)[69]. We visualized these DNA fragments as a heat map with seqMINER software and as a V-plot using a homemade script. In the plot, each dot corresponds to the coordinates of a DNA fragment midpoint and color intensity reflects the number of fragments at that position. When comparing several samples, we chose the color intensity manually and a ratio was applied to reduce the number of fragments to the same level in each sample.

Analysis of the frequency at which subnucleosomal particles are organized in pairs at enhancers and determination of DNA linker length. IGV screenshots of all mouse ES cell enhancers from clusters 1 and 8 (n = 1,430) were analyzed individually and separated into three subgroups on the basis of the enrichment pattern of histone H3, H4, H2A and H2B ChIP-seq peaks for 50–80-bp subnucleosomes: (1) 496 enhancers displayed a single-module organization with two well-separated peaks (examples shown in Fig. 4g, Extended Data Fig. 4a–d, Extended Data Fig. 5, Supplementary Fig. 1d–h and the lower panels of Supplementary Fig. 2); (2) 881 enhancers exhibited three or more discernible histone peaks and were classified as multimodule enhancers (examples shown in Fig. 7, Extended Data Fig. 4e–h, Supplementary Fig. 1a–c and in the upper panels of Supplementary Fig. 2); and (3) 53 enhancers (3.7% of total) presented a single histone peak that could be interpreted either as a rare subcategory of enhancers bearing a single subnucleosomal particle or as single-module enhancer having a pair of two closely located histone peaks fused into a single peak. For the three subgroups, the ChIP-seq peaks of histones H3, H4, H2A and H2B always overlapped in genomic position, confirming the systematic association of the four histones in these 50–80-bp subnucleosomes. We measured the distance D in bp between the centers of the two peaks of the subgroup of 496 single-module enhancers. Assuming that each of these two peaks marked the position of a hemisome protecting an average of 64 bp of DNA from MNase digestion, as proposed in Fig. 4i, we calculated the linker length between these two putative hemisomes as D − 64 bp. We found that this DNA linker's length ranged from 0 to 102 bp (median = 29 bp) (Extended Data Fig. 4i).

Detection of TF motifs at enhancers. We performed motif analysis using the MEME Suite (version 5.3.0)[70]. Detection of OCT4 motifs in Figs. 4g, 5g, 6f,g and 7i, Extended Data Figs. 4 and 10 and Supplementary Figs. 1 and 2 was carried out with Fimo over selected lists of enhancers (clusters 1, 2, 3 and 8 from Extended Data Fig. 1), using two distinct *P* values (0.001 and 0.01) to allow different levels of stringency in the motif sequence matching. The OCT4 motif matrix (MA0142.1) came from the JASPAR database[71]. We defined the OCT4, SOX2, NANOG and KLF4 motif enrichment profiles at mouse ES cell enhancers of clusters 1 and 2 using Centrimo (MEME Suite version 5.3.0) (Extended Data Fig. 2m–p). We also used Centrimo to analyze the distribution of SOX10, microphthalmia-associated transcription factor (MITF) and TFAP2A (ref. 52) motifs at putative enhancers in human 501Mel cells (Extended Data Fig. 7c).

Detection of OCT4 full-size and half-site motifs in the DNA prepared from OCT4-immunopurified 50–80-bp subnucleosomes. OCT4 half-site motifs were taken from the literature[47]. OCT4 full-size motifs and half-sites were detected with Fimo using two distinct *P* values (0.001 and 0.01), as described above. The IGV screenshots of enhancers from a representative cluster (cluster 8, $n = 701$) were analyzed individually to score the presence of OCT4 full-size motifs and half-sites in the DNA of the 50–80-bp subnucleosomes bound by OCT4. These OCT4-enriched regions, which coincided with the histone peaks, are well defined on the IGV screenshots (Figs. 4g, 5g, 6f,g and 7i, Extended Data Figs. 4 and 10 and Supplementary Figs. 1 and 2). When we used the stringent *P* value ($P = 0.001$), we found that 64% of the OCT4-enriched subnucleosomes did not contain an OCT4 full-size consensus motif or a half-site. When we used the relaxed *P* value ($P = 0.01$), allowing the detection of degenerated motifs and half-sites, we found that 18.5% of the OCT4-bound subnucleosomes did not contain an OCT4 full-size motif or a half-site. Note that a large majority of the OCT4 motifs detected with the relaxed *P* value ($P = 0.01$) were not associated with a positive OCT4 ChIP-seq signal on histone-free DNA (for example, Figs. 4g, 6f,g and 7i, Extended Data Figs. 4 and 10 and Supplementary Figs. 1 and 2). It is, thus, unclear whether OCT4 binds these degenerated motifs onto 50–80-bp subnucleosomes in vivo. We concluded that a notable proportion of OCT4-bound subnucleosomes lack both OCT4 full-size motifs and half-sites in the DNA wrapped around the particle.

Analysis of OCT4 occupancy at enhancers. For each enhancer of clusters 1 ($n = 729$), 2 ($n = 600$), 3 ($n = 637$) and 8 ($n = 701$), we first calculated the maximum RPKM value of the OCT4 ChIP-seq signal on the histone-free DNA fraction. Then, for each group of enhancers, we plotted the maximum RPKM values against the number of enhancers associated with each RPKM score. The curve revealed that most enhancers were associated with a low RPKM score, while a minority displayed a higher score. We identified a sharp bending of the curve (knee or elbow point) for each cluster. We chose the RPKM value at the knee point as the threshold defining a low and high OCT4 ChIP-seq signal. The RPKM threshold values were 1,192, 1,264, 1,438 and 1,294 for clusters 1, 2, 3 and 8, respectively. In total, 64 (9%), 54 (9%), 76 (12%) and 71 (10%) enhancers of these clusters had a score above the threshold and were, thus, considered as having a high OCT4 ChIP-seq signal on histone-free DNA. Conversely, 665 (91%), 546 (91%), 561 (88%) and 630 (90%) enhancers of clusters 1, 2, 3 and 8 had a low OCT4 ChIP-seq signal on histone-free DNA. Observations of IGV screenshots confirmed that all enhancers having an RPKM above the threshold displayed well-identified OCT4 ChIP-seq peaks on histone-free DNA, whereas those below the threshold had either low or no detectable signal (for example, Figs. 4g and 6f,g, Extended Data Fig. 4 and Supplementary Figs. 1 and 2). In contrast, the 50–80-bp subnucleosomes had a high OCT4 ChIP-seq signal at most enhancers. Inspection of IGV screenshots of all enhancers of clusters 1, 2, 3 and 8 revealed that even those displaying the lowest RPKM scores had a well-defined OCT4 ChIP-seq enrichment signal. Thus, OCT4 occupancy was constitutively high on 50–80-bp subnucleosomes, in sharp contrast to the low occupancy of the OCT4 motifs present within histone-free DNA.

TF motif detection in the DNA fragments purified from the top gradient fractions. We used MACS2 callpeak (version 2.2.7.1) to identify the genomic regions enriched in histone-free DNA fragments sequenced from the top gradient fractions (DNA purified from a pool of sucrose gradients 2–4). We set the minimal size for a peak to 40 bp. Then, motifs were detected with HOMER (version 4.11) findMotifsGenome.pl for the mouse genome. For Extended Data Fig. 9g, we selected 32 TF motifs with a significant *P* value ($P < 10^{-50}$) in the samples prepared from mouse ES cells expressing wild-type (WT) BRG1 (control samples). We noticed that the number of CTCF motifs detected was unaffected by the depletion of BRG1, in agreement with previous observations based on ATAC-seq experiments[42]. We, thus, chose to normalize the data according to the number of CTCF motifs detected in each sample. Using a homemade R script (R version 4.2.0 and gplots version 3.1.3), the number of CTCF motifs found in control (WT BRG1) samples was divided by the number of CTCF motifs detected in BRG1-depleted samples (https://github.com/Edmri/hist2D/releases/tag/v1.0.0). This coefficient was then applied to 31 other TF motifs to calculate the ratio between the number of motifs detected in chromatin samples prepared from BRG1-depleted and BRG1-expressing mouse ES cells.

SMF analysis. We used published SMF data in mouse ES cells to detect and quantify the presence of subnucleosomes at two examples of enhancers. The data analyzed in Extended Data Fig. 5 were from DNMT-TKO mouse ES cells[3]. We downloaded the selected datasets from the ArrayExpress E-MTAB-9123 series. We analyzed these datasets as described by the Krebs laboratory[72]. We considered that a footprint was indicative of a subnucleosome when at least three GpC or CpG dinucleotides were converted by the bisulfite reaction within the genomic interval of the subnucleosome. To distinguish the pairs of hemisomes from full-length nucleosomes, we considered that at least one CpG or GpC position should be unconverted within the linker region that separates the two hemisomes.

Reporting summary

Further information on research design is available in the Nature Portfolio Reporting Summary linked to this article.

Data availability

We deposited high-throughput sequencing data to the Gene Expression Omnibus (GEO) with accession numbers GSE210780, GSE210444, GSE209914 and GSE255089. The density graphs used in Figs. 4–7, Extended Data Fig. 4 and Supplementary Figs. 1 and 2 were deposited to a Zenodo data repository (https://doi.org/10.5281/zenodo.7056533)[73]. The following public ATAC-seq datasets were obtained from the GEO: mouse ES cells depleted of OCT4 for 24 h (GSM2341274, GSM2341275, GSM2341276, GSM2341284, GSM2341285 and GSM2341286) and 15 h (GSM5327548, GSM5327549, GSM5327538 and GSM5327539). Source data are provided with this paper.

Code availability

The exPATT.R program (https://github.com/jcaude/exPATT) detects OCT4 (or other TF) DNA-binding motifs and changes the genomic coordinates of each enhancer to have the OCT4 motif at its center. The code used to produce the V-plots can be obtained from https://github.com/Edmri/hist2D/releases/tag/v1.0.0.

References

51. Nora, E. P. et al. Targeted degradation of CTCF decouples local insulation of chromosome domains from genomic compartmentalization. *Cell* **169**, 930–944 (2017).

52. Laurette, P. et al. Transcription factor MITF and remodeller BRG1 define chromatin organisation at regulatory elements in melanoma cells. *eLife* **4**, e06857 (2015).
53. Tessarollo, L. Manipulating mouse embryonic stem cells. *Methods Mol. Biol.* **158**, 47–63 (2001).
54. Berlivet, S., Hmitou, I., Picaud, H. & Gérard, M. Efficient depletion of essential gene products for loss-of-function studies in embryonic stem cells. *Methods Mol. Biol.* **1622**, 91–100 (2017).
55. Ran, F. A. et al. Genome engineering using the CRISPR–Cas9 system. *Nat. Protoc.* **8**, 2281–2308 (2013).
56. Dignam, J. D., Lebovitz, R. M. & Roeder, R. G. Accurate transcription initiation by RNA polymerase II in a soluble extract from isolated mammalian nuclei. *Nucleic Acids Res.* **11**, 1475–1489 (1983).
57. Niwa, H., Miyazaki, J. & Smith, A. G. Quantitative expression of OCT-3/4 defines differentiation, dedifferentiation or self-renewal of ES cells. *Nat. Genet.* **24**, 372–376 (2000).
58. Ye, T. et al. seqMINER: an integrated ChIP-seq data interpretation platform. *Nucleic Acids Res.* **39**, e35 (2011).
59. Wasserman, W. W. & Sandelin, A. Applied bioinformatics for the identification of regulatory elements. *Nat. Rev. Genet.* **5**, 276–287 (2004).
60. Heintzman, N. D. et al. Histone modifications at human enhancers reflect global cell-type-specific gene expression. *Nature* **459**, 108–112 (2009).
61. Wang, H. et al. Widespread plasticity in CTCF occupancy linked to DNA methylation. *Genome Res.* **22**, 1680–1688 (2012).
62. Scruggs, B. S. et al. Bidirectional transcription arises from two distinct hubs of transcription factor binding and active chromatin. *Mol. Cell* **58**, 1101–1112 (2015).
63. Mölder, F. et al. Sustainable data analysis with Snakemake. *F1000Res* **10**, 33 (2021).
64. Ewels, P., Magnusson, M., Lundin, S. & Käller, M. MultiQC: summarize analysis results for multiple tools and samples in a single report. *Bioinformatics* **32**, 3047–3048 (2016).
65. Wingett, S. W. & Andrews, S. FastQ Screen: a tool for multi-genome mapping and quality control. *F1000Res* **7**, 1338 (2018).
66. Chen, S., Zhou, Y., Chen, Y. & Gu, J. fastp: an ultra-fast all-in-one FASTQ preprocessor. *Bioinformatics* **34**, i884–i890 (2018).
67. Langmead, B. & Salzberg, S. L. Fast gapped-read alignment with Bowtie 2. *Nat. Methods* **9**, 357–359 (2012).
68. Ramírez, F. et al. deepTools2: a next generation web server for deep-sequencing data analysis. *Nucleic Acids Res.* **44**, W160–W165 (2016).
69. Quinlan, A. R. & Hall, I. M. BEDTools: a flexible suite of utilities for comparing genomic features. *Bioinformatics* **26**, 841–842 (2010).
70. Bailey, T. L. et al. MEME Suite: tools for motif discovery and searching. *Nucleic Acids Res.* **37**, W202–W208 (2009).
71. Fornes, O. et al. JASPAR 2020: update of the open-access database of transcription factor binding profiles. *Nucleic Acids Res.* **48**, D87–D92 (2020).
72. Kleinendorst, R. W. D., Barzaghi, G., Smith, M. L., Zaugg, J. B. & Krebs, A. R. Genome-wide quantification of transcription factor binding at single-DNA-molecule resolution using methyl-transferase footprinting. *Nat. Protoc.* **16**, 5673–5706 (2021).
73. Nocente, M., Mesihovic Karamitsos, A., Drouineau, E., Chantalat, S. & Gérard, M. cBAF generates subnucleosomes that expand OCT4 binding and function beyond DNA motifs at enhancers. *Zenodo* https://doi.org/10.5281/zenodo.7056533 (2024).

Acknowledgements

We thank A. Goldar, A. Leforestier, J. M. Victor, S. Khochbin, K. Yen and S. Mahony for discussions, E. Nora and B. Bruneau (Gladstone Institute of Cardiovascular Disease, San Francisco, CA, USA) for the E14Tg2a-Tir1 cell line, I. Davidson (IGBMC, Illkirch, France) for the 501Mel cell line and discussions and C. Mann for reading the manuscript. This work was supported by the INCA (2017-1-PL BIO-02-CEA-1), Revive (Investissement d'Avenir; ANR-10-LABX-73), ANR (ANR-17-CE12-0001-01), PRC/PICS07434 and Fondation ARC pour la recherche sur le cancer (www.fondation-arc.org) to M.G. The CNRGH sequencing platform was supported by France Génomique (ANR-10-INBS-09). The funders had no role in study design, data collection and analysis, decision to publish or preparation of the manuscript.

Author contributions

M.C.N. designed, performed and analyzed the experiments and bioinformatic analyses. A.M.K. designed, performed and analyzed the experiments. E.D. performed the majority of bioinformatic analyses. M.S. designed, performed and analyzed the experiments. W.A. performed and analyzed the EM experiments. C.D., F.R. and MK performed the experiments. J.-C.A. performed and analyzed the size-exclusion chromatography experiments. H.P. assisted with the experiments. O.A. performed the bioinformatic analyses. J.-C.A. designed tools for the bioinformatic analyses. N.G. supervised the EM experimentation and analysis. F.O. performed modeling of the split nucleosome and contributed to data interpretation. S.C. designed and analyzed the experiments. M.G. conceptualized the project, designed, performed and analyzed the experiments and wrote the manuscript.

Competing interests

The authors declare no competing interests.

Additional information

Extended data is available for this paper at https://doi.org/10.1038/s41594-024-01344-0.

Supplementary information The online version contains supplementary material available at https://doi.org/10.1038/s41594-024-01344-0.

Correspondence and requests for materials should be addressed to Matthieu Gérard.

Peer review information *Nature Structural & Molecular Biology* thanks Sebastian Eustermann and the other, anonymous, reviewer(s) for their contribution to the peer review of this work. Peer reviewer reports are available. Primary Handling Editor: Dimitris Typas, in collaboration with the *Nature Structural & Molecular Biology* team.

https://doi.org/10.1038/s41594-024-01344-0

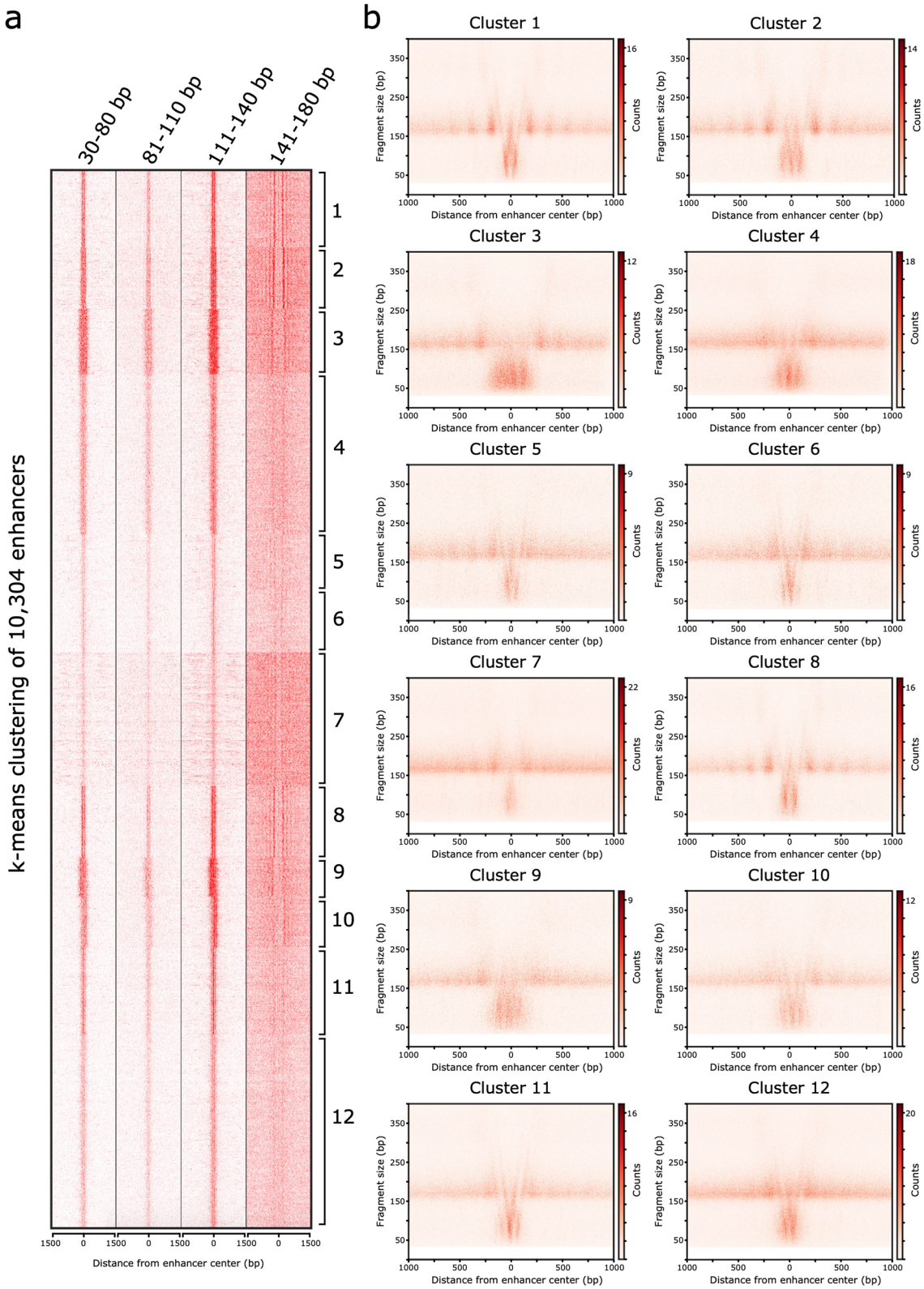

Extended Data Fig. 1 | Integrated nucleosomal and subnucleosomal organization at enhancers. a, Heat map of histone H3 enrichment at 10,304 enhancers determined by MNase-ChIP-seq (left panel). The four columns display histone H3-immunoprecipitated DNA fragments of different size categories. Enhancers were separated into 12 groups by k-means clustering. The enhancer center corresponds to the middle of its DNase I hypersensitivity peak. **b**, For each cluster, the distribution of histone H3 ChIP-seq fragments was analyzed by two-dimensional maps (V-plot), showing the distribution and density of DNA fragments immunoprecipitated with antibodies as a function of the position of their mid-point on the genome (x-axis), and their length (y-axis). The color scale corresponds to the number of DNA fragments. Four biological replicates were performed for each ChIP-seq experiment.

https://doi.org/10.1038/s41594-024-01344-0

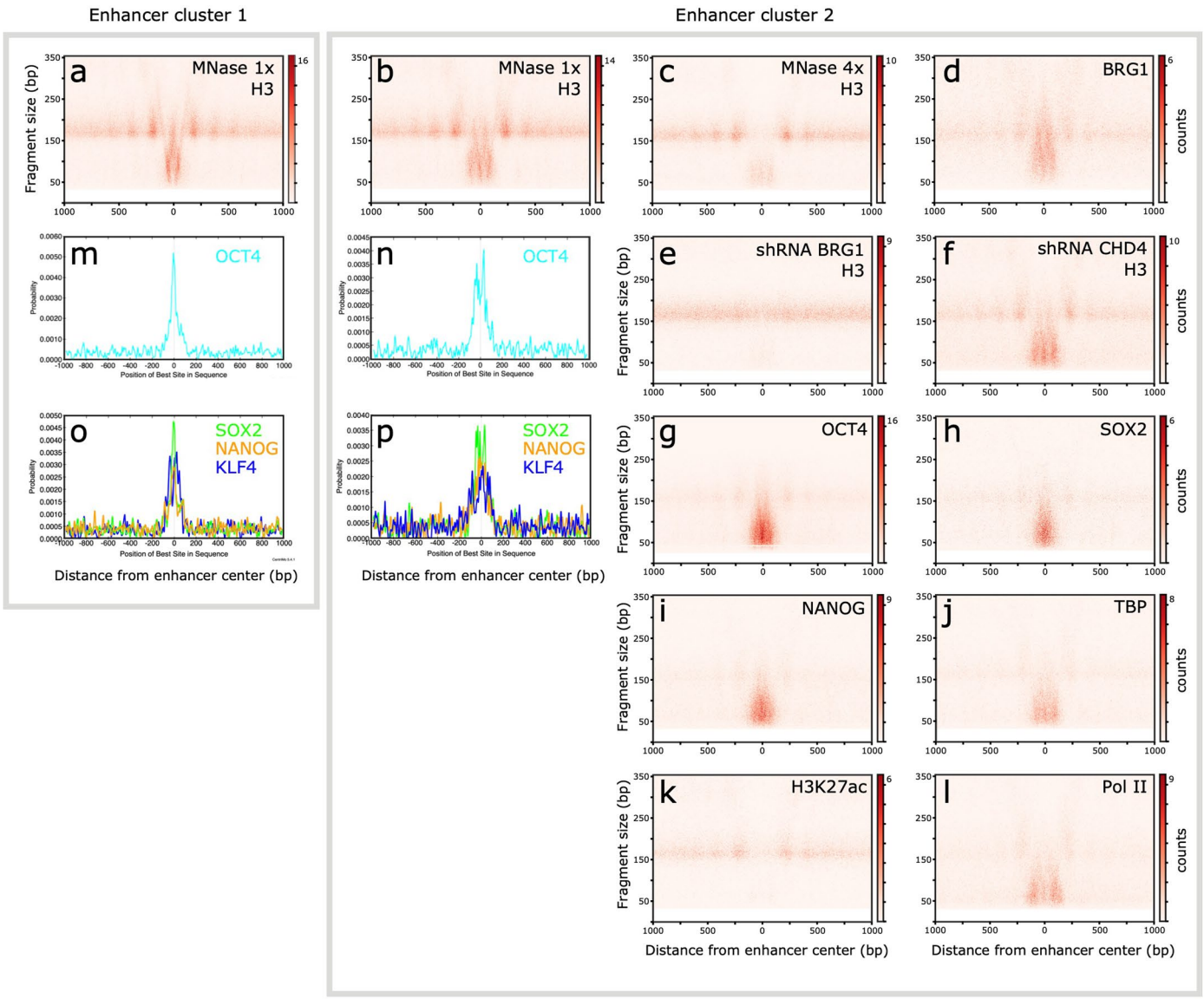

Extended Data Fig. 2 | Nucleosomal and subnucleosomal organization of cluster 2 enhancers. The left and right panels are dedicated to enhancers of clusters 1 and 2, respectively. **a**, **b**, V-plots of histone H3 ChIP-seq fragments spanning ± 1000 bp from the center of enhancer clusters 1 (**a**) and 2 (**b**). **c**, same as in (**b**) using a four-fold excess of MNase. **d**, V-plot of BRG1 ChIP-seq. **e**-**f**, V-plots of histone H3 ChIP-seq in mESCs depleted of either BRG1 (**e**) or CHD4 (**f**), using shRNAs. **g**-**l**, V-plots of OCT4 (**g**), SOX2 (**h**), NANOG (**i**), TBP (**j**), H3K27ac (**k**) and Pol II (**l**) ChIP-seq. The standard MNase dose was used in all panels except in (**c**). Two biological replicates were performed for each ChIP-seq experiment. **m**-**p**, Enrichment for OCT (**m**, **n**), SOX2 (**o**, **p**), NANOG (**o**, **p**), and KLF4 (**o**, **p**) consensus BS, defined by centrimo software, within the same genomic intervals as in (**a**) and (**b**).

https://doi.org/10.1038/s41594-024-01344-0

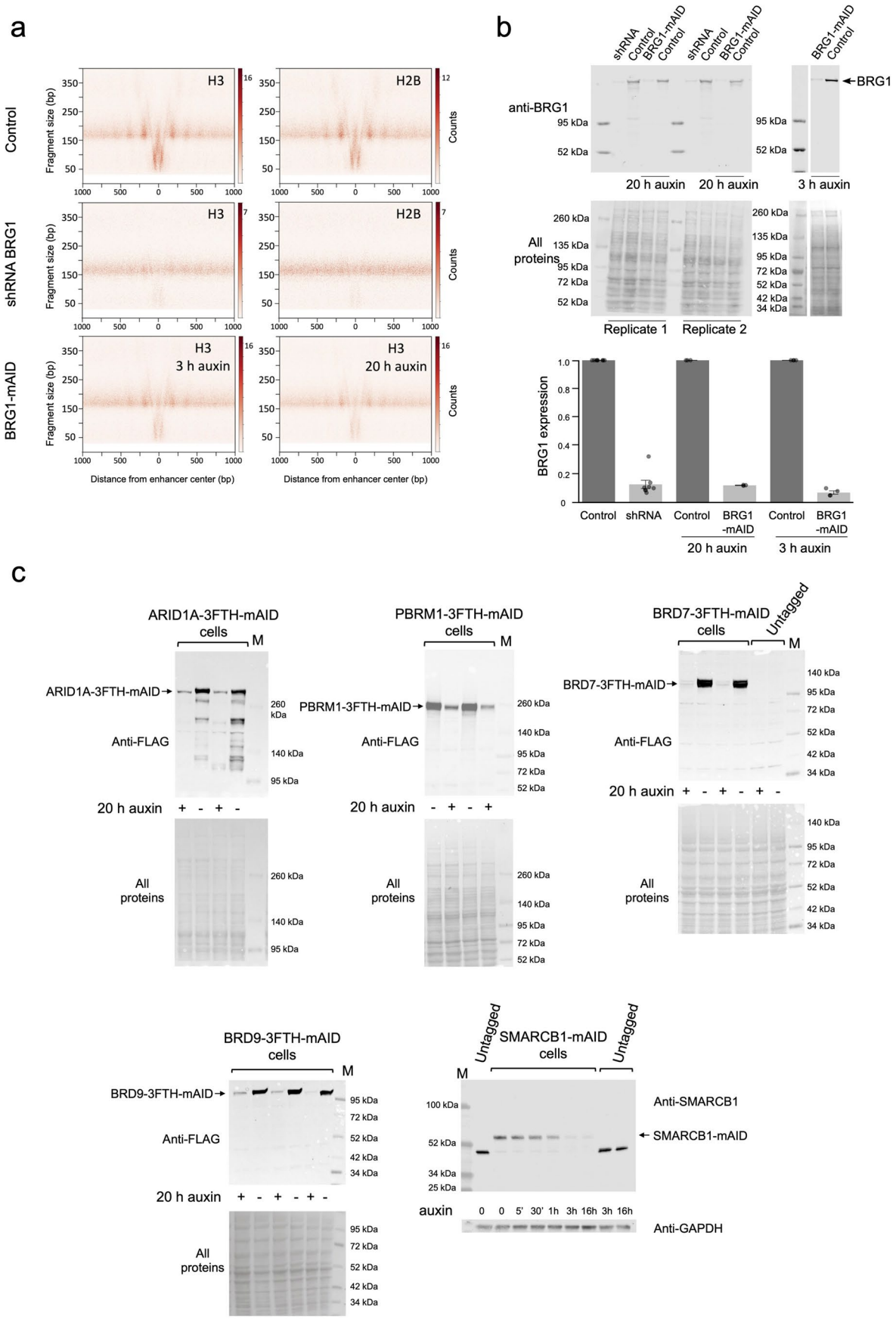

Extended Data Fig. 3 | See next page for caption.

https://doi.org/10.1038/s41594-024-01344-0

Extended Data Fig. 3 | Depletion of BRG1 using shRNA or the auxin system induces similar perturbations at enhancers. a, V-plots of ChIP-seq fragments spanning ± 1000 bp from the center of cluster 1 enhancers. H3 and H2B ChIP-seq were performed on MNase-digested chromatin prepared from mESCs expressing wild-type BRG1 (top panels) or after shRNA-mediated depletion of BRG1 (middle panels). For the H3 ChIP-seq, depletion of BRG1 was obtained using a shRNA distinct from the shRNA used in Fig. 1. H3 ChIP-seq was also performed using chromatin prepared from mESCs depleted of BRG1 using the AID system by either 3 h or 20 h of treatment with 1 mM auxin (bottom panels). Two biological replicates were performed for each ChIP-seq experiment. **b**, Western blot analysis of protein extracts obtained from mESCs transfected with a plasmid expressing a shRNA targeting BRG1, mESCs depleted of BRG1 using the AID system for either 20 or 3 h, and untagged control cells. Ponceau staining of the membrane is shown as a loading control. The bottom panel shows the means ± sd of BRG1 protein levels in replicate experiments (n shRNA = 8, n 20 h auxin = 3 and n 3 h auxin = 4). **c**, Western blot analysis of protein extracts from mESCs depleted of ARID1A, PBRM1, BRD7, BRD9, or SMARCB1 using the AID system.

https://doi.org/10.1038/s41594-024-01344-0

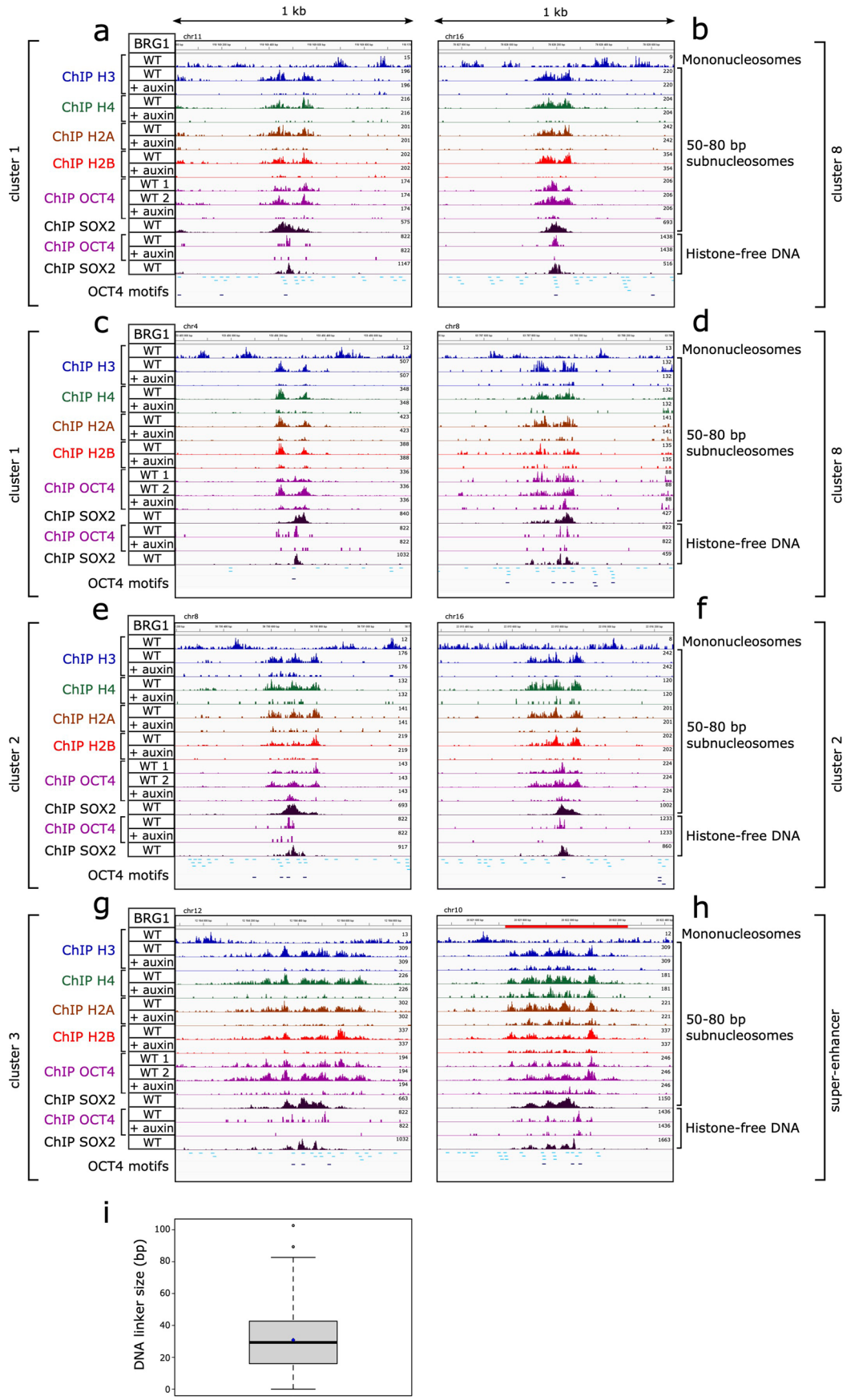

Extended Data Fig. 4 | See next page for caption.

https://doi.org/10.1038/s41594-024-01344-0

Extended Data Fig. 4 | OCT4 enrichment at enhancers coincides with the position of 50-80 bp subnucleosomes. a-**g**, Density graphs showing the distribution of ChIP DNA fragment centers at representative examples of enhancers from clusters 1 (**a**, **c**), 2 (**e**, **f**), 3 (**g**) and 8 (**b**, **d**). The top lane shows the positions of canonical nucleosomes detected by histone H3 ChIP-seq of sucrose gradient fractions 11 and 13. The next eight lanes show the distribution of 50-80 bp subnucleosomes, revealed by histone H3, H4, H2A and H2B ChIP-seq of sucrose gradient fractions 5-6. The following lanes show the OCT4 or SOX2 ChIP-seq signal on 50-80 bp subnucleosomes or histone-free DNA from the top gradient fractions. Experiments were performed with chromatin of cells expressing wild-type (WT) BRG1 or depleted of BRG1 using the AID system (+ auxin). Two distinct antibodies against OCT4 were used in lanes WT 1 and 2. High ($p = 0.001$) and low ($p = 0.01$) confidence OCT4 consensus binding motifs are indicated in black and blue, respectively. Two biological replicates were performed for each ChIP-seq experiment. **h**, Example of an enhancer present within a super-enhancer. **i**, Size distribution of the DNA linker that separates the two 50-80 bp subnucleosomes in single-module enhancers ($n = 496$, median = 29 bp). The box ranges from the first to the third quartile, the line across the box indicates the median, the blue diamond the mean, the whiskers show the maximum and minimum values of the distribution, and open circles represent outliers.

https://doi.org/10.1038/s41594-024-01344-0

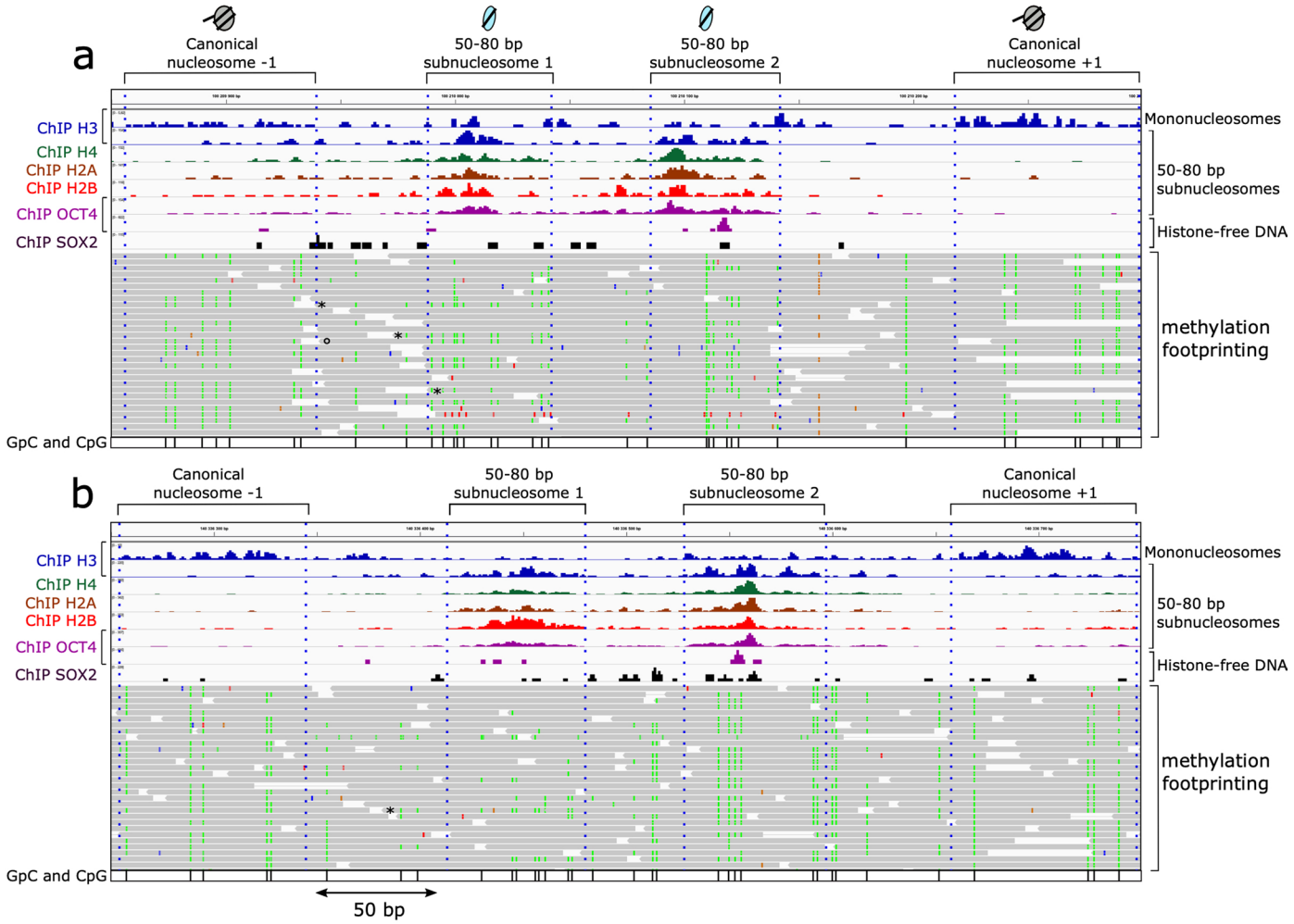

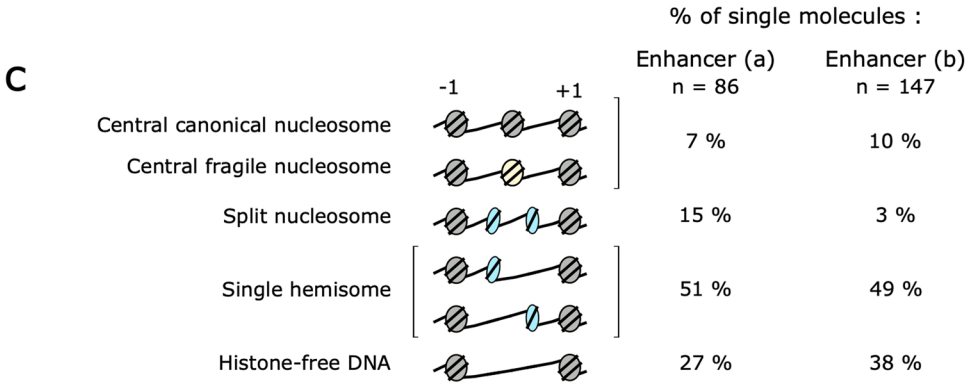

Extended Data Fig. 5 | Methylation footprinting detects the 50-80 bp subnucleosomes at enhancers. a, **b**, Two representative enhancers were analyzed by single-molecule footprinting (SMF). The upper part of each panel displays density graphs of the distribution of ChIP DNA fragment centers. The top five lanes show the positions of canonical nucleosomes and subnucleosomes, as in Fig. 5. The next three lanes show the OCT4 or SOX2 ChIP-seq signal on 50-80 bp subnucleosomes or histone-free DNA, as indicated. The lower part of each panel reveals a subset of the single DNA molecules (grey bars) from the SMF datasets. The green and red marks indicate the genomic positions of the C bases converted by the bisulfite reaction at GpC and CpG dinucleotides. Bisulfite conversion reveals the GpC and CpG protected *in vivo* (footprints). In contrast, unconverted C (grey color) at the same dinucleotide positions indicate that the DNA was accessible *in vivo* (absence of footprint). Other colors indicate polymorphisms linked either to natural genetic variations or sequencing errors. The positions of all GpC and CpG dinucleotides are indicated in black at the bottom of each panel. Asterisks indicate examples of molecules bearing a methylation pattern consistent with a split nucleosome: protection was detected at the level of each subnucleosome but was absent or partial in the linker DNA between the two subnucleosomes. A large footprint covering the locations of the two hemisomes and the linker region reveals the same region's occupancy by a full-length nucleosome (an example is indicated by a black circle). **c**, Interpretation of the footprints observed at each enhancer. Split nucleosomes represent 15% or 3% of the patterns detected for enhancers (**a**) and (**b**), respectively. The most frequent pattern corresponds to a single hemisome with an adjacent region of histone-free DNA (~ 50% of single molecules). Accessible DNA regions (histone-free DNA) represent 27% or 38% of the patterns detected.

https://doi.org/10.1038/s41594-024-01344-0

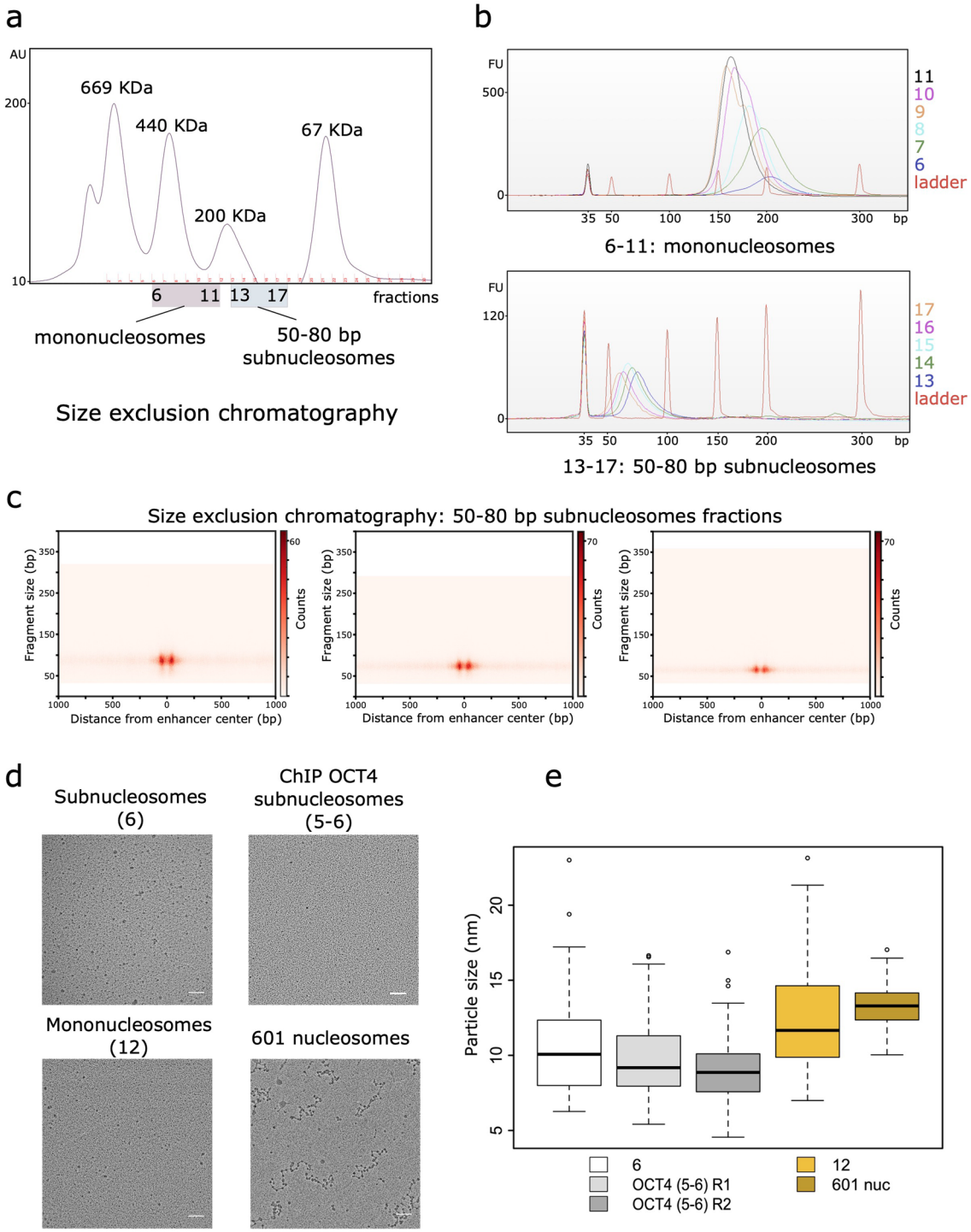

Extended Data Fig. 6 | Size analysis of 50-80 bp subnucleosomes. a-b, Size exclusion chromatography. 50-80bp subnucleosomes (sucrose gradient fraction 6) and mononucleosomes (sucrose gradient fraction 11) were independently fractionated onto a Superdex 200 column. **a**, Elution of the mononucleosomes (Superdex 200 fractions 6-11) occurs before that of 50-80 subnucleosomes (Superdex 200 fractions 13-17). The elution of protein size markers is shown for comparison. **b**, The DNA prepared from the mononucleosomes (top) and the 50-80 bp subnucleosomes (bottom) eluted from the Superdex 200 column were analyzed by high-sensitivity DNA electrophoresis. Numbers on the right side of the panels indicate the Superdex 200 fractions. **c**, V-plot spanning ±1000 bp from the cluster 1 enhancer center of the subnucleosomal particles purified in three consecutive column fractions. **d**, **e**, EM analysis of 50-80 bp subnucleosomes. **d**, The top panels show 50-80 bp subnucleosomes from sucrose gradient fraction 6 and particles from a pool of fractions 5-6 immunopurified with OCT4 antibodies. The bottom panels display mononucleosomes from sucrose fraction 12 and nucleosomes assembled *in vitro* on 601 DNA arrays. **e**, Boxplot showing particle size distribution in the fractions indicated in (**d**). The line across each box indicates the median, boxes indicate the first and third quartile, whiskers the distribution's maximum and minimum values, and open circles outliers. Two independent OCT4 immunopurification experiments (R1 and R2) were analyzed.

https://doi.org/10.1038/s41594-024-01344-0

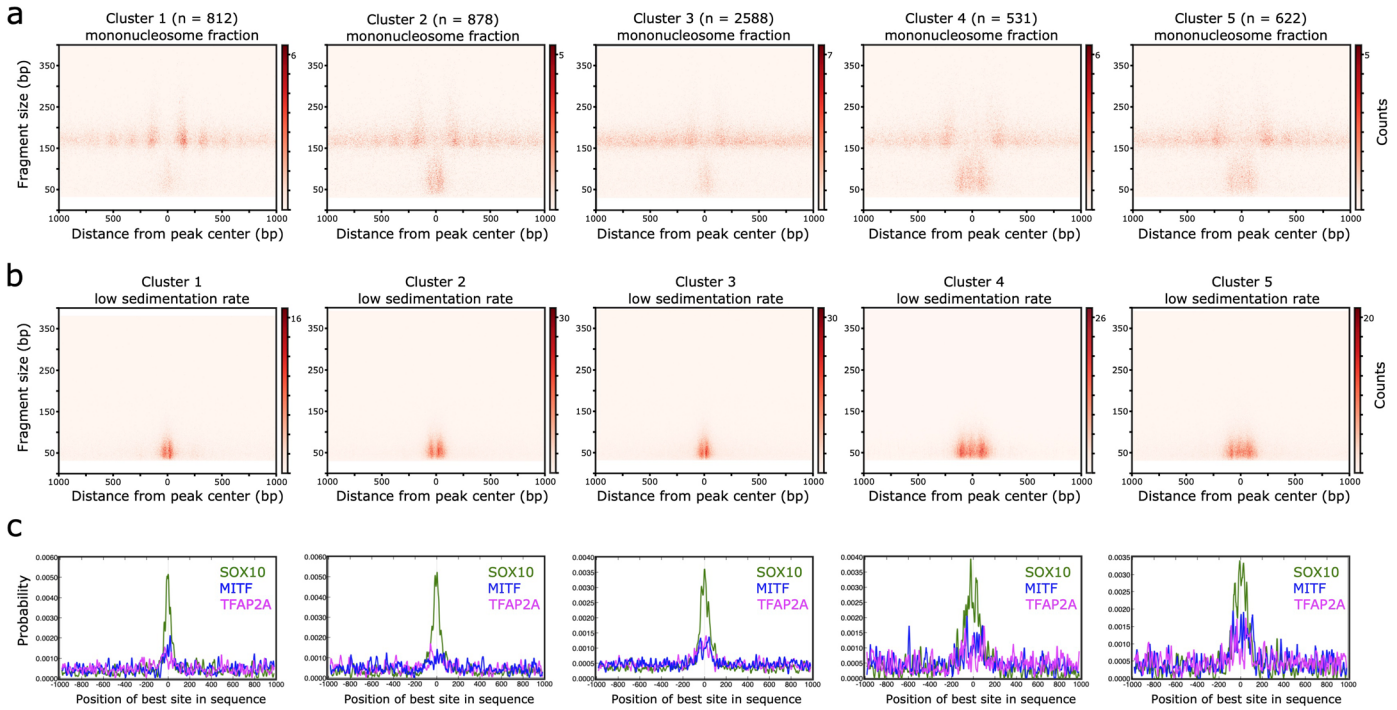

Extended Data Fig. 7 | The subnucleosomal organization of enhancers is conserved in human cells. MNase-digested chromatin prepared from human melanoma 501Mel cells was centrifugated through a 10-30% sucrose gradient, as in Fig. 2. We carried out histone H3 ChIP-seq experiments with gradient fractions containing either mononucleosomes or 50-80 bp subnucleosomes. Two biological replicates were performed for each ChIP-seq experiment. We used these ChIP-seq datasets for k-means clustering of putative enhancers based on nucleosome and subnucleosome distribution patterns. We isolated five clusters of putative enhancers. **a**, **b**, V-plots of histone H3 ChIP-seq experiments performed with gradient fractions containing mononucleosomes (**a**) or 50-80 bp subnucleosomes (**b**), spanning ± 1000 bp from the center of putative enhancers from each of the five clusters. **c**, Enrichment for SOX10, MITF and TFAP2A consensus BS, defined by Centrimo software, within the same genomic intervals as in (**a**, **b**).

https://doi.org/10.1038/s41594-024-01344-0

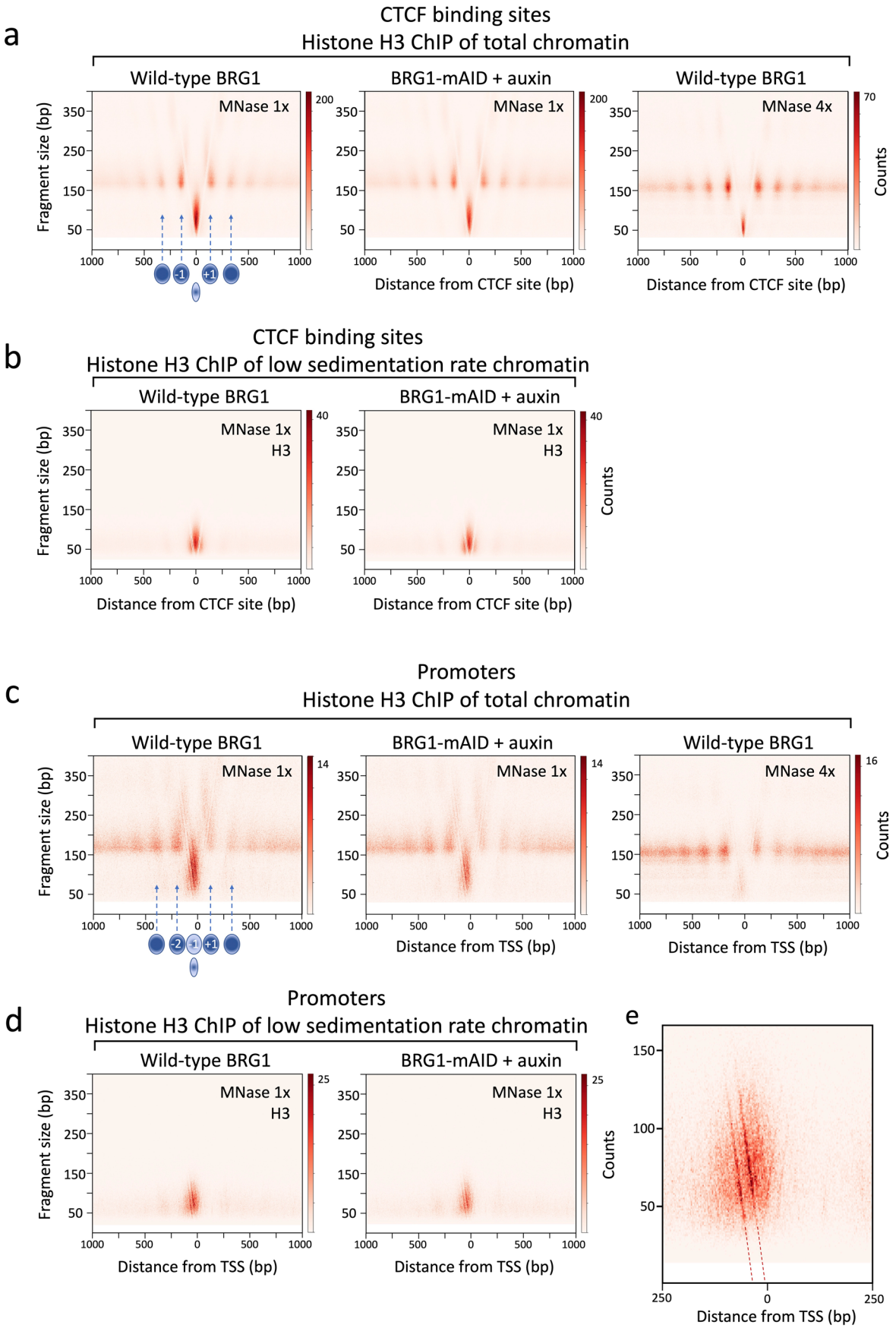

Extended Data Fig. 8 | See next page for caption.

https://doi.org/10.1038/s41594-024-01344-0

Extended Data Fig. 8 | Nucleosomal and subnucleosomal organization at promoters and CTCF sites. a, **c**, V-plots of histone H3 ChIP-seq fragments spanning ±1000 bp from CTCF sites (**a**) and TSSs (**c**), using chromatin prepared from mESCs expressing wild-type BRG1 or from cells depleted of BRG1 using the AID system. Chromatin digestion was performed with the standard MNase dose (left and mid panels) or a four-fold excess (right panel). **b**, **d**, MNase-fragmented chromatin, prepared from mESCs expressing wild-type BRG1, or from cells depleted of BRG1 using the AID system, was centrifugated through a sucrose gradient as in Fig. 2. V-plots of histone H3 ChIP-seq experiments performed with sucrose gradient fractions 5-6 reveal 50-80 bp subnucleosomes at CTCF sites (**b**) and promoters (**d**). At least two biological replicates were performed for each ChIP-seq experiment. The schematic illustrations in (**a**) and (**c**) indicate the positions of nucleosomes and subnucleosomal particles. **e**, Enlargement of **d** (left panel). The two left diagonals result from fragments cleaved precisely on the left and right sides of a region protected from MNase digestion. Extrapolation of the diagonals to y = 0 identifies this region as the -35 to -5 bp interval relative to the TSS. Low molecular weight components of the preinitiation complex might confer this protection.

https://doi.org/10.1038/s41594-024-01344-0

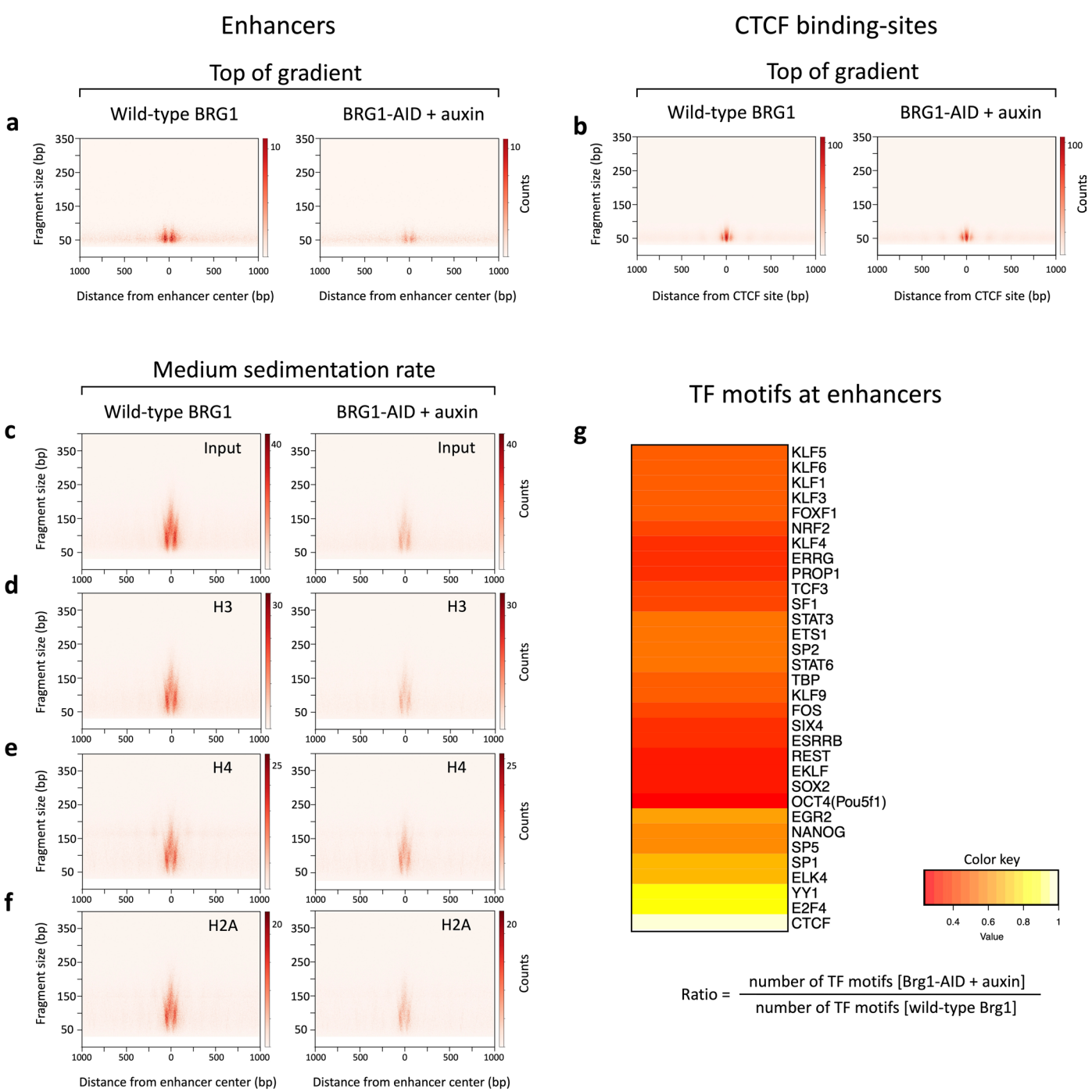

Extended Data Fig. 9 | BRG1 depletion alters the production of histone-free DNA and medium sedimentation rate subnucleosomes at enhancers. Chromatin, prepared from mESCs expressing wild-type BRG1, or from cells depleted of BRG1 using the AID system, was centrifugated through a sucrose gradient as in Fig. 2. **a**, **b** V-plots of DNA fragments purified from the top gradient fractions spanning ± 1000 bp from the enhancer cluster 1 center (**a**), or CTCF sites (**b**). **c**, V-plots of DNA fragments purified from medium sedimentation rate sucrose gradient fractions (pool of fractions 7-8-9) spanning ± 1000 bp from enhancer cluster 1 center. **d**-**f**, V-plots of histone H3 (**d**), H4 (**e**) and H2A (**f**) ChIP-seq experiments performed with the pool of medium sedimentation rate fractions indicated in (**c**) as input. Two biological replicates were performed for each ChIP-seq experiment. The color scales of each pair of panels were adjusted according to the total number of DNA fragments obtained in each dataset. **g**, TF motif detection with the HOMER tool on the DNA fragments revealed in (**a**). The ratio between the number of TF motifs detected in BRG1-depleted versus BRG1-expressing samples was calculated and visualized as a heatmap. The number of CTCF motifs, which was invariant, was used for normalization.

https://doi.org/10.1038/s41594-024-01344-0

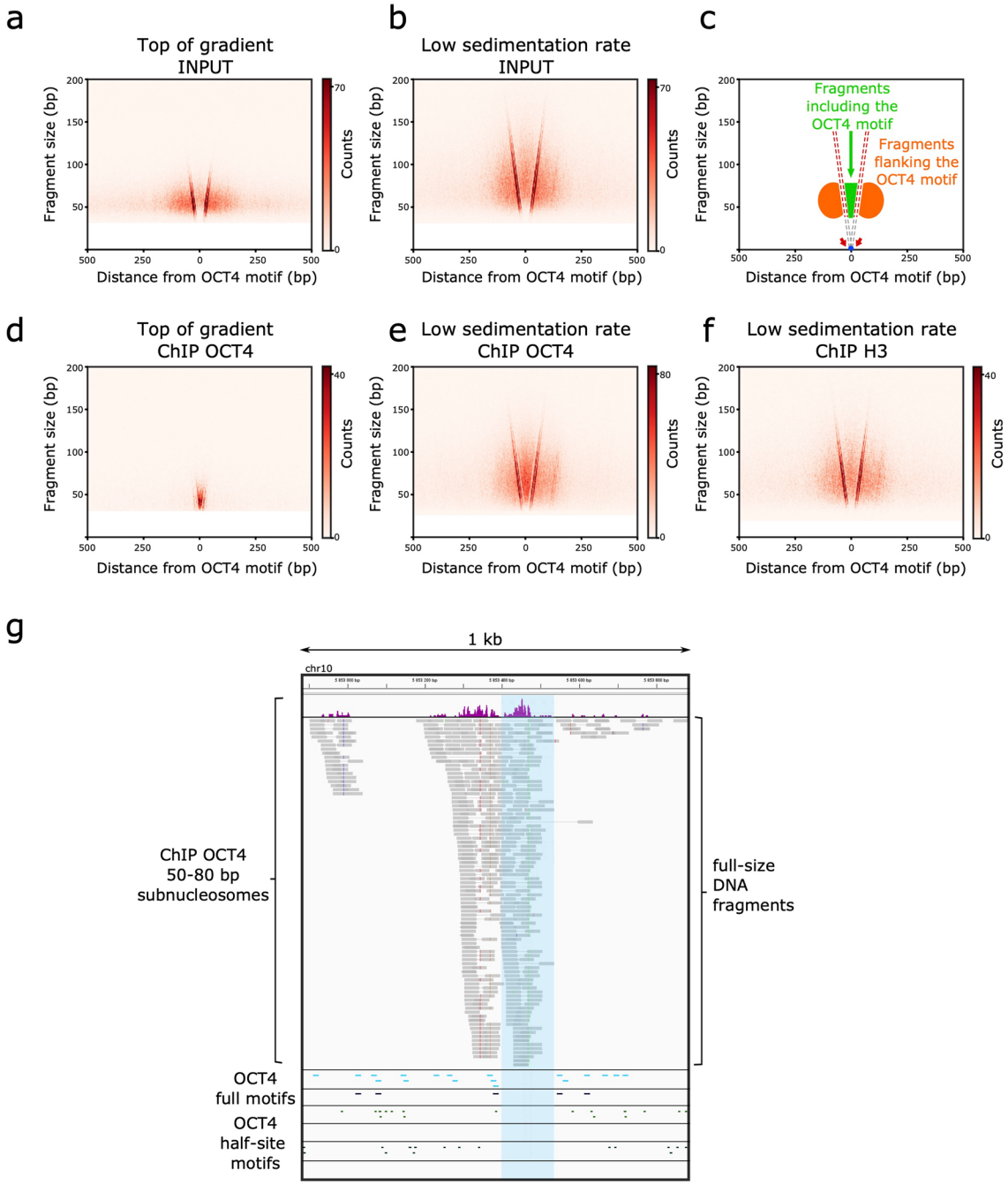

Extended Data Fig. 10 | OCT4 interacts with 50-80 bp subnucleosomes lacking its consensus binding motif. a-**b** and **d**-**f**, V-plots of enhancers centered on their OCT4 motif. Enhancers containing a single OCT4 consensus binding motif were selected for this analysis (n = 1,302). MNase-fragmented chromatin, prepared from mESCs expressing wild-type BRG1, was centrifugated through a sucrose gradient as in Fig. 2. **a**-**b**, V-plots of DNA fragments purified from the top gradient (**a**) and low sedimentation rate (**b**) fractions. **c**, Schematic diagram illustrating key features of V-plots centered on OCT4 motifs. The green area corresponds to MNase-released DNA fragments containing the central OCT4 consensus binding motif. The two orange regions are defined by adjacent or proximal DNA fragments that do not include the OCT4 motif. The red arrows indicate MNase hypersensitive sites on each side of the OCT4 motif, which are at the origin of the diagonals forming the 'V' on each map. **d**-**e**, Maps of OCT4 ChIP-seq experiments of the top gradient (**d**) and low sedimentation rate gradient (**e**) fractions, using as input the fractions shown in (**a**, **b**). **f**, Map of histone H3 ChIP-seq experiment of low sedimentation rate gradient fractions. **g**, Example of a single-module enhancer. The top lane shows in purple the density graph of the DNA fragment centers from OCT4 ChIP-seq 50-80 bp subnucleosomes. Two biological replicates were performed for each ChIP-seq experiment. The genomic position of each individually sequenced fragment is indicated below in grey. Blue shading highlights the DNA fragments that do not contain OCT4 motifs. High (p = 0.001) and low (p = 0.01) stringency OCT4 consensus binding motifs are indicated in black and blue, respectively. The next four lanes show in green the positions of low (p = 0.01) and high (p = 0.001) stringency OCT4 POU_S (top two lanes) and POU_{HD} (bottom) half-sites; no half-site motif was detected at high stringency in the 1 kb interval.

nature portfolio

Corresponding author(s): Matthieu GERARD

Last updated by author(s): 04/23/2024

Reporting Summary

Nature Portfolio wishes to improve the reproducibility of the work that we publish. This form provides structure for consistency and transparency in reporting. For further information on Nature Portfolio policies, see our Editorial Policies and the Editorial Policy Checklist.

Statistics

For all statistical analyses, confirm that the following items are present in the figure legend, table legend, main text, or Methods section.

n/a	Confirmed
☐	☒ The exact sample size (*n*) for each experimental group/condition, given as a discrete number and unit of measurement
☐	☒ A statement on whether measurements were taken from distinct samples or whether the same sample was measured repeatedly
☐	☒ The statistical test(s) used AND whether they are one- or two-sided *Only common tests should be described solely by name; describe more complex techniques in the Methods section.*
☒	☐ A description of all covariates tested
☐	☒ A description of any assumptions or corrections, such as tests of normality and adjustment for multiple comparisons
☐	☒ A full description of the statistical parameters including central tendency (e.g. means) or other basic estimates (e.g. regression coefficient) AND variation (e.g. standard deviation) or associated estimates of uncertainty (e.g. confidence intervals)
☐	☒ For null hypothesis testing, the test statistic (e.g. *F*, *t*, *r*) with confidence intervals, effect sizes, degrees of freedom and *P* value noted *Give P values as exact values whenever suitable.*
☒	☐ For Bayesian analysis, information on the choice of priors and Markov chain Monte Carlo settings
☒	☐ For hierarchical and complex designs, identification of the appropriate level for tests and full reporting of outcomes
☒	☐ Estimates of effect sizes (e.g. Cohen's *d*, Pearson's *r*), indicating how they were calculated

Our web collection on statistics for biologists contains articles on many of the points above.

Software and code

Policy information about availability of computer code

Data collection

Illumina RTA 2.4.11 or 2.11.3 (NextSeq550) and bcl2fastq Conversion Software v2.20.0.422 were used for basecalling and demultiplexing.

Data analysis

Data analysis was performed using Snakemake, Conda and in-house python scripts (https://github.com/Edmri/hist2D/releases/tag/v1.0.0).
Genome versions were Mus musculus mm9 and Homo sapiens hg38.
MNase ChIP-seq reads were controlled using FastQC 0.11.9, fastqScreen 0.14.0 and trimmed using fastp 0.20.1. Reads were mapped by bowtie2 2.4.2. Low quality reads, unmapped reads and duplicates were removed using Picard 2.23.8 and Samtools 1.11. The RPKM normalized genomic coverage was calculated with Deeptools 3.5.0 for MNase data.
Peaks for IGV visualizations used MACS2 2.2.7.1 and V-plots vizualizations used a home-made script and Bedtools 2.29.2 to convert a bam file containing paired-end mapped reads to a bed file containing DNA fragments.
Transcription factors motif detection used MACS2 2.2.7.1, HOMER 4.11, R 4.2.0 and gplots 3.1.3. (https://github.com/Edmri/hist2D/releases/tag/v1.0.0)
Detection of transcription factor motifs at enhancers was performed using Meme 5.3.0.
We developed the exPATT.R tool (https://github.com/jcaude/exPATT) to detect OCT4 DNA binding motifs and change the genomic coordinates of each enhancer to have the OCT4 motif at its center.

For manuscripts utilizing custom algorithms or software that are central to the research but not yet described in published literature, software must be made available to editors and reviewers. We strongly encourage code deposition in a community repository (e.g. GitHub). See the Nature Portfolio guidelines for submitting code & software for further information.

Data

Policy information about availability of data

All manuscripts must include a data availability statement. This statement should provide the following information, where applicable:

- Accession codes, unique identifiers, or web links for publicly available datasets
- A description of any restrictions on data availability
- For clinical datasets or third party data, please ensure that the statement adheres to our policy

We deposited high-throughput sequencing data at the Gene Expression Omnibus with accession GSE210780, GSE210444, GSE209914, and GSE255089. Density graphs have been deposited at the Zenodo Data repository: https://zenodo.org/record/7056534. The following public ATAC-seq datasets were obtained from GEO: mESCs depleted of OCT4 during 24h (GSM2341274, GSM2341275, GSM2341276, GSM2341284, GSM2341285, GSM2341286) and 15h (GSM5327548, GSM5327549, GSM5327538, GSM5327539). We used the Jaspar 2020 and Hocomoco v11 public databases.

Human research participants

Policy information about studies involving human research participants and Sex and Gender in Research.

Reporting on sex and gender	not applicable
Population characteristics	not applicable
Recruitment	not applicable
Ethics oversight	not applicable

Note that full information on the approval of the study protocol must also be provided in the manuscript.

Field-specific reporting

Please select the one below that is the best fit for your research. If you are not sure, read the appropriate sections before making your selection.

☒ Life sciences ☐ Behavioural & social sciences ☐ Ecological, evolutionary & environmental sciences

For a reference copy of the document with all sections, see nature.com/documents/nr-reporting-summary-flat.pdf

Life sciences study design

All studies must disclose on these points even when the disclosure is negative.

Sample size	We indicate sample sizes in the figure legends and the Methods section. We did not predetermine the sample size. For each analysis, we used all the enhancers composing each subgroup. In the Methods section, we describe the criteria used to define the subgroups of each analysis. The large number of enhancers (from 230 to 3266) composing each subgroup ensures that each of them is representative of a significant nucleosomal/subnucleosomal organization and that the conclusion of the analysis can be extended to the majority of the enhancers of the mESC or Mel501 genomes.
Data exclusions	no dataset was excluded
Replication	Between 2 and 4 biological replicates were performed for each experimental situation, as indicated in the Methods section.
Randomization	Randomization was not required for ChIP-seq experiments. ChIP-seq experiments were realized using the same conditions and only modifying a single factor per analysis: nature of the antibody, depletion of a chromatin remodeler, or a transcription factor. The pull-down experiments used the same established conditions with negative controls.
Blinding	Blinding was not applicable to this study. Sequencing biases and artifacts were filtered using dedicated software, and the data were analyzed using either 2D graphs (V-plots), examination of the density graphs at individual enhancers, and average profiling. Prior to comparison, the data were normalized to the sequencing depth. In each analysis, we assessed the qualitative and quantitative differences (or the absence of differences) in the distribution of the ChIP-seq DNA fragments detected in each subgroup of enhancers, promoters, or CTCF sites. All images (V-plots, density graphs, or average profiles) were generated using software with neutral, unbiased quantification features.

Reporting for specific materials, systems and methods

We require information from authors about some types of materials, experimental systems and methods used in many studies. Here, indicate whether each material, system or method listed is relevant to your study. If you are not sure if a list item applies to your research, read the appropriate section before selecting a response.

Materials & experimental systems

n/a	Involved in the study
☐	☒ Antibodies
☐	☒ Eukaryotic cell lines
☒	☐ Palaeontology and archaeology
☒	☐ Animals and other organisms
☒	☐ Clinical data
☒	☐ Dual use research of concern

Methods

n/a	Involved in the study
☐	☒ ChIP-seq
☒	☐ Flow cytometry
☒	☐ MRI-based neuroimaging

Antibodies

Antibodies used

H2A (rabbit polyclonal, ab18255, Abcam), 5 µg/ChIP
H2B (rabbit polyclonal, ab1790, Abcam), 5 µg/ChIP
H3 (rabbit polyclonal, ab1791, Abcam), 5 µg/ChIP
H4 (rabbit polyclonal, ab7311, Abcam), 5 µg/ChIP
H3K27ac (rabbit polyclonal, ab4729), 5 µg/ChIP
Nanog (rabbit polyclonal, RCAB-001P, Reprocell), 20 µg/ChIP
Oct4 (goat polyclonal, sc-8628, Santa Cruz Biotechnology), 20 µg/ChIP
Oct4 (mouse monoclonal C-10, sc-5279, Santa Cruz Biotechnology), 20 µg/ChIP
Oct4 (goat polyclonal, MBS420786, myBioSource), 20 µg/ChIP
RNA Pol II (mouse monoclonal F-12, sc-55492, Santa Cruz Biotechnology), 20 µg/ChIP
Sox2 (goat polyclonal, sc-17320, Santa Cruz Biotechnology), 20 µg/ChIP
TBP (mouse monoclonal, ab51841, abcam), 20 µg/ChIP
Brg1 (rabbit monoclonal, ab110641, Abcam), 0.2 µg/ml for western blotting
Flag (mouse monoclonal M2, F1804, Sigma-Aldrich), dilution 1/1000 for western blotting
IgG, no known specificity (rabbit polyclonal, ab37415, Abcam), 20 µg/ChIP
Smarcb1 (rabbit monoclonal, #8745 Cell Signaling Technology), dilution 1/1000 for western blotting

Validation

Antibodies were validated by western blotting.
Antibodies were also independently validated by the manufacturers:

H2A (rabbit polyclonal, ab18255, Abcam)
https://www.abcam.com/en-fr/products/primary-antibodies/histone-h2a-antibody-chip-grade-ab18255

H2B (rabbit polyclonal, ab1790, Abcam)
https://www.abcam.com/en-fr/products/primary-antibodies/histone-h2b-antibody-chip-grade-ab1790

H3 (rabbit polyclonal, ab1791, Abcam)
https://www.abcam.com/en-fr/products/primary-antibodies/histone-h3-antibody-nuclear-marker-and-chip-grade-ab1791

H4 (rabbit polyclonal, ab7311, Abcam)
https://www.abcam.com/en-fr/products/primary-antibodies/histone-h4-antibody-chip-grade-ab7311

H3K27ac (rabbit polyclonal, ab4729)
https://www.abcam.com/en-fr/products/primary-antibodies/histone-h3-acetyl-k27-antibody-chip-grade-ab4729

Nanog (rabbit polyclonal, RCAB-001P, Reprocell)
https://reprocell.co.jp/wp-content/docs/products/amna/mNanog_Datasheet_20100713%20ver2(RCAB0001P).pdf

Oct4 (goat polyclonal, sc-8628, Santa Cruz Biotechnology)
https://datasheets.scbt.com/sc-8628.pdf

Oct4 (mouse monoclonal C-10, sc-5279, Santa Cruz Biotechnology)
https://datasheets.scbt.com/sc-5279.pdf

Oct4 (goat polyclonal, MBS420786, myBioSource)
https://www.mybiosource.com/dog-human-mouse-rat-antibody/oct4-pou5f1/420786

RNA Pol II (mouse monoclonal F-12, sc-55492, Santa Cruz Biotechnology)
https://datasheets.scbt.com/sc-55492.pdf

Sox2 (goat polyclonal, sc-17320, Santa Cruz Biotechnology)
https://datasheets.scbt.com/sc-17320.pdf

TBP (mouse monoclonal, ab51841, abcam)
https://www.abcam.com/en-fr/products/primary-antibodies/tata-binding-protein-tbp-antibody-mabcam51841-ab300656

Brg1 (rabbit monoclonal, ab110641, Abcam),
https://www.abcam.com/en-fr/products/primary-antibodies/brg1-antibody-epncir111a-ab110641

Flag (mouse monoclonal M2, F1804, Sigma-Aldrich)
https://www.sigmaaldrich.com/FR/fr/product/sigma/f1804

IgG, no known specificity (rabbit polyclonal, ab37415, Abcam)
https://www.abcam.com/en-fr/products/primary-antibodies/rabbit-igg-polyclonal-isotype-control-ab37415

Smarcb1 (rabbit monoclonal, #8745 Cell Signaling Technology)
https://www.cellsignal.com/products/primary-antibodies/smarcb1-baf47-d9c2-rabbit-mab/8745

Eukaryotic cell lines

Policy information about cell lines and Sex and Gender in Research

Cell line source(s)	The Brg1-3FTH mESC line (parental cell line 46C) was generated as described in PMID 26814966. The E14Tg2a-Tir1 mESC cell line was obtained from Dr. E. Nora and B. Bruneau (PMID 28525758). The 501 MEL cell line was obtained from Dr. I. Davidson (PMID 25803486). The ZHBTc4.1 mESC line was obtained from Pr. A. Smith (PMID: 10742100)
Authentication	Genotype of genetically engineered cell lines was tested at the level of DNA sequence and protein by Western blotting.
Mycoplasma contamination	Cell lines tested negative for mycoplasma.
Commonly misidentified lines (See ICLAC register)	No commonly misidentified cell lines were used in this study.

ChIP-seq

Data deposition

☒ Confirm that both raw and final processed data have been deposited in a public database such as GEO.

☒ Confirm that you have deposited or provided access to graph files (e.g. BED files) for the called peaks.

Data access links *May remain private before publication.*	GEO accession GSE210780: Go to https://www.ncbi.nlm.nih.gov/geo/query/acc.cgi?acc=GSE210780 GEO accession GSE210444: Go to https://www.ncbi.nlm.nih.gov/geo/query/acc.cgi?acc=GSE210444 GEO accession GSE209914: Go to https://www.ncbi.nlm.nih.gov/geo/query/acc.cgi?acc=GSE209914 GEO accession GSE255089 Go to https://www.ncbi.nlm.nih.gov/geo/query/acc.cgi?acc=GSE255089
Files in database submission	# MOUSE - Histone H3 MNase ChIP-seq total chromatin replicate 1 WCC_gTIR1_rep1_chipH3_2020_1.fastq.gz ; WCC_gTIR1_rep1_chipH3_2020_2.fastq.gz ; WCC_gTIR1_rep1_chipH3_2020_.bw - Histone H3 MNase ChIP-seq total chromatin replicate 2 WCC_gTIR1_rep2_chipH3_2020_1.fastq.gz ; WCC_gTIR1_rep2_chipH3_2020_2.fastq.gz ; WCC_gTIR1_rep2_chipH3_2020_.bw - Histone H3 MNase ChIP-seq total chromatin replicate 3 WCC_gTIR1_rep3_chipH3_2020_1.fastq.gz ; WCC_gTIR1_rep3_chipH3_2020_2.fastq.gz ; WCC_gTIR1_rep3_chipH3_2020_.bw - Histone H3 MNase ChIP-seq total chromatin 4X MNAse replicate 1 TIR1-4x-H3-Rep1_2019_run1_1.fastq.gz ; TIR1-4x-H3-Rep1_2019_run1_2.fastq.gz ; TIR1-4x-H3-Rep1_2019_run2_1.fastq.gz ; TIR1-4x-H3-Rep1_2019_run2_2.fastq.gz ; TIR1-4x-H3-Rep1_2019_.bw - Histone H3 MNase ChIP-seq total chromatin 4X MNAse replicate 2 TIR1-4x-H3-Rep2_2021_1.fastq.gz ; TIR1-4x-H3-Rep2_2021_2.fastq.gz ; TIR1-4x-H3-Rep2_2021_.bw - Histone H3 MNase ChIP-seq total chromatin 4X MNAse replicate 3 TIR1-4x-H3-Rep3_2021_1.fastq.gz ; TIR1-4x-H3-Rep3_2021_2.fastq.gz ; TIR1-4x-H3-Rep3_2021_.bw - Histone H3 MNase ChIP-seq total chromatin Brg1-depleted auxin 20h replicate 1 WCC_gSMARCA4-AID_rep1_chipH3_2020_1.fastq.gz ; WCC_gSMARCA4-AID_rep1_chipH3_2020_2.fastq.gz ; WCC_gSMARCA4-AID_rep1_chipH3_2020_.bw - Histone H3 MNase ChIP-seq total chromatin Brg1-depleted auxin 20h replicate 2 WCC_gSMARCA4-AID_rep2_chipH3_2020_1.fastq.gz ; WCC_gSMARCA4-AID_rep2_chipH3_2020_2.fastq.gz ;

WCC_gSMARCA4-AID_rep2_chipH3_2020_.bw
- Histone H3 MNase ChIP-seq total chromatin Brg1-depleted auxin 20h replicate 3
WCC_gSMARCA4-AID_rep3_chipH3_2020_1.fastq.gz ; WCC_gSMARCA4-AID_rep3_chipH3_2020_2.fastq.gz ;
WCC_gSMARCA4-AID_rep3_chipH3_2020_.bw
- Histone H3 MNase ChIP-seq total chromatin Brg1-depleted auxin 3h replicate 1
SMARCA4-1B2-A-H3_rep1_2019_1.fastq.gz ; SMARCA4-1B2-A-H3_rep1_2019_2.fastq.gz ;
SMARCA4-1B2-A-H3_rep1_2019_.bw
- Histone H3 MNase ChIP-seq total chromatin Brg1-depleted auxin 3h replicate 2
SMARCA4-1B2-A-H3_rep2_2019_1.fastq.gz ; SMARCA4-1B2-A-H3_rep2_2019_2.fastq.gz ;
SMARCA4-1B2-A-H3_rep2_2019_.bw
- Histone H3 MNase ChIP-seq total chromatin shRNA O7 Brg1 replicate 1
brg1-O7_ChIPH3new_3a_2019_1.fastq.gz ; brg1-O7_ChIPH3new_3a_2019_2.fastq.gz ; brg1-O7_ChIPH3new_3a_2019_.bw
- Histone H3 MNase ChIP-seq total chromatin shRNA O7 Brg1 replicate 2
brg1-O7_chipH3new_4b_2019_1.fastq.gz ; brg1-O7_chipH3new_4b_2019_2.fastq.gz ; brg1-O7_chipH3new_4b_2019_.bw
- Histone H3 MNase ChIP-seq total chromatin shRNA O5 Brg1 replicate 1
brg1-O5_chipH3new_10a_2019_1.fastq.gz ; brg1-O5_chipH3new_10a_2019_2.fastq.gz ;
brg1-O5_chipH3new_10a_2019_.bw
- Histone H3 MNase ChIP-seq total chromatin shRNA O5 Brg1 replicate 2
brg1-O5_chipH3old_12sh_2019_1.fastq.gz ; brg1-O5_chipH3old_12sh_2019_2.fastq.gz ;
brg1-O5_chipH3old_12sh_2019_.bw
- Histone H3 MNase ChIP-seq total chromatin control shRNA replicate 1
Brg1_linker_high_rep1_2018_1.fastq.gz ; Brg1_linker_high_rep1_2018_2.fastq.gz ; Brg1_linker_high_rep1_2018_.bw
- Histone H3 MNase ChIP-seq total chromatin control shRNA replicate 2
Brg1_linker_high_rep2_2018_1.fastq.gz ; Brg1_linker_high_rep2_2018_2.fastq.gz ; Brg1_linker_high_rep2_2018_.bw
- Histone H3 MNase ChIP-seq total chromatin control shRNA replicate 3
Chd4_linker_high_rep1_2018_1.fastq.gz ; Chd4_linker_high_rep1_2018_2.fastq.gz ; Chd4_linker_high_rep1_2018_.bw
- Histone H3 MNase ChIP-seq total chromatin control shRNA replicate 4
Chd4_linker_high_rep2_2018_1.fastq.gz ; Chd4_linker_high_rep2_2018_2.fastq.gz ; Chd4_linker_high_rep2_2018_.bw
- Histone H3 MNase ChIP-seq total chromatin control shRNA replicate 5
Ep400_linker_high_rep1_2018_1.fastq.gz ; Ep400_linker_high_rep1_2018_2.fastq.gz ; Ep400_linker_high_rep1_2018_.bw
- Histone H3 MNase ChIP-seq total chromatin control shRNA replicate 6
Ep400_linker_high_rep2_2018_1.fastq.gz ; Ep400_linker_high_rep2_2018_2.fastq.gz ; Ep400_linker_high_rep2_2018_.bw
- Histone H3 MNase ChIP-seq total chromatin shRNA Chd4 replicate 1
Chd4_high_rep1_2018_1.fastq.gz ; Chd4_high_rep1_2018_2.fastq.gz ; Chd4_high_rep1_2018_.bw
- Histone H3 MNase ChIP-seq total chromatin shRNA Chd4 replicate 2
Chd4_high_rep2_2018_1.fastq.gz ; Chd4_high_rep2_2018_2.fastq.gz ; Chd4_high_rep2_2018_.bw
- Histone H2B MNase ChIP-seq total chromatin shRNA O7 Brg1 replicate 1
brg1-O7_chipH2B_7a_2019_1.fastq.gz ; brg1-O7_chipH2B_7a_2019_2.fastq.gz ; brg1-O7_chipH2B_7a_2019_.bw
- Histone H2B MNase ChIP-seq total chromatin shRNA O7 Brg1 replicate 2
brg1-O7_chipH2B_8b_2019_1.fastq.gz ; brg1-O7_chipH2B_8b_2019_2.fastq.gz ; brg1-O7_chipH2B_8b_2019_.bw
- Histone H2B MNase ChIP-seq total chromatin control shRNA replicate 1
brg1-O7Link_chipH2B_7a_2019_1.fastq.gz ; brg1-O7Link_chipH2B_7a_2019_2.fastq.gz ; brg1-O7Link_chipH2B_7a_2019_.bw
- Histone H2B MNase ChIP-seq total chromatin control shRNA replicate 2
brg1-O7Link_chipH2B_8b_2019_1.fastq.gz ; brg1-O7Link_chipH2B_8b_2019_2.fastq.gz ;
brg1-O7Link_chipH2B_8b_2019_.bw
- Oct4 (sc-8628) MNase ChIP-seq total chromatin replicate 1
Oct4_BRGKD_1_170426_1.fastq.gz ; Oct4_BRGKD_1_170426_2.fastq.gz ; Oct4_BRGKD_1_170426_.bw
- Oct4 (sc-8628) MNase ChIP-seq total chromatin replicate 2
Oct4_BRGKD_2_170426_1.fastq.gz ; Oct4_BRGKD_2_170426_2.fastq.gz ; Oct4_BRGKD_2_170426_.bw
- Oct4 (sc-5279) MNase ChIP-seq total chromatin replicate 1
WCC_13-TIR1-Oct4_rep1_2020_1.fastq.gz ; WCC_13-TIR1-Oct4_rep1_2020_2.fastq.gz ; WCC_13-TIR1-Oct4_rep1_2020_.bw
- Oct4 (sc-5279) MNase ChIP-seq total chromatin replicate 2
WCC_14-TIR1-Oct4_rep2_2020_1.fastq.gz ; WCC_14-TIR1-Oct4_rep2_2020_2.fastq.gz ; WCC_14-TIR1-Oct4_rep2_2020_.bw
- Oct4 (sc-5279) MNase ChIP-seq total chromatin replicate 3
WCC_15-TIR1-Oct4_rep3_2020_1.fastq.gz ; WCC_15-TIR1-Oct4_rep3_2020_2.fastq.gz ; WCC_15-TIR1-Oct4_rep3_2020_.bw
- Sox2 MNase ChIP-seq total chromatin replicate 1
ChIP_Sox2_2018_1.fastq.gz ; ChIP_Sox2_2018_2.fastq.gz ; ChIP_Sox2_2018_.bw
- Sox2 MNase ChIP-seq total chromatin replicate 2
ChIP_Sox2_210218_1.fastq.gz ; ChIP_Sox2_210218_2.fastq.gz ; ChIP_Sox2_210218_.bw
- Nanog MNase ChIP-seq total chromatin replicate 1
ChIP_Nanog_2018_1.fastq.gz ; ChIP_Nanog_2018_2.fastq.gz ; ChIP_Nanog_2018_.bw
- Nanog MNase ChIP-seq total chromatin replicate 2
ChIP_Nanog_rep1_210218_1.fastq.gz ; ChIP_Nanog_rep1_210218_2.fastq.gz ; ChIP_Nanog_rep1_210218_.bw
- Nanog MNase ChIP-seq total chromatin replicate 3
ChIP_Nanog_rep2_210218_1.fastq.gz ; ChIP_Nanog_rep2_210218_2.fastq.gz ; ChIP_Nanog_rep2_210218_.bw
- TBP MNase ChIP-seq total chromatin replicate 1
ChIP_TBP_2018_1.fastq.gz ; ChIP_TBP_2018_2.fastq.gz ; ChIP_TBP_2018_.bw
- TBP MNase ChIP-seq total chromatin replicate 2
ChIP_TBP_210218_1.fastq.gz ; ChIP_TBP_210218_2.fastq.gz ; ChIP_TBP_210218_.bw
- RNA pol II MNase ChIP-seq total chromatin replicate 1
ChIP_PolII_2018_1.fastq.gz ; ChIP_PolII_2018_2.fastq.gz ; ChIP_PolII_2018_.bw
- RNA pol II MNase ChIP-seq total chromatin replicate 2
ChIP_Mnase_Pol2_2020_1.fastq.gz ; ChIP_Mnase_Pol2_2020_2.fastq.gz ; ChIP_Mnase_Pol2_2020_.bw
Brg1 MNase ChIP-seq total chromatin replicate 1
ChIP_Smarca4_200727_run1_1.fastq.gz ; ChIP_Smarca4_200727_run1_2.fastq.gz ; ChIP_Smarca4_200727_run2_1.fastq.gz ;
ChIP_Smarca4_200727_run2_2.fastq.gz ; ChIP_Smarca4_200727_.bw

Brg1 MNase ChIP-seq total chromatin replicate 2
ChIP_Smarca4_2018_1.fastq.gz ; ChIP_Smarca4_2018_2.fastq.gz ; ChIP_Smarca4_2018_.bw
- H3K27ac MNase ChIP-seq total chromatin replicate 1
ChIP_H3K27ac_2018_1.fastq.gz ; ChIP_H3K27ac_2018_2.fastq.gz ; ChIP_H3K27ac_2018_.bw
- H3K27ac MNase ChIP-seq total chromatin replicate 2
ChIP_H3K27ac_rep1_210218_1.fastq.gz ; ChIP_H3K27ac_rep1_210218_2.fastq.gz ; ChIP_H3K27ac_rep1_210218_.bw
- H3K27ac MNase ChIP-seq total chromatin replicate 3
ChIP_H3K27ac_rep2_210218_1.fastq.gz ; ChIP_H3K27ac_rep2_210218_2.fastq.gz ; ChIP_H3K27ac_rep2_210218_.bw
- Sequential Oct4-H2B MNase ChIP-seq total chromatin replicate 1
EL2_Oct4_H2B_seq1_rep1_2021_run1_1.fastq.gz ; EL2_Oct4_H2B_seq1_rep1_2021_run1_2.fastq.gz ;
EL2_Oct4_H2B_seq1_rep1_2021_run2_1.fastq.gz ; EL2_Oct4_H2B_seq1_rep1_2021_run2_2.fastq.gz ;
EL2_Oct4_H2B_seq1_rep1_2021_run3_1.fastq.gz ; EL2_Oct4_H2B_seq1_rep1_2021_run3_2.fastq.gz ;
EL2_Oct4_H2B_seq1_rep1_2021_.bw
- Sequential Oct4-H2B MNase ChIP-seq total chromatin replicate 2
EL2_Oct4_H2B_seq1_rep2_2021_run1_1.fastq.gz ; EL2_Oct4_H2B_seq1_rep2_2021_run1_2.fastq.gz ;
EL2_Oct4_H2B_seq1_rep2_2021_run2_1.fastq.gz ; EL2_Oct4_H2B_seq1_rep2_2021_run2_2.fastq.gz ;
EL2_Oct4_H2B_seq1_rep2_2021_run3_1.fastq.gz ; EL2_Oct4_H2B_seq1_rep2_2021_run3_2.fastq.gz ;
EL2_Oct4_H2B_seq1_rep2_2021_.bw
- Sequential Control IgG-H2B MNase ChIP-seq total chromatin replicate 1
EL2_CTRL_H2B_rep1_2021_run1_1.fastq.gz ; EL2_CTRL_H2B_rep1_2021_run1_2.fastq.gz ;
EL2_CTRL_H2B_rep1_2021_run2_1.fastq.gz ; EL2_CTRL_H2B_rep1_2021_run2_2.fastq.gz ;
EL2_CTRL_H2B_rep1_2021_.bw
- Sequential Control IgG-H2B MNase ChIP-seq total chromatin replicate 2
EL2_CTRL_H2B_rep2_2021_run1_1.fastq.gz ; EL2_CTRL_H2B_rep2_2021_run1_2.fastq.gz ;
EL2_CTRL_H2B_rep2_2021_run2_1.fastq.gz ; EL2_CTRL_H2B_rep2_2021_run2_2.fastq.gz ;
EL2_CTRL_H2B_rep2_2021_.bw
- Histone H3 MNase ChIP-seq top of gradient (3-4) replicate 1
chip_H3_grad1_f3-4_280120_1.fastq.gz ; chip_H3_grad1_f3-4_280120_2.fastq.gz ; chip_H3_grad1_f3-4_280120_.bw
- Histone H3 MNase ChIP-seq top of gradient (3-4) replicate 2
chip_H3_grad2_f3-4_200727_1.fastq.gz ; chip_H3_grad2_f3-4_200727_2.fastq.gz ; chip_H3_grad2_f3-4_200727_.bw
- Histone H3 MNase ChIP-seq top of gradient (2-3-4) replicate 1
TIR1_g2-3-4_rep1_H3_2020_1.fastq.gz ; TIR1_g2-3-4_rep1_H3_2020_2.fastq.gz ; TIR1_g2-3-4_rep1_H3_2020_.bw
- Histone H3 MNase ChIP-seq top of gradient (2-3-4) replicate 2
TIR1_g2-3-4_rep2_H3_2020_1.fastq.gz ; TIR1_g2-3-4_rep2_H3_2020_2.fastq.gz ; TIR1_g2-3-4_rep2_H3_2020_.bw
- Histone H4 MNase ChIP-seq top of gradient (2-3-4) replicate 1
TIR1_g2-3-4_rep1_H4_2020_1.fastq.gz ; TIR1_g2-3-4_rep1_H4_2020_2.fastq.gz ; TIR1_g2-3-4_rep1_H4_2020_.bw
- Histone H4 MNase ChIP-seq top of gradient (2-3-4) replicate 2
TIR1_g2-3-4_rep2_H4_2020_1.fastq.gz ; TIR1_g2-3-4_rep2_H4_2020_2.fastq.gz ; TIR1_g2-3-4_rep2_H4_2020_.bw
- Histone H2B MNase ChIP-seq top of gradient (2-3-4) replicate 1
TIR1_g2-3-4_rep1_H2B_2020_1.fastq.gz ; TIR1_g2-3-4_rep1_H2B_2020_2.fastq.gz ; TIR1_g2-3-4_rep1_H2B_2020_.bw
- Histone H2B MNase ChIP-seq top of gradient (2-3-4) replicate 2
TIR1_g2-3-4_rep2_H2B_2020_1.fastq.gz ; TIR1_g2-3-4_rep2_H2B_2020_2.fastq.gz ; TIR1_g2-3-4_rep2_H2B_2020_.bw
- Histone H2A MNase ChIP-seq top of gradient (2-3-4) replicate 1
TIR1_g2-3-4_rep1_H2A_2020_1.fastq.gz ; TIR1_g2-3-4_rep1_H2A_2020_2.fastq.gz ; TIR1_g2-3-4_rep1_H2A_2020_.bw
- Histone H2A MNase ChIP-seq top of gradient (2-3-4) replicate 2
TIR1_g2-3-4_rep2_H2A_2020_1.fastq.gz ; TIR1_g2-3-4_rep2_H2A_2020_2.fastq.gz ; TIR1_g2-3-4_rep2_H2A_2020_.bw
- Histone H3 MNase ChIP-seq low sedimentation rate (5-6) replicate 1
chip_H3_grad1_f5-6_280120_1.fastq.gz ; chip_H3_grad1_f5-6_280120_2.fastq.gz ; chip_H3_grad1_f5-6_280120_.bw
- Histone H3 MNase ChIP-seq low sedimentation rate (5-6) replicate 2
chip_H3_grad2_f5-6_200727_1.fastq.gz ; chip_H3_grad2_f5-6_200727_2.fastq.gz ; chip_H3_grad2_f5-6_200727_.bw
- Histone H3 MNase ChIP-seq low sedimentation rate (5-6) replicate 3
TIR1_g5-6_rep1_H3_2020_1.fastq.gz ; TIR1_g5-6_rep1_H3_2020_2.fastq.gz ; TIR1_g5-6_rep1_H3_2020_.bw
- Histone H3 MNase ChIP-seq low sedimentation rate (5-6) replicate 4
TIR1_g5-6_rep2_H3_2020_1.fastq.gz ; TIR1_g5-6_rep2_H3_2020_2.fastq.gz ; TIR1_g5-6_rep2_H3_2020_.bw
- Histone H4 MNase ChIP-seq low sedimentation rate (5-6) replicate 1
TIR1_g5-6_rep1_H4_2020_1.fastq.gz ; TIR1_g5-6_rep1_H4_2020_2.fastq.gz ; TIR1_g5-6_rep1_H4_2020_.bw
- Histone H4 MNase ChIP-seq low sedimentation rate (5-6) replicate 2
TIR1_g5-6_rep2_H4_2020_1.fastq.gz ; TIR1_g5-6_rep2_H4_2020_2.fastq.gz ; TIR1_g5-6_rep2_H4_2020_.bw
- Histone H2B MNase ChIP-seq low sedimentation rate (5-6) replicate 1
TIR1_g5-6_rep1_H2B_2020_1.fastq.gz ; TIR1_g5-6_rep1_H2B_2020_2.fastq.gz ; TIR1_g5-6_rep1_H2B_2020_.bw
- Histone H2B MNase ChIP-seq low sedimentation rate (5-6) replicate 2
TIR1_g5-6_rep2_H2B_2020_1.fastq.gz ; TIR1_g5-6_rep2_H2B_2020_2.fastq.gz ; TIR1_g5-6_rep2_H2B_2020_.bw
- Histone H2A MNase ChIP-seq low sedimentation rate (5-6) replicate 1
TIR1_g5-6_rep1_H2A_2020_1.fastq.gz ; TIR1_g5-6_rep1_H2A_2020_2.fastq.gz ; TIR1_g5-6_rep1_H2A_2020_.bw
- Histone H2A MNase ChIP-seq low sedimentation rate (5-6) replicate 2
TIR1_g5-6_rep2_H2A_2020_1.fastq.gz ; TIR1_g5-6_rep2_H2A_2020_2.fastq.gz ; TIR1_g5-6_rep2_H2A_2020_.bw
- Histone H3 MNase ChIP-seq low sedimentation rate (5-6) - Brg1-depleted auxin 20h replicate 1
SMARCA4-AID_g5-6_rep1_H3_2020_1.fastq.gz ; SMARCA4-AID_g5-6_rep1_H3_2020_2.fastq.gz ;
SMARCA4-AID_g5-6_rep1_H3_2020_.bw
- Histone H3 MNase ChIP-seq low sedimentation rate (5-6) - Brg1-depleted auxin 20h replicate 2
SMARCA4-AID_g5-6_rep2_H3_2020_1.fastq.gz ; SMARCA4-AID_g5-6_rep2_H3_2020_2.fastq.gz ;
SMARCA4-AID_g5-6_rep2_H3_2020_.bw
- Histone H4 MNase ChIP-seq low sedimentation rate (5-6) - Brg1-depleted auxin 20h replicate 1
SMARCA4-AID_g5-6_rep1_H4_2020_1.fastq.gz ; SMARCA4-AID_g5-6_rep1_H4_2020_2.fastq.gz ;
SMARCA4-AID_g5-6_rep1_H4_2020_.bw
- Histone H4 MNase ChIP-seq low sedimentation rate (5-6) - Brg1-depleted auxin 20h replicate 2

SMARCA4-AID_g5-6_rep2_H4_2020_1.fastq.gz ; SMARCA4-AID_g5-6_rep2_H4_2020_2.fastq.gz ;
SMARCA4-AID_g5-6_rep2_H4_2020_.bw
- Histone H2B MNase ChIP-seq low sedimentation rate (5-6) - Brg1-depleted auxin 20h replicate 1
SMARCA4-AID_g5-6_rep1_H2B_2020_1.fastq.gz ; SMARCA4-AID_g5-6_rep1_H2B_2020_2.fastq.gz ;
SMARCA4-AID_g5-6_rep1_H2B_2020_.bw
- Histone H2B MNase ChIP-seq low sedimentation rate (5-6) - Brg1-depleted auxin 20h replicate 2
SMARCA4-AID_g5-6_rep2_H2B_2020_1.fastq.gz ; SMARCA4-AID_g5-6_rep2_H2B_2020_2.fastq.gz ;
SMARCA4-AID_g5-6_rep2_H2B_2020_.bw
- Histone H2A MNase ChIP-seq low sedimentation rate (5-6) - Brg1-depleted auxin 20h replicate 1
SMARCA4-AID_g5-6_rep1_H2A_2020_1.fastq.gz ; SMARCA4-AID_g5-6_rep1_H2A_2020_2.fastq.gz ;
SMARCA4-AID_g5-6_rep1_H2A_2020_.bw
- Histone H2A MNase ChIP-seq low sedimentation rate (5-6) - Brg1-depleted auxin 20h replicate 2
SMARCA4-AID_g5-6_rep2_H2A_2020_1.fastq.gz ; SMARCA4-AID_g5-6_rep2_H2A_2020_2.fastq.gz ;
SMARCA4-AID_g5-6_rep2_H2A_2020_.bw
- Histone H3 MNase ChIP-seq medium sedimentation rate (7-8) replicate 1
ChIP_H3_grad1_f7-8_200128_run1_1.fastq.gz ; ChIP_H3_grad1_f7-8_200128_run1_2.fastq.gz ;
ChIP_H3_grad1_f7-8_200128_run2_1.fastq.gz ; ChIP_H3_grad1_f7-8_200128_run2_2.fastq.gz ;
ChIP_H3_grad1_f7-8_200128_.bw
- Histone H3 MNase ChIP-seq medium sedimentation rate (7-8) replicate 2
ChIP_H3_grad2_f7-8_200128_run1_1.fastq.gz ; ChIP_H3_grad2_f7-8_200128_run1_2.fastq.gz ;
ChIP_H3_grad2_f7-8_200128_run2_1.fastq.gz ; ChIP_H3_grad2_f7-8_200128_run2_2.fastq.gz ;
ChIP_H3_grad2_f7-8_200128_.bw
- Histone H3 MNase ChIP-seq medium sedimentation rate (7-8-9) replicate 1
TIR1_g7-8-9_rep1_H3_2020_1.fastq.gz ; TIR1_g7-8-9_rep1_H3_2020_2.fastq.gz ; TIR1_g7-8-9_rep1_H3_2020_.bw
- Histone H3 MNase ChIP-seq medium sedimentation rate (7-8-9) replicate 2
TIR1_g7-8-9_rep2_H3_2020_1.fastq.gz ; TIR1_g7-8-9_rep2_H3_2020_2.fastq.gz ; TIR1_g7-8-9_rep2_H3_2020_.bw
- Histone H4 MNase ChIP-seq medium sedimentation rate (7-8-9) replicate 1
TIR1_g7-8-9_rep1_H4_2020_1.fastq.gz ; TIR1_g7-8-9_rep1_H4_2020_2.fastq.gz ; TIR1_g7-8-9_rep1_H4_2020_.bw
- Histone H4 MNase ChIP-seq medium sedimentation rate (7-8-9) replicate 2
TIR1_g7-8-9_rep2_H4_2020_1.fastq.gz ; TIR1_g7-8-9_rep2_H4_2020_2.fastq.gz ; TIR1_g7-8-9_rep2_H4_2020_.bw
- Histone H2A MNase ChIP-seq medium sedimentation rate (7-8-9) replicate 1
TIR1_g7-8-9_rep1_H2A_2020_1.fastq.gz ; TIR1_g7-8-9_rep1_H2A_2020_2.fastq.gz ; TIR1_g7-8-9_rep1_H2A_2020_.bw
- Histone H2A MNase ChIP-seq medium sedimentation rate (7-8-9) replicate 2
TIR1_g7-8-9_rep2_H2A_2020_1.fastq.gz ; TIR1_g7-8-9_rep2_H2A_2020_2.fastq.gz ; TIR1_g7-8-9_rep2_H2A_2020_.bw
- Histone H3 MNase ChIP-seq medium sedimentation rate (7-8-9) - Brg1-depleted auxin 20h replicate 1
SMARCA4-AID_g7-8-9_rep1_H3_2020_1.fastq.gz ; SMARCA4-AID_g7-8-9_rep1_H3_2020_2.fastq.gz ;
SMARCA4-AID_g7-8-9_rep1_H3_2020_.bw
- Histone H3 MNase ChIP-seq medium sedimentation rate (7-8-9) - Brg1-depleted auxin 20h replicate 2
SMARCA4-AID_g7-8-9_rep2_H3_2020_1.fastq.gz ; SMARCA4-AID_g7-8-9_rep2_H3_2020_2.fastq.gz ;
SMARCA4-AID_g7-8-9_rep2_H3_2020_.bw
- Histone H4 MNase ChIP-seq medium sedimentation rate (7-8-9) - Brg1-depleted auxin 20h replicate 1
SMARCA4-AID_g7-8-9_rep1_H4_2020_1.fastq.gz ; SMARCA4-AID_g7-8-9_rep1_H4_2020_2.fastq.gz ;
SMARCA4-AID_g7-8-9_rep1_H4_2020_.bw
- Histone H4 MNase ChIP-seq medium sedimentation rate (7-8-9) - Brg1-depleted auxin 20h replicate 2
SMARCA4-AID_g7-8-9_rep2_H4_2020_1.fastq.gz ; SMARCA4-AID_g7-8-9_rep2_H4_2020_2.fastq.gz ;
SMARCA4-AID_g7-8-9_rep2_H4_2020_.bw
- Histone H2A MNase ChIP-seq medium sedimentation rate (7-8-9) - Brg1-depleted auxin 20h replicate 1
SMARCA4-AID_g7-8-9_rep1_H2A_2020_1.fastq.gz ; SMARCA4-AID_g7-8-9_rep1_H2A_2020_2.fastq.gz ;
SMARCA4-AID_g7-8-9_rep1_H2A_2020_.bw
- Histone H2A MNase ChIP-seq medium sedimentation rate (7-8-9) - Brg1-depleted auxin 20h replicate 2
SMARCA4-AID_g7-8-9_rep2_H2A_2020_1.fastq.gz ; SMARCA4-AID_g7-8-9_rep2_H2A_2020_2.fastq.gz ;
SMARCA4-AID_g7-8-9_rep2_H2A_2020_.bw
- Histone H3 MNase ChIP-seq medium sedimentation rate (9-10) replicate 1
chip_H3_grad1_f9-10_200128_run1_1.fastq.gz ; chip_H3_grad1_f9-10_200128_run1_2.fastq.gz ;
chip_H3_grad1_f9-10_200128_run2_1.fastq.gz ; chip_H3_grad1_f9-10_200128_run2_2.fastq.gz ;
chip_H3_grad1_f9-10_200128_.bw
- Histone H3 MNase ChIP-seq medium sedimentation rate (9-10) replicate 2
chip_H3_grad2_f9-10_200727_run1_1.fastq.gz ; chip_H3_grad2_f9-10_200727_run1_2.fastq.gz ;
chip_H3_grad2_f9-10_200727_run2_1.fastq.gz ; chip_H3_grad2_f9-10_200727_run2_2.fastq.gz ;
chip_H3_grad2_f9-10_200727_.bw
- Histone H3 MNase ChIP-seq mononucleosomes (11) replicate 1
chip_H3_grad1_f11_200128_run1_1.fastq.gz ; chip_H3_grad1_f11_200128_run1_2.fastq.gz ;
chip_H3_grad1_f11_200128_run2_1.fastq.gz ; chip_H3_grad1_f11_200128_run2_2.fastq.gz ;
chip_H3_grad1_f11_200128_.bw
- Histone H3 MNase ChIP-seq mononucleosomes (11) replicate 2
chip_H3_grad2_f11_200727_run1_1.fastq.gz ; chip_H3_grad2_f11_200727_run1_2.fastq.gz ;
chip_H3_grad2_f11_200727_run2_1.fastq.gz ; chip_H3_grad2_f11_200727_run2_2.fastq.gz ;
chip_H3_grad2_f11_200727_.bw
- Histone H3 MNase ChIP-seq mononucleosomes (13) replicate 1
chip_H3_grad1_f13_200128_run1_1.fastq.gz ; chip_H3_grad1_f13_200128_run1_2.fastq.gz ;
chip_H3_grad1_f13_200128_run2_1.fastq.gz ; chip_H3_grad1_f13_200128_run2_2.fastq.gz ;
chip_H3_grad1_f13_200128_.bw
- Histone H3 MNase ChIP-seq mononucleosomes (13) replicate 2
chip_H3_grad2_f13_200727_run1_1.fastq.gz ; chip_H3_grad2_f13_200727_run1_2.fastq.gz ;
chip_H3_grad2_f13_200727_run2_1.fastq.gz ; chip_H3_grad2_f13_200727_run2_2.fastq.gz ;
chip_H3_grad2_f13_200727_.bw

- Oct4 (sc-5279) MNase ChIP-seq top of gradient (2-3-4) replicate 1
1-TIR1-2-3-4-Oct4_rep1_1.fastq.gz ; 1-TIR1-2-3-4-Oct4_rep1_2.fastq.gz ; 1-TIR1-2-3-4-Oct4_rep1_.bw
- Oct4 (sc-5279) MNase ChIP-seq top of gradient (2-3-4) replicate 2
2-TIR1-2-3-4-Oct4_rep2_1.fastq.gz ; 2-TIR1-2-3-4-Oct4_rep2_2.fastq.gz ; 2-TIR1-2-3-4-Oct4_rep2_.bw
- Oct4 (sc-5279) MNase ChIP-seq top of gradient (2-3-4) - Brg1-depleted auxin 20h replicate 1
3-SMARCA4-2-3-4-Oct4_rep1_1.fastq.gz ; 3-SMARCA4-2-3-4-Oct4_rep1_2.fastq.gz ; 3-SMARCA4-2-3-4-Oct4_rep1_.bw
- Oct4 (sc-5279) MNase ChIP-seq top of gradient (2-3-4) - Brg1-depleted auxin 20h replicate 2
4-SMARCA4-2-3-4-Oct4_rep2_1.fastq.gz ; 4-SMARCA4-2-3-4-Oct4_rep2_2.fastq.gz ; 4-SMARCA4-2-3-4-Oct4_rep2_.bw
- Oct4 (sc-5279) MNase ChIP-seq low sedimentation rate (5-6) replicate 1
5-TIR1-5-6-Oct4_rep1_1.fastq.gz ; 5-TIR1-5-6-Oct4_rep1_2.fastq.gz ; 5-TIR1-5-6-Oct4_rep1_.bw
- Oct4 (sc-5279) MNase ChIP-seq low sedimentation rate (5-6) replicate 2
6-TIR1-5-6-Oct4_rep2_1.fastq.gz ; 6-TIR1-5-6-Oct4_rep2_2.fastq.gz ; 6-TIR1-5-6-Oct4_rep2_.bw
- Oct4 (sc-5279) MNase ChIP-seq low sedimentation rate (5-6) - Brg1-depleted auxin 20h replicate 1
7-SMARCA4-5-6-Oct4_rep1_1.fastq.gz ; 7-SMARCA4-5-6-Oct4_rep1_2.fastq.gz ; 7-SMARCA4-5-6-Oct4_rep1_.bw
- Oct4 (sc-5279) MNase ChIP-seq low sedimentation rate (5-6) - Brg1-depleted auxin 20h replicate 2
8-SMARCA4-5-6-Oct4_rep2_1.fastq.gz ; 8-SMARCA4-5-6-Oct4_rep2_2.fastq.gz ; 8-SMARCA4-5-6-Oct4_rep2_.bw
- Oct4 (MBS420786) MNase ChIP-seq low sedimentation rate (5-6) replicate 1
EL_PEP_Oct4_5-6_Rep1_C002K7S_1.fastq.gz ; EL_PEP_Oct4_5-6_Rep1_C002K7S_2.fastq.gz ;
EL_PEP_Oct4_5-6_Rep1_C002K7S_.bw
- Oct4 (MBS420786) MNase ChIP-seq low sedimentation rate (5-6) replicate 2
EL_PEP_Oct4_5-6_Rep2_C002K7T_1.fastq.gz ; EL_PEP_Oct4_5-6_Rep2_C002K7T_2.fastq.gz ;
EL_PEP_Oct4_5-6_Rep2_C002K7T_.bw
- MNase-seq top of gradient (2-3-4) replicate 1
input_Tir1_rep1_g2-3-4_1.fastq.gz ; input_Tir1_rep1_g2-3-4_2.fastq.gz ; input_Tir1_rep1_g2-3-4_.bw
- MNase-seq top of gradient (2-3-4) replicate 2
input_Tir1_rep2_g2-3-4_1.fastq.gz ; input_Tir1_rep2_g2-3-4_2.fastq.gz ; input_Tir1_rep2_g2-3-4_.bw
- MNase-seq top of gradient (2-3-4) replicate 3
input_Tir1_rep3_g2-3-4_1.fastq.gz ; input_Tir1_rep3_g2-3-4_2.fastq.gz ; input_Tir1_rep3_g2-3-4_.bw
- MNase-seq top of gradient (2-3-4) replicate 4
input_Tir1_rep4_g2-3-4_1.fastq.gz ; input_Tir1_rep4_g2-3-4_2.fastq.gz ; input_Tir1_rep4_g2-3-4_.bw
- MNase-seq top of gradient (2-3-4) - Brg1-depleted auxin 20h replicate 1
input_Smarca4_rep1_g2-3-4_1.fastq.gz ; input_Smarca4_rep1_g2-3-4_2.fastq.gz ; input_Smarca4_rep1_g2-3-4_.bw
- MNase-seq top of gradient (2-3-4) - Brg1-depleted auxin 20h replicate 2
input_Smarca4_rep2_g2-3-4_1.fastq.gz ; input_Smarca4_rep2_g2-3-4_2.fastq.gz ; input_Smarca4_rep2_g2-3-4_.bw
- MNase-seq top of gradient (2-3-4) - Brg1-depleted auxin 20h replicate 3
input_Smarca4_rep3_g2-3-4_1.fastq.gz ; input_Smarca4_rep3_g2-3-4_2.fastq.gz ; input_Smarca4_rep3_g2-3-4_.bw
- MNase-seq top of gradient (2-3-4) - Brg1-depleted auxin 20h replicate 4
input_Smarca4_rep4_g2-3-4_1.fastq.gz ; input_Smarca4_rep4_g2-3-4_2.fastq.gz ; input_Smarca4_rep4_g2-3-4_.bw
- MNase-seq low sedimentation rate (5-6) replicate 1
input_Tir1_rep1_g5-6_1.fastq.gz ; input_Tir1_rep1_g5-6_2.fastq.gz ; input_Tir1_rep1_g5-6_.bw
- MNase-seq low sedimentation rate (5-6) replicate 2
input_Tir1_rep2_g5-6_1.fastq.gz ; input_Tir1_rep2_g5-6_2.fastq.gz ; input_Tir1_rep2_g5-6_.bw
- MNase-seq low sedimentation rate (5-6) replicate 3
input_Tir1_rep3_g5-6_1.fastq.gz ; input_Tir1_rep3_g5-6_2.fastq.gz ; input_Tir1_rep3_g5-6_.bw
- MNase-seq low sedimentation rate (5-6) replicate 4
input_Tir1_rep4_g5-6_1.fastq.gz ; input_Tir1_rep4_g5-6_2.fastq.gz ; input_Tir1_rep4_g5-6_.bw
- MNase-seq low sedimentation rate (5-6) - Brg1-depleted auxin 20h replicate 1
input_Smarca4_rep1_g5-6_1.fastq.gz ; input_Smarca4_rep1_g5-6_2.fastq.gz ; input_Smarca4_rep1_g5-6_.bw
- MNase-seq low sedimentation rate (5-6) - Brg1-depleted auxin 20h replicate 2
input_Smarca4_rep2_g5-6_1.fastq.gz ; input_Smarca4_rep2_g5-6_2.fastq.gz ; input_Smarca4_rep2_g5-6_.bw
- MNase-seq low sedimentation rate (5-6) - Brg1-depleted auxin 20h replicate 3
input_Smarca4_rep3_g5-6_1.fastq.gz ; input_Smarca4_rep3_g5-6_2.fastq.gz ; input_Smarca4_rep3_g5-6_.bw
- MNase-seq low sedimentation rate (5-6) - Brg1-depleted auxin 20h replicate 4
input_Smarca4_rep4_g5-6_1.fastq.gz ; input_Smarca4_rep4_g5-6_2.fastq.gz ; input_Smarca4_rep4_g5-6_.bw
- MNase-seq medium sedimentation rate (7-8-9) replicate 1
input_Tir1_rep1_g7-8-9_1.fastq.gz ; input_Tir1_rep1_g7-8-9_2.fastq.gz ; input_Tir1_rep1_g7-8-9_.bw
- MNase-seq medium sedimentation rate (7-8-9) replicate 2
input_Tir1_rep2_g7-8-9_1.fastq.gz ; input_Tir1_rep2_g7-8-9_2.fastq.gz ; input_Tir1_rep2_g7-8-9_.bw
- MNase-seq medium sedimentation rate (7-8-9) replicate 3
input_Tir1_rep3_g7-8-9_1.fastq.gz ; input_Tir1_rep3_g7-8-9_2.fastq.gz ; input_Tir1_rep3_g7-8-9_.bw
- MNase-seq medium sedimentation rate (7-8-9) replicate 4
input_Tir1_rep4_g7-8-9_1.fastq.gz ; input_Tir1_rep4_g7-8-9_2.fastq.gz ; input_Tir1_rep4_g7-8-9_.bw
- MNase-seq medium sedimentation rate (7-8-9) - Brg1-depleted auxin 20h replicate 1
input_Smarca4_rep1_g7-8-9_1.fastq.gz ; input_Smarca4_rep1_g7-8-9_2.fastq.gz ; input_Smarca4_rep1_g7-8-9_.bw
- MNase-seq medium sedimentation rate (7-8-9) - Brg1-depleted auxin 20h replicate 2
input_Smarca4_rep2_g7-8-9_1.fastq.gz ; input_Smarca4_rep2_g7-8-9_2.fastq.gz ; input_Smarca4_rep2_g7-8-9_.bw
- MNase-seq medium sedimentation rate (7-8-9) - Brg1-depleted auxin 20h replicate 3
input_Smarca4_rep3_g7-8-9_1.fastq.gz ; input_Smarca4_rep3_g7-8-9_2.fastq.gz ; input_Smarca4_rep3_g7-8-9_.bw
- MNase-seq medium sedimentation rate (7-8-9) - Brg1-depleted auxin 20h replicate 4
input_Smarca4_rep4_g7-8-9_1.fastq.gz ; input_Smarca4_rep4_g7-8-9_2.fastq.gz ; input_Smarca4_rep4_g7-8-9_.bw
HUMAN
- Histone H3 MNase ChIP-seq low sedimentation rate (4-5-6-7) replicate 1
Chip-H3_4-5-6-7_M1_C002K7Y_1.fastq.gz ; Chip-H3_4-5-6-7_M1_C002K7Y_2.fastq.gz ; Chip-H3_4-5-6-7_M1_C002K7Y_.bw
- Histone H3 MNase ChIP-seq low sedimentation rate (4-5-6-7) replicate 2
Chip-H3_4-5-6-7_M2_C002K7Z_1.fastq.gz ; Chip-H3_4-5-6-7_M2_C002K7Z_2.fastq.gz ; Chip-H3_4-5-6-7_M2_C002K7Z_.bw
- Histone H3 MNase ChIP-seq mononucleosomes (11) replicate 1

Chip-H3_frac11_M1_C002K81_1.fastq.gz ; Chip-H3_frac11_M1_C002K81_2.fastq.gz ; Chip-H3_frac11_M1_C002K81_.bw
- Histone H3 MNase ChIP-seq mononucleosomes (11) replicate 2
Chip-H3_frac11_M2_C002K82_1.fastq.gz ; Chip-H3_frac11_M2_C002K82_2.fastq.gz ; Chip-H3_frac11_M2_C002K82_.bw
- Histone H3 MNase ChIP-seq low sedimentation rate (5-6) - Smarcb1-depleted auxin 20h replicate 1
SMCB1-H3_5-6-R1_1.fastq.gz; SMCB1-H3_5-6-R1_2.fastq.gz; SMCB1-H3_5-6-R1_.bw
- Histone H3 MNase ChIP-seq low sedimentation rate (5-6) - Smarcb1-depleted auxin 20h replicate 2
SMCB1-H3_5-6-R2_1.fastq.gz; SMCB1-H3_5-6-R2_2.fastq.gz; SMCB1-H3_5-6-R2_.bw
- Histone H3 MNase ChIP-seq low sedimentation rate (5-6) - Arid1a-depleted auxin 20h replicate 1
ARID1A-H3_5-6-R1_1.fastq.gz; ARID1A-H3_5-6-R1_2.fastq.gz; ARID1A-H3_5-6-R1_.bw
- Histone H3 MNase ChIP-seq low sedimentation rate (5-6) - Arid1a-depleted auxin 20h replicate 2
ARID1A-H3_5-6-R2_1.fastq.gz; ARID1A-H3_5-6-R2_2.fastq.gz; ARID1A-H3_5-6-R2_.bw
- Histone H3 MNase ChIP-seq low sedimentation rate (5-6) – PBRM1-depleted auxin 20h replicate 1
PBRM1-5-6-H3-R1_1.fastq.gz; PBRM1-5-6-H3-R1_2.fastq.gz; PBRM1-5-6-H3-R1_.bw
- Histone H3 MNase ChIP-seq low sedimentation rate (5-6) – PBRM1-depleted auxin 20h replicate 2
PBRM1-5-6-H3-R2_1.fastq.gz; PBRM1-5-6-H3-R2_2.fastq.gz; PBRM1-5-6-H3-R2_.bw
- Histone H3 MNase ChIP-seq low sedimentation rate (5-6) – BRD7-depleted auxin 20h replicate 1
BRD7-5-6-H3-R1_1.fastq.gz; BRD7-5-6-H3-R1_2.fastq.gz; BRD7-5-6-H3-R1_.bw
- Histone H3 MNase ChIP-seq low sedimentation rate (5-6) – BRD7-depleted auxin 20h replicate 2
BRD7-5-6-H3-R2_1.fastq.gz; BRD7-5-6-H3-R2_2.fastq.gz; BRD7-5-6-H3-R2_.bw
- Histone H3 MNase ChIP-seq low sedimentation rate (5-6) - Brd9-depleted auxin 20h replicate 1
BRD9-H3_5-6-R1_1.fastq.gz; BRD9-H3_5-6-R1_2.fastq.gz; BRD9-H3_5-6-R1_.bw
- Histone H3 MNase ChIP-seq low sedimentation rate (5-6) - Brd9-depleted auxin 20h replicate 2
BRD9-H3_5-6-R2_1.fastq.gz; BRD9-H3_5-6-R2_2.fastq.gz; BRD9-H3_5-6-R2_.bw
- Histone H3 MNase ChIP-seq low sedimentation rate (5-6) replicate 5
TIR1-H3_5-6-R1_1.fastq.gz; TIR1-H3_5-6-R1_2.fastq.gz; TIR1-H3_5-6-R1_.bw
- Histone H3 MNase ChIP-seq low sedimentation rate (5-6) replicate 6
TIR1-H3_5-6-R2_1.fastq.gz; TIR1-H3_5-6-R2_2.fastq.gz; TIR1-H3_5-6-R2_.bw
- Oct4 (sc-5279) MNase ChIP-seq low sedimentation rate (5-6-7) - Smarcb1-depleted auxin 20h replicate 1
SMARCB1_ChIP-Oct4_5-6-7_R1_1.fastq.gz; SMARCB1_ChIP-Oct4_5-6-7_R1_2.fastq.gz; SMARCB1_ChIP-Oct4_5-6-7_R1_.bw
- Oct4 (sc-5279) MNase ChIP-seq low sedimentation rate (5-6-7) - Smarcb1-depleted auxin 20h replicate 2
SMARCB1_ChIP-Oct4_5-6-7_R2_1.fastq.gz; SMARCB1_ChIP-Oct4_5-6-7_R2_2.fastq.gz; SMARCB1_ChIP-Oct4_5-6-7_R2_.bw
- Oct4 (sc-5279) MNase ChIP-seq low sedimentation rate (5-6-7) - Arid1a-depleted auxin 20h replicate 1
ARID1A_ChIP-Oct4_5-6-7_R1_1.fastq.gz; ARID1A_ChIP-Oct4_5-6-7_R1_2.fastq.gz; ARID1A_ChIP-Oct4_5-6-7_R1_.bw
- Oct4 (sc-5279) MNase ChIP-seq low sedimentation rate (5-6-7) - Arid1a-depleted auxin 20h replicate 2
ARID1A_ChIP-Oct4_5-6-7_R2_1.fastq.gz; ARID1A_ChIP-Oct4_5-6-7_R2_2.fastq.gz; ARID1A_ChIP-Oct4_5-6-7_R2_.bw
- Oct4 (sc-5279) MNase ChIP-seq low sedimentation rate (5-6-7) - Brd7-depleted auxin 20h replicate 1
BRD7_ChIP-Oct4_5-6-7_R1_1.fastq.gz; BRD7_ChIP-Oct4_5-6-7_R1_2.fastq.gz; BRD7_ChIP-Oct4_5-6-7_R1_.bw
- Oct4 (sc-5279) MNase ChIP-seq low sedimentation rate (5-6-7) - Brd7-depleted auxin 20h replicate 2
BRD7_ChIP-Oct4_5-6-7_R2_1.fastq.gz; BRD7_ChIP-Oct4_5-6-7_R2_2.fastq.gz; BRD7_ChIP-Oct4_5-6-7_R2_.bw

- Oct4 (sc-5279) MNase ChIP-seq low sedimentation rate (5-6-7) - Pbrm1-depleted auxin 20h replicate 1
PBRM1_ChIP-Oct4_5-6-7_R1_1.fastq.gz; PBRM1_ChIP-Oct4_5-6-7_R1_2.fastq.gz; PBRM1_ChIP-Oct4_5-6-7_R1_.bw
- Oct4 (sc-5279) MNase ChIP-seq low sedimentation rate (5-6-7) - Pbrm1-depleted auxin 20h replicate 2
PBRM1_ChIP-Oct4_5-6-7_R2_1.fastq.gz; PBRM1_ChIP-Oct4_5-6-7_R2_2.fastq.gz; PBRM1_ChIP-Oct4_5-6-7_R2_.bw
- Oct4 (sc-5279) MNase ChIP-seq low sedimentation rate (5-6-7) - Brd9-depleted auxin 20h replicate 1
BRD9_ChIP-Oct4_5-6-7_R1_1.fastq.gz; BRD9_ChIP-Oct4_5-6-7_R1_2.fastq.gz; BRD9_ChIP-Oct4_5-6-7_R1_.bw
- Oct4 (sc-5279) MNase ChIP-seq low sedimentation rate (5-6-7) - Brd9-depleted auxin 20h replicate 2
BRD9_ChIP-Oct4_5-6-7_R2_1.fastq.gz; BRD9_ChIP-Oct4_5-6-7_R2_2.fastq.gz; BRD9_ChIP-Oct4_5-6-7_R2_.bw
- Oct4 (sc-5279) MNase ChIP-seq low sedimentation rate (5-6-7) - Smarca4-depleted auxin 20h replicate 1
SMARCA4_ChIP-Oct4_5-6-7_R1_1.fastq.gz; SMARCA4_ChIP-Oct4_5-6-7_R1_2.fastq.gz; SMARCA4_ChIP-Oct4_5-6-7_R1_.bw
- Oct4 (sc-5279) MNase ChIP-seq low sedimentation rate (5-6-7) - Smarca4-depleted auxin 20h replicate 2
SMARCA4_ChIP-Oct4_5-6-7_R2_1.fastq.gz; SMARCA4_ChIP-Oct4_5-6-7_R2_2.fastq.gz; SMARCA4_ChIP-Oct4_5-6-7_R2_.bw
- Oct4 (sc-5279) MNase ChIP-seq low sedimentation rate (5-6-7) replicate 1
TIR1_ChIP-Oct4_5-6-7_R1_1.fastq.gz; TIR1_ChIP-Oct4_5-6-7_R1_2.fastq.gz; TIR1_ChIP-Oct4_5-6-7_R1_.bw
- Oct4 (sc-5279) MNase ChIP-seq low sedimentation rate (5-6-7) replicate 2
TIR1_ChIP-Oct4_5-6-7_R2_1.fastq.gz; TIR1_ChIP-Oct4_5-6-7_R2_2.fastq.gz; TIR1_ChIP-Oct4_5-6-7_R2_.bw
- Sox2 (sc-17320) MNase ChIP-seq low sedimentation rate (5-6) replicate 1
TIR1_ChIP-Sox2_5-6_R1_1.fastq.gz; TIR1_ChIP-Sox2_5-6_R1_2.fastq.gz; TIR1_ChIP-Sox2_5-6_R1_.bw
- Sox2 (sc-17320) MNase ChIP-seq low sedimentation rate (5-6) replicate 2
TIR1_ChIP-Sox2_5-6_R2_1.fastq.gz; TIR1_ChIP-Sox2_5-6_R2_2.fastq.gz; TIR1_ChIP-Sox2_5-6_R2_.bw
- Sox2 (sc-17320) MNase ChIP-seq low sedimentation rate (2-3-4) replicate 1
TIR1_ChIP-Sox2_2-3-4_R1_1.fastq.gz; TIR1_ChIP-Sox2_2-3-4_R1_2.fastq.gz; TIR1_ChIP-Sox2_2-3-4_R1_.bw
- Sox2 (sc-17320) MNase ChIP-seq low sedimentation rate (2-3-4) replicate 2
TIR1_ChIP-Sox2_2-3-4_R2_1.fastq.gz; TIR1_ChIP-Sox2_2-3-4_R2_2.fastq.gz; TIR1_ChIP-Sox2_2-3-4_R2_.bw
- Histone H3 MNase ChIP-seq low sedimentation rate (5-6) Control ZHBTc4 replicate1
ZHBTc4_NT_ChIPH3_5-6_R1_1.fastq.gz; ZHBTc4_NT_ChIPH3_5-6_R1_2.fastq.gz; ZHBTc4_NT_ChIPH3_5-6_R1_.bw
- Histone H3 MNase ChIP-seq low sedimentation rate (5-6) Control ZHBTc4 replicate2
ZHBTc4_NT_ChIPH3_5-6_R2_1.fastq.gz; ZHBTc4_NT_ChIPH3_5-6_R2_2.fastq.gz; ZHBTc4_NT_ChIPH3_5-6_R2_.bw
- Histone H3 MNase ChIP-seq low sedimentation rate (5-6) Oct4-depleted ZHBTc4 replicate1
ZHBTc4_DOX_ChIPH3_5-6_R1_1.fastq.gz; ZHBTc4_DOX_ChIPH3_5-6_R1_2.fastq.gz; ZHBTc4_DOX_ChIPH3_5-6_R1_.bw
- Histone H3 MNase ChIP-seq low sedimentation rate (5-6) Oct4-depleted ZHBTc4 replicate2
ZHBTc4_DOX_ChIPH3_5-6_R2_1.fastq.gz; ZHBTc4_DOX_ChIPH3_5-6_R2_2.fastq.gz; ZHBTc4_DOX_ChIPH3_5-6_R2_.bw
- Histone H3.3-TAG MNase ChIP-seq low sedimentation rate (5-6) replicate 1
N-ChIP-H3.3-TAG_R1_1.fastq.gz; N-ChIP-H3.3-TAG_R1_2.fastq.gz; N-ChIP-H3.3-TAG_R1_.bw
- Histone H3.3-TAG MNase ChIP-seq low sedimentation rate (5-6) replicate 2
N-ChIP-H3.3-TAG_R2_1.fastq.gz; N-ChIP-H3.3-TAG_R2_2.fastq.gz; N-ChIP-H3.3-TAG_R2_.bw

- Histone H3.3-TAG MNase ChIP-seq low sedimentation rate (5-6) replicate 3
N-ChIP-H3.3-TAG_R3_1.fastq.gz; N-ChIP-H3.3-TAG_R3_2.fastq.gz; N-ChIP-H3.3-TAG_R3_.bw
- Histone H3.3-TAG MNase ChIP-seq low sedimentation rate (5-6) replicate 4
N-ChIP-H3.3-TAG_R4_1.fastq.gz; N-ChIP-H3.3-TAG_R4_2.fastq.gz; N-ChIP-H3.3-TAG_R4_.bw
- Oct4-pull-down replicate 1
Oct4-Pull-down_N-ChIP-H3.3-TAG_R1_1.fastq.gz; Oct4-Pull-down_N-ChIP-H3.3-TAG_R1_2.fastq.gz; Oct4-Pull-down_N-ChIP-H3.3-TAG_R1_.bw
- Oct4-pull-down replicate 2
Oct4-Pull-down_N-ChIP-H3.3-TAG_R2_1.fastq.gz; Oct4-Pull-down_N-ChIP-H3.3-TAG_R2_2.fastq.gz; Oct4-Pull-down_N-ChIP-H3.3-TAG_R2_.bw
- Oct4-pull-down replicate 3
Oct4-Pull-down_N-ChIP-H3.3-TAG_R3_1.fastq.gz; Oct4-Pull-down_N-ChIP-H3.3-TAG_R3_2.fastq.gz; Oct4-Pull-down_N-ChIP-H3.3-TAG_R3_.bw
Oct4-pull-down replicate 4
Oct4-Pull-down_N-ChIP-H3.3-TAG_R4_1.fastq.gz; Oct4-Pull-down_N-ChIP-H3.3-TAG_R4_2.fastq.gz; Oct4-Pull-down_N-ChIP-H3.3-TAG_R4_.bw

Genome browser session
(e.g. UCSC)

Density graphs and bed files have been deposited at the Zenodo Data repository: https://zenodo.org/record/7056534.

MM10 mouse BW files : density graphs shown in Fig. 4, 5, 6, 7 and in Extended Data Fig. 4, 11, 12
https://zenodo.org/record/7056534/files/mouseES_mm10_fusion_Histone_H2A_MNase_ChIP-seq_lowSedimentationRate5-6.bw?download=1
https://zenodo.org/record/7056534/files/mouseES_mm10_fusion_Histone_H2A_MNase_ChIP-seq_lowSedimentationRate_5-6_Brg1-depleted_auxin_20h.bw?download=1
https://zenodo.org/record/7056534/files/mouseES_mm10_fusion_Histone_H2B_MNase_ChIP-seq_lowSedimentationRate5-6.bw?download=1
https://zenodo.org/record/7056534/files/mouseES_mm10_fusion_Histone_H2B_MNase_ChIP-seq_lowSedimentationRate5-6_Brg1-depleted_auxin_20h.bw?download=1
https://zenodo.org/record/7056534/files/mouseES_mm10_fusion_Histone_H3_MNase_ChIP-seq_lowSedimentationRate5-6.bw?download=1
https://zenodo.org/record/7056534/files/mouseES_mm10_fusion_Histone_H3_MNase_ChIP-seq_lowSedimentationRate5-6_Brg1-depleted_auxin_20h.bw?download=1
https://zenodo.org/record/7056534/files/mouseES_mm10_fusion_Histone_H3_MNase_ChIP-seq_mononucleosomes_fractions11-13.bw?download=1
https://zenodo.org/record/7056534/files/mouseES_mm10_fusion_Histone_H4_MNase_ChIP-seq_lowSedimentationRate5-6.bw?download=1
https://zenodo.org/record/7056534/files/mouseES_mm10_fusion_Histone_H4_MNase_ChIP-seq_lowSedimentationRate5-6_Brg1-depleted_auxin_20h.bw?download=1
https://zenodo.org/record/7056534/files/mouseES_mm10_fusion_Oct4_MBS420786_MNase_ChIP-seq_lowSedimentationRate_5-6.bw?download=1
https://zenodo.org/record/7056534/files/mouseES_mm10_fusion_Oct4_MNase_ChIP-seq_lowSedimentationRate5-6.bw?download=1
https://zenodo.org/record/7056534/files/mouseES_mm10_fusion_Oct4_MNase_ChIP-seq_lowSedimentationRate5-6_Brg1-depleted_auxin_20h.bw?download=1
https://zenodo.org/record/7056534/files/mouseES_mm10_fusion_Oct4_MNase_ChIP-seq_topGradient2-3-4.bw?download=1
https://zenodo.org/record/7056534/files/mouseES_mm10_fusion_Oct4_MNase_ChIP-seq_topGradient2-3-4_Brg1-depleted_auxin_20h.bw?download=1
https://zenodo.org/records/10609917/files/mouseES_mm10_low100_fusion2_ARID1A_ChIP-Oct4_5-6-7.bw?download=1
https://zenodo.org/records/10609917/files/mouseES_mm10_low100_fusion2_BRD7_ChIP-Oct4_5-6-7.bw?download=1
https://zenodo.org/records/10609917/files/mouseES_mm10_low100_fusion2_BRD9_ChIP-Oct4_5-6-7.bw?download=1
https://zenodo.org/records/10609917/files/mouseES_mm10_low100_fusion2_PBRM1_ChIP-Oct4_5-6-7.bw?download=1
https://zenodo.org/records/10609917/files/mouseES_mm10_low100_fusion2_SMARCB1_ChIP-Oct4_5-6-7.bw?download=1
https://zenodo.org/records/10609917/files/mouseES_mm10_low100_fusion4_N-ChIP-H3-3-TAG.bw?download=1
https://zenodo.org/records/10609917/files/mouseES_mm10_low100_fusion4_Oct4-Pull-down_N-ChIP-H3-3-TAG.bw?download=1
https://zenodo.org/records/10609917/files/mouseES_mm10_low500_fusion2_ARID1A-H3_5-6.bw?download=1
https://zenodo.org/records/10609917/files/mouseES_mm10_low500_fusion2_BRD7-5-6-H3.bw?download=1
https://zenodo.org/records/10609917/files/mouseES_mm10_low500_fusion2_BRD9-H3_5-6.bw?download=1
https://zenodo.org/records/10609917/files/mouseES_mm10_low500_fusion2_PBRM1-5-6-H3.bw?download=1
https://zenodo.org/records/10609917/files/mouseES_mm10_low500_fusion2_SMARCB1-H3_5-6.bw?download=1
https://zenodo.org/records/10609917/files/mouseES_mm10_low500_fusion2_TIR1_ChIP-Sox2_2-3-4.bw?download=1
https://zenodo.org/records/10609917/files/mouseES_mm10_low500_fusion2_TIR1_ChIP-Sox2_5-6.bw?download=1
https://zenodo.org/records/10609917/files/mouseES_mm10_low500_fusion2_ZHBTc4_DOX_ChIPH3_5-6.bw?download=1
https://zenodo.org/records/10609917/files/mouseES_mm10_low500_fusion2_ZHBTc4_NT_ChIPH3_5-6.bw?download=1

MM10 mouse BED files : selection of enhancer lists shown in Extended Data Fig. 1
https://zenodo.org/record/7056534/files/mouseES_mm10_enhancers_10304.bed?download=1
https://zenodo.org/record/7056534/files/mouseES_mm10_enhancers_cluster1.bed?download=1
https://zenodo.org/record/7056534/files/mouseES_mm10_enhancers_cluster2.bed?download=1
https://zenodo.org/record/7056534/files/mouseES_mm10_enhancers_cluster3.bed?download=1
https://zenodo.org/record/7056534/files/mouseES_mm10_enhancers_cluster8.bed?download=1

MM10 mouse BED files : lists of promoters and CTCF binding sites used in Extended Data Fig. 8
https://zenodo.org/record/7056534/files/mouseES_mm10_TSS_g0.bed?download=1
https://zenodo.org/record/7056534/files/mouseES_mm10_ctcf.bed?download=1

HG38 human BED files: enhancer lists used in Extended Data Fig. 10c-e
https://zenodo.org/record/7056534/files/human501Mel_enhancers_cluster1.bed?download=1
https://zenodo.org/record/7056534/files/human501Mel_enhancers_cluster2.bed?download=1

Methodology

Replicates	Between 2 and 4 biological replicates were performed for each experimental situation
Sequencing depth	All ChIP-seq samples were sequenced paired-end, as 26, 37, 38, 42, 76 or 150 mers. Sequencing depth is given in Supplementary Table 4.
Antibodies	H2A (rabbit polyclonal, ab18255, Abcam) H2B (rabbit polyclonal, ab1790, Abcam) H3 (rabbit polyclonal, ab1791, Abcam) H4 (rabbit polyclonal, ab7311, Abcam) H3K27ac (rabbit polyclonal, ab4729, Abcam) Nanog (rabbit polyclonal, RCAB-001P, Reprocell) Oct4 (goat polyclonal, sc-8628, Santa Cruz Biotechnomogy) Oct4 (mouse monoclonal C-10, sc-5279, Santa Cruz Biotechnology) Oct4 (goat polyclonal, MBS420786, myBioSource) RNA Pol II (mouse monoclonal F-12, sc-55492, Santa Cruz Biotechnology) Sox2 (goat polyclonal, sc-17320, Santa Cruz Biotechnology) TBP (mouse monoclonal, ab51841, abcam) Flag (mouse monoclonal M2, F1804, Sigma-Aldrich) HA (mouse monoclonal HA-7, H3663, Sigma-Aldrich) IgG, no known specificity (rabbit polyclonal, ab37415, Abcam)
Peak calling parameters	For IGV visualizations, peaks from each TF or histone dataset were identified using MACS2 (v 2.2.7.1) using default parameters. MACS2 was used without the control option. For TF motif detection, replicate datasets were merged and peaks were identified using MACS2 (v 2.2.7.1; parameters -f BAMPE -g mm --min-length 40).
Data quality	ChIP-seq sample quality was analysed using the following criteria: - technical quality: proper sequencing depth and unique-hit mapping rates - reproducibility was controlled by comparing the V-plots and IGV browser patterns of replicate experiments.
Software	Illumina RTA 2.4.11 or 2.11.3 (NextSeq550) and bcl2fastq Conversion was used for basecalling and demultiplexing. Software v2.20.0.422 was used for basecalling and demultiplexing. MNase ChIP-seq analysis were performed using Snakemake, Conda and in-house python script. Peak calling: MACS2 v 2.2.7.1. Transcription factor motif detection was performed with HOMER v 4.11 or Meme v 5.3.0. Heatmap analysis was performed with seqMINER v 1.3.3e. R 4.2.0. was used for boxplots and bar charts.